NON-POLYSACCHARIDE PLANT POLYMERIC MATERIALS

EDITED BY : José Alejandro Heredia-Guerrero and Athanassia Athanassiou

frontiers Research Topics

About Frontiers

Frontiers is more than just an open-access publisher of scholarly articles: it is a pioneering approach to the world of academia, radically improving the way scholarly research is managed. The grand vision of Frontiers is a world where all people have an equal opportunity to seek, share and generate knowledge. Frontiers provides immediate and permanent online open access to all its publications, but this alone is not enough to realize our grand goals.

Frontiers Journal Series

The Frontiers Journal Series is a multi-tier and interdisciplinary set of open-access, online journals, promising a paradigm shift from the current review, selection and dissemination processes in academic publishing. All Frontiers journals are driven by researchers for researchers; therefore, they constitute a service to the scholarly community. At the same time, the Frontiers Journal Series operates on a revolutionary invention, the tiered publishing system, initially addressing specific communities of scholars, and gradually climbing up to broader public understanding, thus serving the interests of the lay society, too.

Dedication to quality

Each Frontiers article is a landmark of the highest quality, thanks to genuinely collaborative interactions between authors and review editors, who include some of the world's best academicians. Research must be certified by peers before entering a stream of knowledge that may eventually reach the public - and shape society; therefore, Frontiers only applies the most rigorous and unbiased reviews.

Frontiers revolutionizes research publishing by freely delivering the most outstanding research, evaluated with no bias from both the academic and social point of view.

By applying the most advanced information technologies, Frontiers is catapulting scholarly publishing into a new generation.

What are Frontiers Research Topics?

Frontiers Research Topics are very popular trademarks of the Frontiers Journals Series: they are collections of at least ten articles, all centered on a particular subject. With their unique mix of varied contributions from Original Research to Review Articles, Frontiers Research Topics unify the most influential researchers, the latest key findings and historical advances in a hot research area! Find out more on how to host your own Frontiers Research Topic or contribute to one as an author by contacting the Frontiers Editorial Office: **researchtopics@frontiersin.org**

NON-POLYSACCHARIDE PLANT POLYMERIC MATERIALS

Topic Editors:
José Alejandro Heredia-Guerrero, Smart Materials, Istituto Italiano di Tecnologia, Italy
Athanassia Athanassiou, Smart Materials, Istituto Italiano di Technologia, Italy
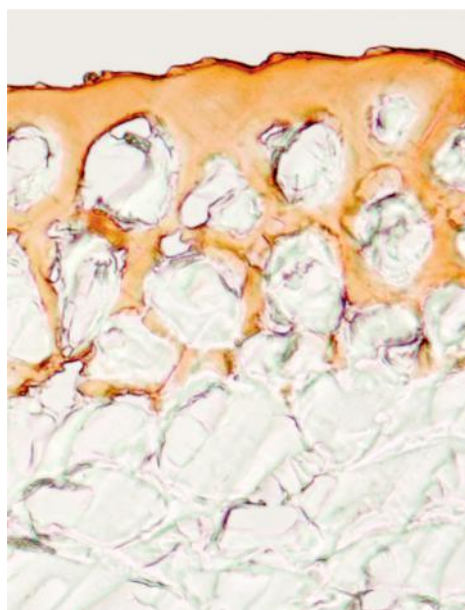
Plants are the most important renewable source of feedstock for polymeric materials. They are a resource of monomers and macromolecules after the appropriate chemical treatment. By analogy with the petrochemistry industry, plant macromolecules are depolymerized into simpler units which are generally chemically modified and re-bound to produce new polymers. The properties of these polymers are usually tailored by small chemical changes in their molecular structure, or by the polymerization of plant monomers with other molecules. Another interesting strategy for the formation of polymeric materials is the direct use of plant macromolecules in the form of blends, composites, grafted polymers, multilayer systems, etc. The interactions and assemblies of the different components allow the control of the final features of such materials.

Traditionally, polysaccharides, with cellulose as the main protagonist, have been the most used substances. However, as consequence of a growing demand of functional plastics, other plant macromolecules, habitually considered wastes, have started to become valuable raw materials. Lignin and plant proteins (mainly, soy protein, wheat gluten, and zein) are classical examples. Also, suberin has been highlighted in this field. Other plant polymers such as the cutin and the sporopollenin are promising alternatives. Furthermore, other minority plant polymers, e.g. cutan or algaenan, could be potential sources of materials. The different chemistry, structure, intrinsic properties and functions of these macromolecules in the plants are a strong inspiration for the development of novel and interesting polymeric materials.

Fruit pericarp cross-section of the tomato wild species Solanum cheesmaniae. Cuticle stained with Sudan IV.

Image by Eva Domínguez

Here, in this Research Topic, we welcome the submission of manuscripts related to the production, extraction, processability, synthesis, characterization and applications of non-polysaccharides plant materials.

Citation: Heredia-Guerrero, J. A., Athanassiou, A., eds. (2016). Non-Polysaccharide Plant Polymeric Materials. Lausanne: Frontiers Media. doi: 10.3389/978-2-88919-853-5

Table of Contents

Editorial: Non-polysaccharide Plant Polymeric Materials

José Alejandro Heredia-Guerrero* and Athanassia Athanassiou*

Smart Materials, Nanophysics, Fondazione Istituto Italiano di Tecnologia (IIT), Genoa, Italy

The Editorial on the Research Topic

Non-polysaccharide Plant Polymeric Materials

> This is a plastic's age, man, a plastic's age.
> Julio Cortázar (Hopscotch, 1963)

Plastics are everywhere. Their unique combination of properties (lightweight, durability, wide range of mechanical properties, different degrees of hydrophobicity, processability, etc.), as well as the low cost in comparison with materials of similar characteristics, has allowed an impressive development of such macromolecules. Moreover, the ease of change of plastic's features by small chemical modification or by addition of fillers is an important advantage to be considered. However, they have a serious drawback related to their sustainability. Mainly plastics are derived from fossil resources, being most of them non-biodegradable in human scale of time, which leads to important environmental problems as, for instance, the alteration and destruction of ecosystems or adverse health effects.

As an alternative, biopolymers combine similar performances as common plastics with high rates of biodegradation in short times. Despite these facts, the lack of a specific large-scale technology for them and the relatively high costs for their isolation and process have been hindering their use. Nevertheless, the depletion of fossil resources and an increasingly green conscience, reflected on different new policies and regulations, have promoted the industrial interest on biopolymers. In this sense, plants are the most important renewable source of feedstock for monomers and macro-molecules after appropriate chemical treatment. Traditionally, polysaccharides, with cellulose as the main protagonist, have been the most used substances. Nonetheless, as consequence of a growing demand of functional materials, other plant macromolecules habitually considered wastes have started to become valuable raw materials.

One characteristic example is the cutin, an amorphous, insoluble and hydrophobic polyester composed by polyhydroxylated fatty acids and, to a lesser extent, glycerol. It is the main component of plant cuticle, i.e., the external membrane that covers the epidermis of non-lignified parts of aerial plant organs, such as fruits, leaves, and green stems. The distribution of cutin in the plant cuticle and its interaction with other cuticular components present a significant interest and recently has been tracked by Confocal Raman Microscopy (Prats Mateu et al.) Cutin can be hydrolyzed into monomers in basic solutions, which can be repolymerized to form films with application in food packaging. For instance, cutin monomers and derivatives can be easily polymerized by non-catalyzed melt-polycondensation (Benítez et al.) At 150°C, free-standing polyesters with very similar properties to cutin are obtained. Also, the reaction can be catalyzed by Lewis acidic ionic liquids, such as choline chloride·2ZnCl$_2$ (Gómez-Patiño et al.) In this case, viscous and mainly linear polymers with potential biomedical applications are synthesized.

Another kind of interesting plant barrier polymer is the suberin (Graça). It is a lipid polymer formed by α,ω-bifunctional fatty acids and glycerol. These α,ω-bifunctional fatty acids have multiple

uses, for example, in the synthesis of polyurethanes and thermoset resins, in the fabrication of high-resistant fibers, or in the water-proofing of cellulose-base films. Additionally, they are promising for biomedical applications due to their cancer-preventing antimutagenic properties and their firming anti-wrinkle action in human skin (Graça). Cork is one of the main sources of suberin. This natural material can be used in the manufacture of high number of products, such as mechanical, thermal, and acoustic insulators in the form of panels, blocks, or sandwich structures for the construction industry (Gil).

Sporopollenin, the main component of the outer shells (exines) of pollen grains and plant spores, is another non-polysaccharide plant polymer. It shows a high chemical inertness. These exines can be employed as microcapsules and filled with substances of different nature, such as enzymes or drugs, and used in biomedical applications. Also, the sporopollenin exine surface can be chemically functionalized in several ways and used as solid support for peptide synthesis, catalysis, and ion-exchange chromatography (Mackenzie et al.)

Interestingly, some of these non-polysaccharide plant polymers, before being fully biodegraded, can be transformed into a useful and energetic macropolymer named kerogen, whose final composition depends on the chemical nature of the biological input (Gupta).

Here, we have shown just few alternatives to plastics. It should be our responsibility (for us and for future generations) to continue and expand these research lines and make them suitable for large-scale production. It is time, reinterpreting the famous Argentine writer Julio Cortázar, for a new green plastic's age.

AUTHOR CONTRIBUTIONS

All authors listed have made substantial, direct, and intellectual contribution to the work and approved it for publication.

ACKNOWLEDGMENTS

FUNDING

Cork: sustainability and new applications

Luís Gil *

Laboratório Nacional de Energia e Geologia I.P., Lisboa, Portugal
*Correspondence: luis.gil@lneg.pt

Cork is a strategic material used in multiple applications and its use has accompanied mankind since the days of Ancient Egypt. The cork oak forests are extremely well adapted to the semi-arid regions of southern Europe and northern Africa (western Mediterranean). These forests help to prevent the advance of desertification, improve water penetration into the soil and hydrological regulation, promote soil conservation, and being the perfect habitat for many animal and vegetables species. Consequently, these forests promote biodiversity (Pereira, 2007; Gil, 2011, 2014).

Save the cork forests, increasing the area and the quantity and quality of cork produced and develop new products with high added value are essential actions. The loss of the economic importance of the cork activity would lead to an uncertain future of cork oak forests, promoting biodiversity loss, land abandonment (social desertification), and also social imbalance. This could lead to the disappearance of one of the most sustainable industries based on forest products, beyond the environmental and nature problems created.

One of the ways to decrease the amount of carbon dioxide in the atmosphere is the production of long-life products based on plant biomass, which include without doubt, cork products. Furthermore, these materials are "carbon neutral" at the time of decomposition or energy recovery.

A very important aspect has to do with the increase in production due to cork extraction. This is caused by the need of the tree to be rapidly protected from the environment after the removal of its bark. This operation will serve as a stimulus to the production of new suberous material, particularly in the early years after the extraction. During the tree lifetime in operation, an average cork oak produces about four times more cork bark than the cork tree would produce if it were not subject to stripping. The sum of the various layers of cork produced and harvested is greater than the single layer of cork produced if there was no extraction during the life of a tree (Gil, 1998, 2011).

Related to environmental aspects of the transformation of the cork raw material, it can be mentioned the production of expanded cork agglomerate. The manufacture of this cork product only uses superheated steam, using generators fueled with cork waste, not introducing any other products not exclusively cork, and giving up agglomeration based on resins of the cork itself. So, this is a completely natural and ecological product. In addition, in the processing of this and other cork products an important residue is produced, cork powder. This powder is commonly burned to produce steam and/or power used in the factories themselves, given the high energy content of this material. Also, all other industrial cork wastes are reused or valorized in another way (Gil, 1998). So, there is really no wasted cork.

Meanwhile, cork products for the construction industry, are ones of the most suitable for sustainable and efficient energy construction, given its mentioned ecological characteristics. These materials are good thermal insulators, conferring to the buildings good thermal quality and good thermal behavior according to the energy certification systems. In addition, these products contribute to the general comfort and also indoor air quality (Gil, 2007).

In this regard, it should be noted that there are a number of new derivatives products of cork or incorporating new technologies applied to traditional products, which are still in various stages of development. These may have or be adapted for use in construction, one of the most interesting areas of application although several other fields of applications are also under consideration. These are new products that may eventually contribute to a greater sustainability in the construction business and also in the cork sector. A short selection on these new materials that can be foreseen for building applications is as follows.

For example, we can start by addressing a new product derived from cork that is being introduced in the market, consisting of a flexible tubular cork pipe coating obtained by extruding a mixture of granulated cork with a polyurethane resin binder (Esteves, 2010). This product is intended for industrial and residential applications for mechanical, thermal, and acoustic insulation. Its application is foreseen particularly under conditions where the outer wear caused by photo-degradation, chemical, physical, and biological conditions is very heavy, resisting better than competing insulation materials. It is anticipated a widespread use in piping insulation, e.g., in air conditioning and central heating, water heating systems, solar energy and water pipes, etc. This material may also be buried in the ground or embedded in construction.

Another product that is also being developed is a block of concrete with cork, with optimized geometry, light weight and good thermal and acoustic performance, maintaining good physical and mechanical behavior (Branco et al., 2008). This block can be used as a construction element, e.g.,

as a brick. It is also being developed a constructive solution, which is a prefabricated vertical partition element incorporating cork, having a high thermal and acoustic performance. It is expected to reduce walls' construction costs, adding the reduction of labor time and of the waste generated, reducing the overall ecological footprint.

It is also foreseen increasing the use of cork products in combination with other materials for structural purposes, as well as uses of very high value (functional materials) such as innovative new applications in the construction industry and other specific fields. As an example, it can also be foreseen the use of agglomerated cork as component material in sandwich structures (Soares, 2007; Silva et al., 2010). Hybrid sandwich panels with a new cork-based plastic composite material as core material were investigated and compared with other materials proving that the new core cork-based material is competitive (Kim, 2011).

In this field can be further highlighted new products previously studied but not yet in the market, such as corkboards with ligands based on lignin residues (Gil, 2007a); products obtained with mixtures of mortar, plaster, and other materials with cork; cork composites with pulp and various natural fibers combined (Fernandes et al., 2009); cork waste-polymer composites (Fernandes et al., 2011); and still different textiles using cork.

It is also under development an eco-efficient partition wall. This material uses by-products of other industrial productions such as gypsum from the desulfurization of flue gases from power plants and textile fibers from the recycling of old tires, together with the expanded cork regranulate. The composite material can be used in partitions or walls in new buildings rehabilitation.

A new patented composite of cork and beverage cartons was developed. The process aimed at the utilization of packing materials as cork stoppers and multilayer (card, aluminum, polyethylene) packages. These packing materials are ground, mixed, and hot pressed, using operational conditions, which allow the thermoplastic and cork composition materials to act as binding agents. A wide range of physical and mechanical characteristics was obtained depending on the cork:beverage carton

ratio and on the temperature and pressure conditions, among other parameters (Gil and Silva, 2005).

There are also plans to use some structural building elements made of cork and the use of "three-dimensional" pieces (irregular shapes, reliefs). The aim is to contribute to a greater architectural value, in particular, through the use of CAD/CAM technologies (especially at the end of their production chain), which allows a great geometric freedom and customization possibilities, as can be seen in SOFALCA homepage [http://sofalca.pt/corkwave/index.html (accessed on 2014.12.15)].

Different cork layered plywood composites (plywood board + cork core) and plywood board with cork core and cork face layers were produced, tested, and compared with standard particle boards and plywood boards. The cork layered plywood showed some better characteristics in comparison with these marketed products (Král et al., 2014).

Reference is also done to new composites based on cork powder and reinforced with carbon nanotubes (Daveiga and Ferreira, 2005), which are anticipated with high tensile strength and ductility, foreseeing applications such as acoustic and thermal insulation construction materials. A new composite has also just being divulged [see link http://webcache.googleusercontent.com/search?q=cache:AU635p1xh24J:www.greenfibertech.com/file_bank/Materia_Brochura.pdf+&cd=2&hl=pt-PT&ct=clnk&gl=pt (accessed on 2014.12.15)] based on plastic, wood fibers, and cork (a kind of plastic timber) for different applications including building.

It should be noted here too the possibility of future use of paints incorporating cork particles. These particles can have different particle sizes and different proportions, resulting in a lower thermal conductivity and a higher acoustic absorption compared with standard paints, thus contributing to a better housing (Gil and Marreiros, 2011a).

Cork agglomerates and cork rubber composites can be a solution to provide damping capacity also including low weight and thermal and acoustic insulation (Policarpo et al., 2013).

In some recent meetings of relatively narrow scope was also released information

on projects and studies in which new products are being developed based on the projected cork and cork products with fiberglass, resin, and cork and even combining ceramic and cork.

Concluding here were described some aspects related to sustainability and the contribution of new products based on cork to this concept, prefiguring an interesting future in this field. Cork, which is a material that comes from the past, is walking to the future.

REFERENCES

Branco, F. G., Reis, M. L. B. C., and Tadeu, A. (2008). Experimental evaluation of the durability of cork concrete. *Int J Hous Sci* 32, 149–162.

Daveiga, J., and Ferreira, P. (2005). "Smart and nano materials in architecture," in *Conference ACADIA 05: Smart Architecture* (Savannah: SCAD), 58–67.

Esteves, D. (2010). *Desenvolvimento, caracterização e avaliação do comportamento termomecânico de um novo material constituído principalmente por cortiça.* MSc. thesis, Lisbon: Instituto Superior Técnico.

Fernandes, E. M., Corelo, V. M., Chagas, J. A. M., Mano, J. F., and Reis, R. L. (2009). *Compósitos à base de cortiça reforçados com fibras.* Portuguese patent PT 104704.

Fernandes, E. M., Corelo, V. M., Chagas, J. A. M., Mano, J. F., and Reis, R. L. (2011). Properties of new cork-polymer composites: advantages and drawbacks as compared with commercially available fibreboard materials. *Compos Struct* 93, 3120–3129.

Gil, L. (1998). *Cortiça – Produção, Tecnologia e Aplicação.* Lisboa: INETI.

Gil, L. (2007). *Cork as a Building Material. Technical Manual.* Santa Maria de Lamas: APCOR.

Gil, L. (2007a). "New cork agglomerates based on modified lignin ecobinders," in *15th European Biomass Conference & Exhibition* (Berlin).

Gil, L. (2011). Environmental, sustainability and ecological aspects of cork products for building. *Sci Technol Mater* 23, 87–90.

Gil, L. (2014). Cork: a strategic material. *Front Chem* 2:16. doi:10.3389/fchem.2014.00016

Gil, L., and Marreiros, N. (2011a). Tintas com incorporação de partículas de cortiça para melhor comportamento térmico e acústico. *Sci Technol Mater* 23, 15–17.

Gil, L., and Silva, P. (2005). *Processo para a produção de aglomerados compósitos e produtos obtidos pelo processo.* Portuguese patent PT 102992.

Kim, S. (2011). *A Study on Cork-Based Plastic Composite Material,* Thesis for Engineer's Degree, Massachusetts Institute of Technology, Cambridge.

Král, P., Klémek, P., Mishra, P. K., Rademacher, P., and Wimmer, R. (2014). Preparation and characterization of cork layered composite plywood boards. *Bioresources* 9, 1977–1985. doi:10.15376/biores.9.2.1977-1985

Pereira, H. (2007). *Cork: Biology, Production and Uses.* Amesterdam: Elsevier.

Policarpo, H., Diogo, A. C., Neves, M. M., and Maia, N. M. M. (2013). "A note on the estimation of cork composite elasto-dynamic properties and their frequency dependence," in *ICEDyn*

2013 – International Conference on Structural Engineering Dynamics (Sesimbra: Hindowi Publishing Corporation).

Silva, J. M., Devezas, T., Silva, A., Gil, L., Nunes, C., and Franco, N. (2010). Exploring the use of cork based composites for aerospace applications. *Mater Sci Forum* 636-637, 260–265. doi:10.4028/www.scientific.net/MSF.636-637.260

Soares, B. (2007). *Estruturas sandwich com utilização de núcleos de cortiça*. MSc. thesis, Instituto Superior Técnico, Lisbon.

Suberin: the biopolyester at the frontier of plants

José Graça *

Centro de Estudos Florestais, Instituto Superior de Agronomia, Universidade de Lisboa, Lisboa, Portugal

Suberin is a lipophilic macromolecule found in specialized plant cell walls, wherever insulation or protection toward the surroundings is needed. Suberized cells form the periderm, the tissue that envelops secondary stems as part of the bark, and develop as the sealing tissue after wounding or leaf abscission. Suberin is a complex polyester built from poly-functional long-chain fatty acids (suberin acids) and glycerol. The suberin acids composition of a number of plant tissues and species is now established, but how the polyester macromolecule is assembled within the suberized cell walls is not known. In the last years contributions from several areas have however significantly enriched our understanding of suberin. The primary structure of the polyester, i.e., how the suberin acids and glycerol are sequentially linked was revealed, together with the stereochemistry of the mid-chain functional groups some suberin acids have; solid-state NMR studies showed the presence of methylene chains spatially separated and with different molecular mobility; biophysical studies showed the membrane behavior of suberin acids derivatives, allowing new insights on structure-properties relationships; and a number of candidate genes were conclusively related to suberin biosynthesis. The comprehension of suberin as a macromolecule will be essential to understand its vital protective roles in plants and how they will deal with eventual environmental changes. Suberin is also expected to be a source for high-performing bio-based chemicals, taking advantage of the structural uniqueness of their constituent suberin acids.

SUBERIZED CELL WALLS FORM A PROTECTIVE BARRIER IN PLANTS

When plants emerged from the sea and start evolving in the more aggressive land environment, they faced a number of survival challenges, including control of water loss, insulation against climatic variability, and protection against abiotic aggressions (Delaux et al., 2012). As an answer, plants developed tissues with barrier properties enveloping all parts of their body. Plant tissues of primary growth, like leaves, fruits, and stems, are covered by a single cell layer, the epidermis; in plants with secondary growth, like trees and shrubs, a multi-cell layer forms, the periderm, as part of the outer bark (Evert, 2006). To fulfill their frontier roles, epidermis and periderm cells have specialized biomacromolecules as a major component of their cell walls, cutin, and suberin, respectively.

Cutinized and suberized cell walls are however complex structures including, besides cutin and suberin, other biomacromolecules and non-polymeric components (the "extractives"). Polyaromatics, which can be analytically determined as lignin, are found associated

(and covalently linked) to suberin, and in a lesser extent to cutin (Riley and Kolattukudy, 1975). Polysaccharides are also part of these cell walls, but in comparatively smaller proportions. Non-polymeric lipids, the "waxes," are deposited in suberized and cutinized cells, sometimes in very significant amounts, and probably have a major role in the hydrophobicity and low permeability of these cell walls (Schreiber et al., 2005). Although cutin and suberin share many chemical and structural affinities, their building units ("monomers") and macromolecular arrangement, follow different patterns in the respective cell walls. The focus of this mini-review is suberin, seen as a macromolecule in the context of the structure of suberized cell walls. Polyaromatics are briefly reviewed, taking into account their association with suberin; polysaccharides and non-polymeric lipids are not discussed, except on their putative roles in the overall structure of suberized cell walls.

Suberized cells are found not only as part of periderms, but also in other plant tissues, some of them internal, where control of water flow or transport to the surroundings is needed (Schreiber, 2010). Also, suberized cells form as wound tissue after physical injuries, as well as the sealing layer that leads to the abscission of plant parts (Vandoorn and Stead, 1997). However, it is in periderm of some plants that sometimes massive amounts of suberized cells are found. The periderm is formed by the phellogen, a meristematic cell layer that divides to the outside phellem, and to the inside phelloderm (**Figures 1A,B**). The phellem cells differentiate as suberized cells, and since the division of phelloderm is (in many cases) minimal, periderms are mostly made of suberized cells (**Figures 1C,D**).

In the context of trees biology, the suberized tissue of periderms is known as "cork." Some trees and shrubs have a "corky" outer bark, because its phellogen is very active and divide large number of suberized cell layers each year of growth. Plants developed corky barks as an adaptation against fire, since they are found mostly in ecosystems prone to it, such as savannah and sub-tropical biomes (Dantas and Pausas, 2013). An exceptional corky outer bark is the one of the cork oak (*Quercus suber* L.), a tree found in the west Mediterranean and neighboring Atlantic regions, from which commercial cork is harvested. Cork have a large set of properties, making it a technological performing material, used worldwide in a high number of industrial applications, for some of them without proper substitute (Pereira, 2007). Many of these technical properties mimic the original functions of suberized cells in plants, and derive from the presence of suberin in their cell walls.

Periderms also form in underground stems, of which potato (*Solanum tuberosum*) tubers are a typical example. When potatoes are harvested, the suberization process keeps evolving in the periderm cells for a few days, making the "mature" potato skin (Lulai and Orr, 1994). The protection afforded by the periderm's suberized cells is essential for potatoes conservation, and the breaking of its integrity by physical or biotic damage a major problem in the respective agroindustry (Neubauer et al., 2013). When potato tubers are cut through, a sealing tissue made of suberized cells forms in a few days, making a "wound periderm" (Lulai and Corsini, 1998). Due to their abundance and industrial importance, the suberins of *Quercus suber* cork and potato

periderm are the ones most extensively studied. Other aspects of the suberization process, like its physiology, genomics or suberin biosynthesis, were in many cases also carried out in potato wound periderms, due to the relatively short times and simplicity to get them.

SUBERIZED CELL WALLS HAVE A POLY-LAMELLATE ORGANIZATION

The specificities of suberized cell walls, in terms of their histology and structure, as observed at microscopic level, were early recognized. Still in the XIX century van Wisselingh observed that suberized cells walls showed three main layers, one more external corresponding to the primary wall, a thicker secondary wall faintly lamellate, and an internal tertiary wall (Vanwisselingh, 1888). The primary and tertiary cell wall layers were comparatively thin and stained positively for cellulose and lignin; the secondary wall was marked by lipid and fat stains and therefore included suberin in its composition. Some suberized cell walls also show deposited internally to the tertiary wall (or apparently in its substitution), other materials, which in some cases can represent a significant fraction of the wall's total thickness. These materials, the latter to be synthesized and deposited, are mainly extractable "waxes": for instance, in potato periderm, this waxy layer in very significant (**Figure 1F**), accounting for 20% of the tissue weight (Graça and Pereira, 2000b). Suberized cell walls can be very thin: primary and tertiary walls have a thickness of 0.1 to 0.2 μm in cross section; the suberin secondary wall can have approximately 0.5 μm, and the extractives layer, when present, up to 0.3 μm (**Figures 1E,F**).

With the advent of the transmission electron microscopy (TEM), the pioneering work of Sitte (mostly based in cork) postulated in a comprehensive manner the ultrastructure of suberized cell walls. Besides confirming the overall structure proposed by van Wisselingh, the main observation of Sitte was that the secondary suberin wall is thinly lamellate (Sitte, 1959). Two types of alternating lamellae are observed: the "light," electron translucent lamellae, and the "dark," electron-opaque ones. In cork, Sitte measured for light lamellae an even thickness of 3 nm, and for the dark lamellae a variable thickness, from 7 to 10 nm. In all, from 30 to 60 light and dark lamellae could be counted across cork's suberized cell wall (Sitte, 1962). The number of observed lamellae is however highly variable depending on the particular tissue or plant species, and as rule, less in number than in *Q. suber* cork (Kolattukudy and Espelie, 1989). In some suberized cell walls the lamellae are very well-defined and straight, like in potato periderm (**Figure 1E**), but in others, they can look more undulated, particularly in the inner (lately differentiated) part of the secondary wall (**Figure 1F**).

The presence of this mostly organized poly-lamellate structure, besides tissue identity and location, has been used to define suberized cells (Kolattukudy and Espelie, 1989). In rare cases the lamellae were not observed in suberized walls (Teixeira and Pereira, 2010), but care should be taken since methodological choices can affect the visibility of the lamellae. The key question that remains to be answered is how the
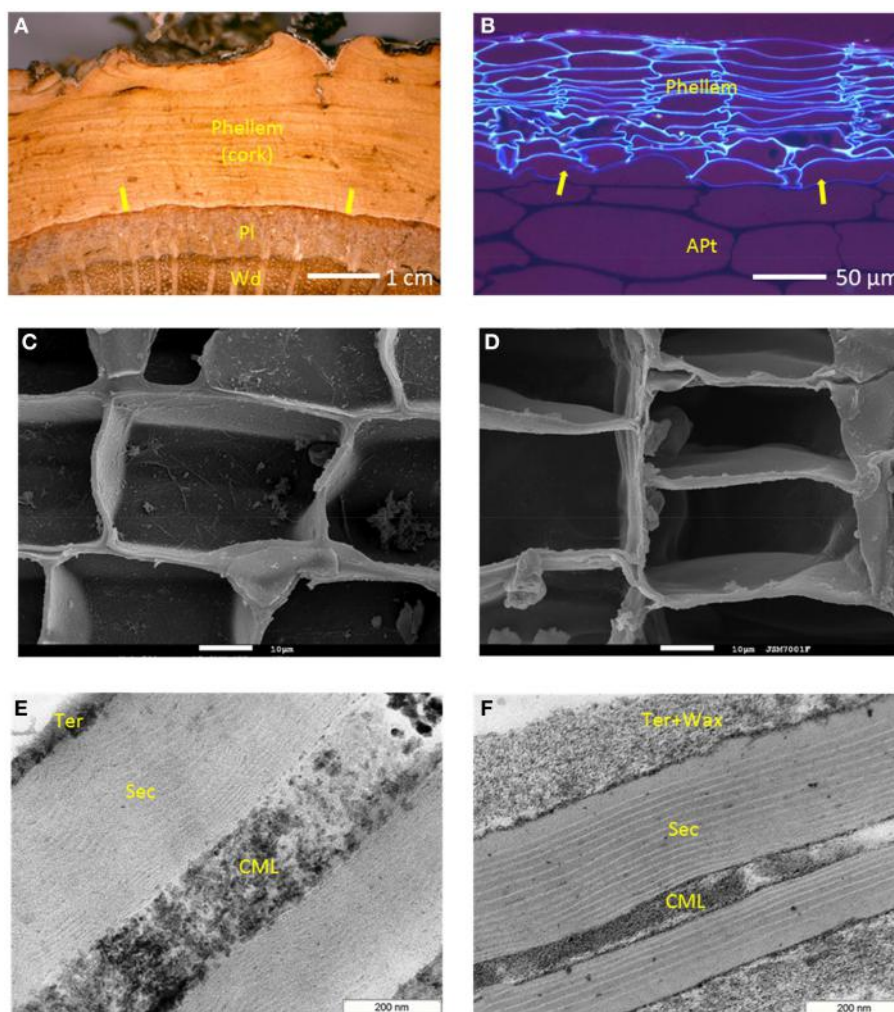
FIGURE 1 | Periderm and suberized cells in cork (*Quercus suber*) and potato tubers (*Solanum tuberosum*). (A) *Q. suber* trunk outer tissues, showing the periderm, made of phellem (suberized tissue, the *cork*), *phellogen* (the mother-cell layer, arrows), and phelloderm (not visible); *Pl*, phloem; *Wd*, xylem (wood). **(B)** Potato tuber outer tissues, showing the periderm, made of *phellem* (the suberized tissue), *phellogen* (arrows), and phelloderm (not visible); *Apt*, amylaceous parenchyma tissue. Suberized cells as seen by SEM, in cork **(C)** and potato periderm **(D)** (white bars = 10 μm). Ultrastructure of suberized cell walls as seen by TEM, in cork **(E)** and potato periderm **(F)**; *CML*, compound middle lamella (mostly primary wall); *Sec*, the poly-lamellate secondary wall; *Ter*, tertiary wall with the non-polymeric waxes, *Wax*, deposited.

chemical composition of suberized cell walls is related to the observed ultrastructure; in particular, how the molecular (or supramolecular) arrangement of suberin, and other associated macromolecules, like polyaromatics, can explain the lamellate structure found in secondary walls. This will be addressed below together with the discussion of the macromolecular structure of suberin.

SUBERIN IS BUILT FROM α,ω-BIFUNCTIONAL FATTY ACIDS AND GLYCEROL

All types of ester breaking reactions can be used to depolymerize suberin, showing that its building units are interlinked as a polyester macromolecule. Alkaline hydrolysis was an initial favorite, but later, less aggressive techniques like base and acid-catalyzed methanolysis, and hydrogenolysis, have been preferred for analytical convenience (Kolattukudy, 2001). The major component of suberin depolymerisates are long-chain aliphatic acids, representing typically 80–90% in mass of all monomers released (**Figure 2**). Although a few ancient works had unequivocally showed that glycerol was also released when suberin was depolymerized (Ribas and Blasco, 1940), the presence of glycerol and its important role in suberin was ignored for a long time. Most of the suberin analysis put their focus on its aliphatic acids, which were recovered to an organic phase in partition with water, the latter carrying the glycerol away when discarded. Quantitative determinations of glycerol in suberins are relatively few, but values from 5 to 20% of all suberin monomers

have been measured (Graça and Pereira, 2000a). Finally, when suberin is depolymerized, "phenolic acids" are also released; in particular ferulic acid is always present in small amounts. The role of this phenolic moieties in suberin is discussed in Section Polyaromatics are a Substantial Component of Suberized Cell Walls.

The total suberin content has been accessed as the organic soluble component of the depolymerization products (therefore not including glycerol) or more correctly, as the mass-loss after suberin depolymerization (Graça and Pereira, 2000a). Suberin content determinations in plant materials varied from 1% to more than 50%. However, besides the question of how the suberin content was calculated, these values are relative to plant materials which included very different proportions of suberized cells. In carefully isolated "pure" suberized tissue, after the removal of non-polymeric extractives, the suberin content is typically higher, from 10 to 60% (Holloway, 1983). This value should correspond to the proportion of suberin in the composition of suberized cell walls, and the one to take into account in the discussion in Section Suberin Make the Light, and Polyaromatics the Dark Lamellae in Suberized Cell walls.

The exact structure of suberin acids was long controversial, but by the middle of the XX century their chemistry was elucidated (Jensen, 1952; Ribas, 1952; Guillemonat, 1960). In the early 1970s, with the development of gas chromatography hyphenated with mass spectrometry (GC-MS), the analysis of complex mixtures of suberin acids become straightforward, and the works of Kolattukudy and Holloway pioneered the studies of suberin composition from a number of plant sources (Kolattukudy et al., 1975; Holloway, 1983). The main characteristic of suberin acids is that they are α,ω-bifunctional, i.e., they have linking groups at both ends of their hydrocarbon chains. Two main families of fatty acids are thus defined: the α,ω-diacids, with carboxylic acids at both the α and ω positions; and the ω-hydroxyacids, with a carboxylic acid in the α position and a hydroxyl group in the ω position (**Figure 2**). The existence of at least these two linking positions in suberin monomers is necessary for them to be part of a polymeric structure. Mono-functional fatty acids (alkanoic acids) and fatty alcohols (alkanols) are also commonly found among the depolymerization products of most suberins (**Figure 2**), but as a rule, they represent a comparatively small part of the long-chain monomers ($< 10\%$); due to their single linking group they can only act as dead ends in the suberin macromolecule.

The chain length of both α,ω-diacids and ω-hydroxyacids in suberins range typically from C_{16} to C_{26}, with the even numbered chains largely dominant (Holloway, 1983; Kolattukudy, 2002). In some suberins the mono-functional fatty acids and alcohols can reach much higher chain lengths, up to C_{30} (Rios et al., 2014). Within the α,ω-diacids and ω-hydroxyacids classes of suberin monomers, two groups are found: the C_{18} with mid-chain modifications (discussed below), and the ones with saturated chains, starting at C_{16} (skipping the C_{18}) and going up to C_{28}. Other types of fatty acids are also found in some suberins, including α-hydroxyacids, α,ω-alkanediols, and C_{16} ω-dihydroxyacids (Kolattukudy, 2002), the latter more typical of cutins.

The C_{18} mid-chain modified α,ω-diacids and ω-hydroxyacids are quantitatively relevant, or even dominant, in the composition of many suberins, and therefore must play a crucial role in its macromolecular structure. Three main types of mid-chain modifications are found at the C-9 and C-10 carbons: a double bond, an epoxide ring or two vicinal hydroxyl groups (*vic*-diol) (**Figure 2**). The stereochemistry of this mid-chain groups was studied in cork suberin: both the double bonds and the epoxide ring have a *cis* configuration, and the *vic*-diols are *threo*, using the nomenclature developed for carbohydrates for their relative configuration, meaning that both the *9R,10R*, and *9S,10S* absolute configurations can be present (Santos et al., 2013; Santos and Graça, 2014). These secondary groups at mid-chain can impact significantly the molecular packing of the suberin macromolecule due to steric effects, derived from their specific stereochemistry and volumetric hindrance, or provide cross-links though intra-molecular bonding (discussed below).

The relative proportion of the different families of monomers, and of the individual suberin acids, are highly variable in suberins, depending on plant species and tissue location (Holloway, 1983; Kolattukudy, 2002). The number of suberins which have been thoroughly analyzed so far is limited, but patterns in suberin composition can be recognized. As a rule, ω-hydroxyacids are always an important class of monomers; the α,ω-diacids can be second to ω-hydroxyacids, but can also be more abundant, as in the cases of *Q. suber* cork and potato periderm suberins (Graça and Pereira, 2000a,b). Two main types of suberins can be recognized taking into account their dominant suberin acids (Holloway, 1983): there is a group of suberins where the C_{18} epoxide and *vic*-diol α,ω-diacids and ω-hydroxyacids are overwhelming, with minor proportions of saturated chain monomers, like in *Kielmeyera coriacea* bark periderm (Rios et al., 2014); and there is another group of suberins where the mono-unsaturated $C_{18:1}$ and saturated chain monomers are dominant, and the C_{18} epoxide and *vic*-diol suberin acids are present in small amounts or event absent, as are the cases in *Pseudotsuga menziessii* bark and potato periderm (Graça and Santos, 2007). This means that there are different patterns in the macromolecular structure of suberin. However, all kinds of in-between cases exist: for instance, in *Q. suber* cork, all types of the above monomers are found, and its suberin cannot be assigned to one of the groups (Graça and Santos, 2007). The reasons behind this variability are not clear, and can either be related to the ontogeny of the tissue, the physiological stress faced or genetics related to phylogeny.

THE PRIMARY STRUCTURE OF SUBERIN: HOW ARE THE SUBERIN MONOMERS SEQUENTIALLY LINKED?

How are the suberin monomers, namely the α,ω-bifunctional fatty acids, glycerol, and the phenolic acids inter-linked in the suberin macromolecule? So far our knowledge is limited to the so-called primary structure of the macromolecule, i.e., how the monomer residues are sequentially linked. Most of what
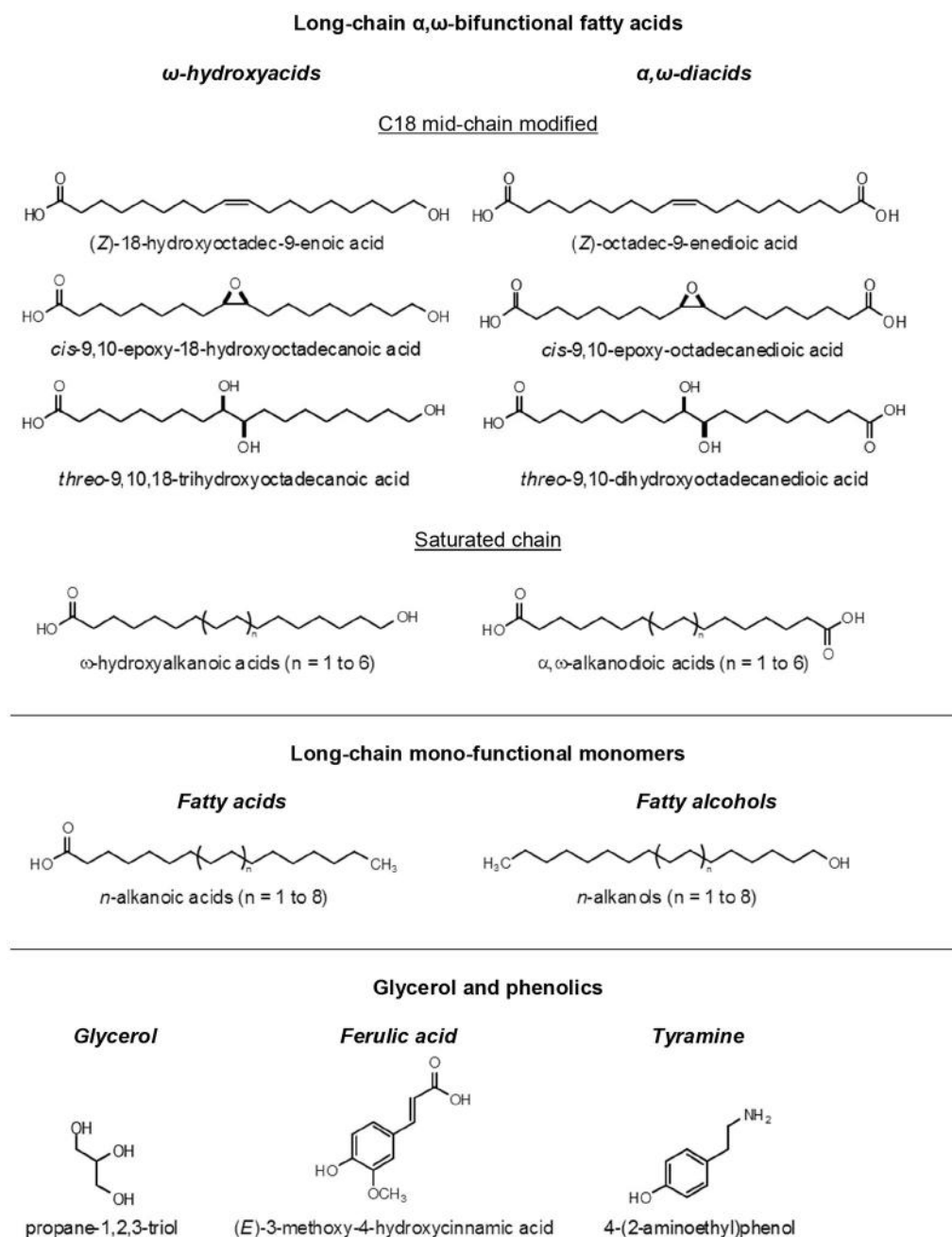
FIGURE 2 | Structural formula of the main suberin monomers.

is known comes from the analysis of oligomers, fragments of the suberin macromolecule still carrying some of their *in situ* inter-monomer ester linkages (Graça and Pereira, 1997; Wang et al., 2010). These oligomers (together with monomers) are obtained by the partial depolymerization of the suberin polyester, using mild or partial hydrolysis conditions. The structure of the solubilized oligomers is identified combining information from GC-MS, electrospray ionization coupled to tandem mass spectrometry (ESI-MS/MS) and high-resolution

one and two-dimensional NMR. Oligomers including 2–5 monomer residues of all the main suberin monomers were found (Graça et al., 2015). Most of these results, discussed below, were obtained from *Q. suber* cork and potato periderm suberins.

The dominant oligomer species in the suberin partial depolymerisates are glycerides having as acyl moieties all types of suberin acids, namely α,ω-diacids, ω-hydroxyacids, and alkanoic acids (Graça and Pereira, 1999, 2000b). Acylglycerol

species involving all the glycerol positions were found as suberin oligomers: 1(3)- and 2-monoacylglycerols, 1,2- and 2,3-diacylglycerols and triacylglycerols (Graça et al., 2015). Besides, α,ω-diacids were found esterified at both ends to two different glycerol moieties, with both 1(3)- and 2-glycerol positions involved in the ester linkages (Graça and Santos, 2006a). Oligomers showing the continuum of this glycerol—α,ω-diacid—glycerol structure units were also identified in the potato suberin partial depolymerisates (Graça et al., 2015). This glycerol—α,ω-diacid—glycerol block can therefore be one of the main backbones from which the suberin grows to macromolecular dimensions. In all, these results, together with the quantitative importance of the involved monomers, imply that suberin is structurally an acylglycerol lipid.

Besides linked to glycerol, suberin acids linked head-to-tail were also obtained as oligomer fragments from the partial depolymerization of suberins. These linear aliphatic esters included mainly as monomer residues ω-hydroxyacids, since the ω-hydroxyl group is necessary to make the ester bond; however, linear ester oligomers including α,ω-diacids were also detected (Graça and Santos, 2006b). The number of suberin acids included in these linear esters were no more than three, as found in the partial depolymerisates of the analyzed suberins (Graça et al., 2015). Some of these rows of interesterified suberin acids were further linked at their end to glycerol. This means that the suberin macromolecule also grows linearly, by the successive addition of ω-hydroxyacids at end chain.

The other significant ester structure found in the oligomers released from the partial depolymerisation of suberins are ferulates of ω-hydroxyacids. In the suberins analyzed so far (Q. suber cork, P. menziesii bark cork and potato periderm), all ω-hydroxyacids which were found as monomers, were also found esterified though their ω-hydroxyl group to ferulic acid as oligomer species (Graça and Pereira, 1998, 1999, 2000b). Also, the trimeric structure of glycerol esterified to ferulates of ω-hydroxyacids, through the acidic end group of the latter, was found in the partial depolymerisates of suberins (Santos and Graça, 2006; Graça et al., 2015). This means that one of the main roles of the ω-hydroxyl group of ω-hydroxyacids is to link the acylglycerol matrix of suberin to phenolic moieties. Due to the high proportion of ω-hydroxyacids found as suberin monomers, and the relative abundance of their ferulates found as suberin oligomers, these aliphatic-aromatic linkages can be an important feature in the organization of suberized cell walls. The discussion of the association of the suberin polyester with aromatics follows.

POLYAROMATICS ARE A SUBSTANTIAL COMPONENT OF SUBERIZED CELL WALLS

Suberized cell walls include non-soluble polyphenolic materials, the "polyaromatics," in significant quantities: in cork, assessed as lignin, they represent approximately 25% of all structural components ("extractive-free" basis) (Pereira, 1988); in native

potato periderm, 31% of insoluble phenolics were determined based on the initial weight, after suberin, polysaccharides and extractives removal (Mattinen et al., 2009); even higher values have been found in wound-induced potato periderm, with a ratio of polymeric phenolics to aliphatic suberin of 2:1, as measured by the respective carbon peak areas in solid-state ^{13}C NMR analysis (Garbow et al., 1989); in the periderm of six subterranean periderms, residual polyaromatics, after the removal of ester-linked suberin, represented from 25 to 30% of the extractive-free initial material (Kolattukudy et al., 1975). A differential scanning calorimetry (DSC) analysis of a potato periderm extract enriched in suberin and polyaromatics showed two different polymer softening temperatures, at 45°C and 59°C, with the latter eventually arising from the polyaromatics moiety (Mattinen et al., 2009). What exactly these polyaromatics are and how similar they are to conventional lignins, remains controversial.

Besides the insoluble polyaromatics, when the suberin polyester is depolymerized by any ester breaking technique, small amounts of phenolics are co-solubilized together with the main aliphatic suberin monomers. Values from 1 to 10% of all suberin depolymerized materials have been found (Kolattukudy et al., 1975; Borgolivier and Monties, 1993). Among the soluble phenolics detected, the hydroxycinnamic ferulic acid is always present in comparatively higher quantities (**Figure 2**), and can have a significant role in the overall structure of suberized cell walls (Graça, 2010). Aminated phenolics have also been found co-solubilized from suberin, namely tyramine (**Figure 2**), both in native and wound induced potato periderm, however in quantities even smaller than ferulic acid (Borgolivier and Monties, 1993). Also, in potato periderms, two ferulic acid amides, feruloyltyramine, and feruloyloctopamine, were found ether linked in the insoluble polyaromatics, but there was no proof of their direct linkage to suberin (Negrel et al., 1996).

The analysis of the insoluble suberin-associated polyaromatics have included, besides degradative lignin techniques, like thioacidolysis and analytical pyrolysis coupled to mass spectrometry (Py-GC-MS), also *in situ* studies by ^{13}C solid state NMR (^{13}C ssNMR). A model for the suberin polyaromatics as a poly(ferulic acid) structure, built from ferulic acid units linked by condensation and ether linkages similar to lignin, was developed: after feeding ^{13}C labeled phenylalanine in suberizing wound potato periderm, signal enhancement was found mostly in carbons assignable to hydroxycinnamates (Bernards et al., 1995; Bernards and Lewis, 1998). This ferulic-acid based polymer was interpreted as a "non-lignin" biomacromolecule (Bernards and Razem, 2001). However, a number of results showed that the suberin-associated polyaromatics behaved analytically (at least in part) as typical lignins. Work carried out in the cork periderms of a few trees and also in native potato periderm, showed these polyaromatics to be dominantly a guaiacyl lignin (Neto et al., 1996; Mattinen et al., 2009; Marques and Pereira, 2013), although in wound potato periderm comparatively high proportions of syringyl units were also found (Lapierre et al., 1996; Yan and Stark, 2000). The exact structure and homogeneity of the suberin-associated polyaromatics remains an open question.

SUBERIN IS A POLY(ACYLGLYCEROL) MACROMOLECULE IN PART ARRANGED AS A LIPID MEMBRANE

A key question to be answered is how we define suberin. The original term "subérine" (in French) is attributed to the famed XIX century chemist Chevreul, who used it to define all the non-soluble materials specific of cork (Gilson, 1890). Later, suberin was considered as the component susceptible to be depolymerized by ester-breaking treatments, thus corresponding to the aliphatic polyester. In a more recent interpretation, suberin has being used to name the two main components of suberized cell walls, thus including two "domains": the aliphatic polyester named the "suberin poly(aliphatic) domain" (SPAD), and the insoluble polyaromatics, named the "suberin poly(phenolic) domain" (SPPD) (Kolattukudy et al., 1975; Bernards, 2002). In our point of view, the name suberin should be kept for the aliphatic polyester (as followed in this review) for several reasons: first, the aliphatic suberin can be analytically isolated as such; second, the polyaromatics are chemically and structurally distinct and in part, spatially separated in suberized cell walls; and finally, the suberin aliphatic polyester can have a defined macromolecular and independent structure (as discussed below). This doesn't preclude the existence of extensive contact and covalent linkages between suberin and the associated polyaromatics, such as those known between other biomacromolecules in plant cell walls.

Based in the above assumptions and in our present knowledge, suberin can be defined as a poly(acylglycerol) macromolecule. Glycerol units linked in succession to α,ω-diacids will be the core backbone of the suberin macromolecule (as illustrated in **Figure 3**); this successive glycerol—α,ω-diacid—glycerol connections can grow as a reticulated and disordered net, giving rise to a random structure (Pollard et al., 2008), or the hydrocarbon chains can dispose in a more orderly packed manner, building membrane-like regions within the suberin macromolecule (Graça and Santos, 2007). Some other indirect evidence can be seen as supportive of the above proposed structure. Suberin-like glycerol—α,ω-diacid—glycerol model molecules were shown to self-assembly *in vitro*: synthesized glycerol—1,16-hexadecanedioic acid—glycerol formed stable lipid vesicles in aqueous media; these vesicles became fluid only at relatively high temperatures (57°C), and their membrane thickness could be estimated close to the length of the C_{16} chain when stretched (Douliez et al., 2005). ^{13}C ssNMR molecular dynamics studies in both cork and potato periderm suberins revealed the presence of two different populations of aliphatic CH_2 (methylene) groups, one more mobile, and the other, presumably close to ester groups (as shown by their chemical shifts), much more rigid in molecular motion (Gil et al., 1997; Yan and Stark, 1998); relating these results to the acylglycerol structure proposed here for suberin, the rigid methylene moieties can correspond to the hydrocarbon chains in the more orderly organized parts of the suberin polyester, and the ones with more motional freedom to the hydrocarbon chains in less constrained regions, further apart from the glycerol anchorage points.
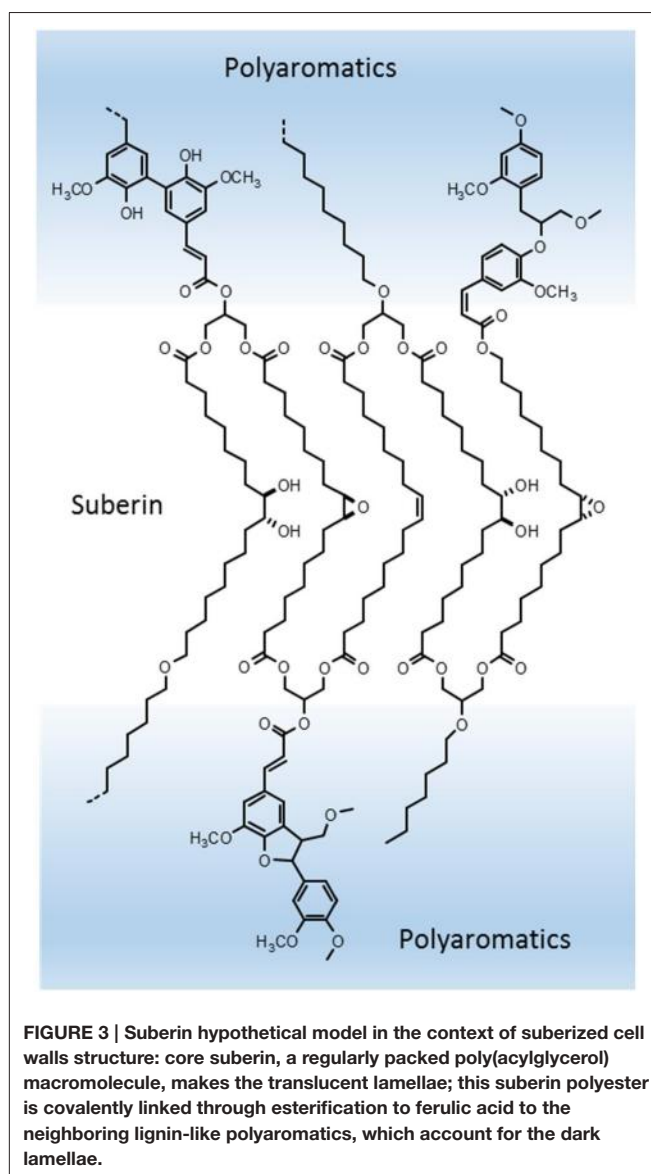
FIGURE 3 | Suberin hypothetical model in the context of suberized cell walls structure: core suberin, a regularly packed poly(acylglycerol) macromolecule, makes the translucent lamellae; this suberin polyester is covalently linked through esterification to ferulic acid to the neighboring lignin-like polyaromatics, which account for the dark lamellae.

Mid-chain modifications in the C_{18} ω-hydroxyacids and α,ω-diacids, dominant in many suberins, can add further complexity to its macromolecular structure and affect the overall properties of suberized cell walls. Unsaturated $C_{18:1}$ suberin monomers, due to its *cis*-configuration, can bend the hydrocarbon chain to a kinked position; fatty acids with mid-chain *cis*-double bonds are known to impart fluidity to lipid membranes, which could be the case in the suberins where these $C_{18:1}$ suberin are dominant. In the opposite direction, the C_{18} 9,10-epoxide and 9,10-*vic*-diol substituted monomers can eventually carry rigidity to the structure: they can also bend at mid-chain, favoring the establishment of intra-monomer secondary bonds, namely hydrogen bridges, cross-linking the hydrocarbon chains, and thus reinforcing an eventual packed arrangement of the suberin acylglycerol structure (**Figure 3**).

As discussed above, we know that ω-hydroxyacids (at their ω-hydroxyl end) show up commonly in suberin oligomers as ferulates. This means that ω-hydroxyacids, besides being part of the acylglycerol suberin matrix, linked through their acidic end group to glycerol, can act at the same time as connectors to the neighboring polyaromatics, through esterification to ferulic acid; the latter can be part of, or be linked to the periphery of those polyaromatics (**Figure 3**). We also know that ω-hydroxyacids are ester linked head-to-tail as linear structures. How long this rows of long-chain monomers grow, we don't know. They can eventually be part of a continuum of the aliphatic polyester across the suberized cell walls. As mentioned, since there are suberins with different proportions of ω-hydroxyacids, α,ω-diacids and glycerol, together with different monomer compositions, the existence of variable suberin macromolecular arrangements are to be expected.

SUBERIN MAKE THE LIGHT, AND POLYAROMATICS THE DARK LAMELLAE IN SUBERIZED CELL WALLS

How does the proposed model for the suberin polyester and associated polyaromatics can fit into the ultrastructure of suberized cell walls as observed by TEM? We know that the suberized cell walls have a lamellate structure, in which the light-contrast lamellae have a regular thickness, and the dark-contrast lamellae a not so regular thickness. Initially, the light lamellae were attributed to non-polymeric waxes and the dark lamellae to suberin (Sitte, 1962). This idea was supported by the observation that in wound potato periderm, the light lamellae did not form after the specific inhibition of waxes synthesis (its chain elongation impaired by trichloroacetate), without affecting significantly suberin monomer composition (Soliday et al., 1979). But other results are consistent with the location of the suberin aliphatic polyester in the light lamellae. In the suberized fibers of cotton, the application *in vitro* of a specific inhibitor of fatty acid elongases (EPTC), led to a suberin with shorter long-chain monomers; besides, the suberized cell walls after this treatment showed less, and in some cases thinner, light lamellae; the conclusion was that the glycerol-suberin acids structure was necessary for the lamellae formation, and that the long-chain monomers would be perpendicular to the light lamellae plane (Schmutz et al., 1996). Also in potato periderm, the silencing of a key gene involved in the ω-hydroxylation of fatty acids in suberin, *CYP86A33,* led to much less suberin, highly deficient in C18 ω-hydroxicadis and α,ω-diacids; as a result, the lamellar structure was disrupted (Serra et al., 2009).

The analysis of suberized cell walls *in situ* by ^{13}C ssNMR techniques allowed direct information on the location and molecular mobility of their aliphatic and aromatic components, both in potato periderm (Stark and Garbow, 1992; Yan and Stark, 1998) and in cork (Neto et al., 1995; Gil et al., 1999). The aliphatic polyester is spatially separated from the polyaromatics, and the latter have two populations, one in the vicinity of the aliphatic polyester and the other close to polysaccharides. Considering all the available information above discussed, we can hypothesize the

following role of suberin as part of the topochemical arrangement of suberized cell walls: light lamellae are made by the core of the suberin polyester, namely glycerol—C18 α,ω-diacids—glycerol and the glycerol—C18 ω-hydroxyacids moieties; in this suberin regions, hydrocarbon long-chains will be in part orderly arranged, accounting for the regular thickness of the light lamellae; the dark lamellae are mostly made by the polyaromatics, though locally crossed by aliphatic chains; suberin and the vicinal polyaromatics are extensively covalently linked at their interface through ferulic acid, the latter esterified to ω-hydroxyacids and glycerol on the polyester side, and with lignin-like linkages on the polyaromatics side; this polyaromatics are a ferulic-acid rich lignin-like macromolecule; the polyaromatics not vicinal to the suberin polyester are a standard, dominantly guaiacyl lignin, that together with polysaccharides, build the primary wall (and tertiary wall when present); inner to the suberin cell wall, non-polymeric materials, namely "waxes," are deposited as a more or less thick layer, depending on their relative abundance (**Figure 2**).

GENOMICS AND BIOSYNTHESIS STUDIES GO TOGETHER WITH THE SUBERIN CHEMISTRY STRUCTURAL RESULTS

Studies on the biosynthetic pathways leading to suberin (and cutin) monomers started in the 1970s (Kolattukudy and Espelie, 1989), but most of the knowledge on the specific genes and proteins involved on the monomers synthesis and their assembling as a polyester in suberizing plant cells was obtained in the last decade. Biosynthesis studies were done mostly in suberizing wound potato, but also in other plants and tissues where cutin is formed, since they share a number of monomers (Kolattukudy, 2002). Many of the genomics and associated biochemical and functional studies were carried out in the model *Arabidopsis*, namely through silencing and/or overexpressing of suberin candidate genes, and assessing the phenotypical modifications at the polyester structure and composition (Beisson et al., 2012; Franke et al., 2012). Biosynthesis studies showed that the mono-functional 9-unsaturated $C_{18:1}$(oleic) acid was the starting point for the mid-chain 9,10 modified suberin monomers: the terminal C-18 carbon is first ω-hydroxylated forming the $C_{18:1}$ω-hydroxyacid, and further oxidized to the corresponding $C_{18:1}$α,ω-diacid; the epoxidation at the C-9/C-10 carbons, and its further hydration, give rise respectively to the C_{18} 9,10 epoxide and C_{18}9,10-diol monomers. Straight chain suberin acids followed the known pathway starting at acetyl and malonyl CoA, down to the C_{16} saturated chain fatty acid, followed by its successive elongation, together with its eventual end chain oxidation to ω-hydroxyacids and α,ω-diacids (Kolattukudy, 2002).

Recent genomics approaches allowed the identification of enzymes, and their encoding genes, that lead not only to suberin acids, but also to the different ester structures found in suberin known from the chemical analysis. Cytochrome P450(CYP) oxygenases were proved to play a crucial role in the end- and mid-chain oxidation steps, starting from mono-functional fatty acids, and leading to ω-hydroxyacids and α,ω-diacids, either with

saturated chains or with secondary oxygenated groups (Pinot and Beisson, 2011). Some genes and the corresponding enzymes seem to be selective for specific suberin monomers: genes encoding ω-hydroxylases more specific to C_{16}–C_{18} (*CYP86A1*) or to C_{22}–C_{24} fatty acids (*CYP86B1*), were found associated with the suberization process; the epoxidation *in vitro* of the C-9 double bond of the $C_{18:1}$ (oleic) acid by the CYP94A1 oxygenase, gave rise to dominantly (*9R,10S*) and much less (*9S,10R*) stereoisomers, both corresponding to the *cis* configuration found in suberin epoxyacids discussed above. The silencing of the *CYP83A33* gene in potato, which promotes the ω-hydroxylation step in its periderm suberin, led to a highly modified polyester structure and the distortion of the lamellar arrangement in the cell walls (Serra et al., 2009).

Acyltransferases, and the corresponding genes, able to synthesize two of the main ester structures found in suberin have been identified, promoting the esterification of suberin acids to glycerol, and the esterification of ω-hydroxyacids (through their ω-hydroxyl group) to ferulic acid. A glycerol-3-phosphate acyltransferase (GPAT5) was found to direct the esterification of ω-hydroxyacids and α,ω-diacids at the *sn*-2 position (the "middle" hydroxyl) of glycerol (Yang et al., 2010), and other GPATs are expected to carry the esterification at the *sn*-1(3) positions (Beisson et al., 2012). Feruloyl transferases from the BAHD family able to ester-link ferulic acid to ω-hydroxyacids (and *n*-alkanols) were found in suberizing tissues, and their role in the suberin biosynthesis proved after their silencing in mutant plants (Molina et al., 2009); these ω-hydroxyacid ferulate connections were discussed above as the putative preferential structure that links the suberin aliphatic polyester to the neighboring aromatics. In spite of these significant advances, how the suberin monomers assemble *in situ* building the macromolecular structure, and the transport processes involved, remains in most part to be elucidated.

THE CHEMICAL SINGULARITY OF SUBERIN MAKES IT VALUABLE FOR INDUSTRIAL APPLICATIONS

The chemical uniqueness of suberin long-chain α,ω-bifunctional monomers, or the polyester macromolecule as a whole, makes them of high industrial interest. A key point is their bi- or poly-functionality: each suberin acid have at least two reactive groups in the α,ω-positions, or more in the case of the C_{18} mid-chain modified ones; besides, they carry the properties derived from the long hydrocarbon chains, such as molecular flexibility and hydrophobicity. The preparation of technical polymers with

designed properties, starting from these bi- or polyfunctional suberin monomers, is one of the more promising areas (Olsson et al., 2007; De Geus et al., 2010; Sousa et al., 2011). Because of this, considerable efforts have been done to obtain suberin-like fatty acids by biotechnological means (Huf et al., 2011) and chemical synthesis (Yokota and Watanabe, 1990). However, suberin-rich plant materials are available as residues in thousands of tons from some industries, like cork transformation (cork powders), potato processing (potato skins) or birch (*Betula* sp.) trees harvesting (outer bark) (Pinto et al., 2009). In the perspective of its industrial use, the extraction of suberin from the suberized matrices has been made by conventional hydrolytic means, and more recently, was achieved using ionic liquids, specifically targeting the acylglycerol linkages (Ferreira et al., 2014).

The efforts to obtain isolated suberin acids in industrial scale date back to the 1940s when a company named "Suber" was installed in France, offering "Subéryl," a product obtained from suberin after cork saponification (Guillemonat, 1949). At research level, the number of assayed applications and potential uses for suberin and suberin acids keeps growing: hybrid co-polymers like polyurethanes were made from cork suberin extracts and isocyanate monomers (Cordeiro et al., 1999), and thermoset resins from epoxy ω-hydroxyacids and methacrylates (Torron et al., 2014); polymers built from the polymerization of long-chain ω-hydroxyacids were used to obtain high-resistant fibers (De Geus et al., 2010); and suberin fatty acids were shown to improve significantly the water vapor imperviousness of cellulose-based films (Heinäemäeki et al., 2015). Moreover, suberin seems to be of potential interest in many other areas. For instance, suberin extracts showed cancer-preventing anti-mutagenic properties (Krizkova et al., 1999) and a firming anti-wrinkle action in human skin (Coquet et al., 2005). Suberin has also been regarded as an inspiring source for biomimetic materials, including "superhydrophilic" and "superhydrophobic" surfaces (Koch and Barthlott, 2009). Finally, another major asset of these suberin-based products is that they can be obtained from renewable and sustainable plant sources, thus insuring its future development.

ACKNOWLEDGMENTS

REFERENCES

Beisson, F., Li-Beisson, Y., and Pollard, M. (2012). Solving the puzzles of cutin and suberin polymer biosynthesis. *Curr. Opin. Plant Biol.* 15, 329–337. doi: 10.1016/j.pbi.2012.03.003

Bernards, M. A. (2002). Demystifying suberin. *Canad. J. Bot. Revue* 80, 227–240. doi: 10.1139/b02-017

Bernards, M. A., and Lewis, N. G. (1998). The macromolecular aromatic domain in suberized tissue: a changing paradigm. *Phytochemistry* 47, 915–933. doi: 10.1016/s0031-9422(98)80052-6

Bernards, M. A., Lopez, M. L., Zajicek, J., and Lewis, N. G. (1995). Hydroxycinnamic acid-derived polymers constitute the polyaromatic domain of suberin. *J. Biol. Chem.* 270, 7382–7386.

Bernards, M. A., and Razem, F. A. (2001). The poly(phenolic) domain of potato suberin: a non-lignin cell wall bio-polymer. *Phytochemistry* 57, 1115–1122. doi: 10.1016/s0031-9422(01)00046-2

Borgolivier, O., and Monties, B. (1993). Lignin, suberin, phenolic-acids and tyramine in the suberized, wound-induced potato periderm. *Phytochemistry* 32, 601–606. doi: 10.1016/s0031-9422(00)95143-4

Coquet, C., Bauza, E., Oberto, G., Berghi, A., Farnet, A. M., Ferré, E., et al. (2005). Quercus suber cork extract displays a tensor and smoothing effect on human skin: an *in vivo* study. *Drugs Exp. Clin. Res.* 31, 89–99.

Cordeiro, N., Belgacem, M. N., Gandini, A., and Neto, C. P. (1999). Urethanes and polyurethanes from suberin 2: synthesis and characterization. *Ind. Crops Prod.* 10, 1–10. doi: 10.1016/s0926-6690(98)00029-6

Dantas, V. D., and Pausas, J. G. (2013). The lanky and the corky: fire-escape strategies in savanna woody species. *J. Ecol.* 101, 1265–1272. doi: 10.1111/1365-2745.12118

De Geus, M., van der Meulen, I., Goderis, B., van Hecke, K., Dorschu, M., van der Werff, H., et al. (2010). Performance polymers from renewable monomers: high molecular weight poly(pentadecalactone) for fiber applications. *Polym. Chem.* 1, 525–533. doi: 10.1039/b9py00360f

Delaux, P. M., Nanda, A. K., Mathe, C., Sejalon-Delmas, N., and Dunand, C. (2012). Molecular and biochemical aspects of plant terrestrialization. *Perspect. Plant Ecol. Evol. Syst.* 14, 49–59. doi: 10.1016/j.ppees.2011.09.001

Douliez, J. P., Barrault, J., Jerome, F., Heredia, A., Navailles, L., and Nallet, F. (2005). Glycerol derivatives of cutin and suberin monomers: Synthesis and self-assembly. *Biomacromolecules* 6, 30–34. doi: 10.1021/bm049325o

Evert, R. F. (2006). *Esau's Plant Anatomy: Meristems, Cells, and Tissues of the Plant Body: Their Structure, Function, and Development.* Hoboken, NJ: John Wiley & Sons.

Ferreira, R., Garcia, H., Sousa, A. F., Guerreiro, M., Duarte, F. J. S., Freire, C. S. R., et al. (2014). Unveiling the dual role of the cholinium hexanoate ionic liquid as solvent and catalyst in suberin depolymerisation. *RSC Adv.* 4, 2993–3002. doi: 10.1039/c3ra45910a

Franke, R. B., Dombrink, I., and Schreiber, L. (2012). Suberin goes genomics: use of a short living plant to investigate a long lasting polymer. *Front. Plant Sci.* 3:4. doi: 10.3389/fpls.2012.00004

Garbow, J. R., Ferrantello, L. M., and Stark, R. E. (1989). C-13 Nuclear magnetic-resonance study of suberized potato cell-wall. *Plant Physiol.* 90, 783–787. doi: 10.1104/pp.90.3.783

Gil, A. M., Lopes, M. H., Neto, C. P., and Rocha, J. (1999). Very high-resolution H-1 MAS NMR of a natural polymeric material. *Solid State Nucl. Magn. Reson.* 15, 59–67. doi: 10.1016/s0926-2040(99)00047-8

Gil, A. M., Lopes, M., Rocha, J., and Neto, C. P. (1997). A C-13 solid state nuclear magnetic resonance spectroscopic study of cork cell wall structure: the effect of suberin removal. *Int. J. Biol. Macromol.* 20, 293–305. doi: 10.1016/s0141-8130(97)00029-9

Gilson, E. (1890). La subérine e les cellules du liège. *La Cell. (Louvain)* 6, 63–114.

Graça, J. (2010). Hydroxycinnamates in suberin formation. *Phytochem. Rev.* 9, 85–91. doi: 10.1007/s11101-009-9138-4

Graça, J., Cabral, V., Santos, S., Lamosa, P., Serra, O., Molinas, M., et al. (2015). Partial depolymerization of genetically modified potato tuber periderm reveals intermolecular linkages in suberin polyester. *Phytochemistry* 117, 209–219. doi: 10.1016/j.phytochem.2015.06.010

Graça, J., and Pereira, H. (1997). Cork suberin: a glyceryl based polyester. *Holzforschung* 51, 225–234. doi: 10.1515/hfsg.1997.51.3.225

Graça, J., and Pereira, H. (1998). Feruloyl esters of omega-hydroxyacids in cork suberin. *J. Wood Chem. Technol.* 18, 207–217. doi: 10.1080/02773819809349577

Graça, J., and Pereira, H. (1999). Glyceryl-acyl and aryl-acyl dimers in Pseudotsuga menziesii bark suberin. *Holzforschung* 53, 397–402. doi: 10.1515/hf.1999.066

Graça, J., and Pereira, H. (2000a). Methanolysis of bark suberins: analysis of glycerol and acid monomers. *Phytochem. Anal.* 11, 45–51. doi: 10.1002/(sici)1099-1565(200001/02)11:1<45::aid-pca481>3.0.co;2-8

Graça, J., and Pereira, H. (2000b). Suberin structure in potato periderm: glycerol, long-chain monomers, and glyceryl and feruloyl dimers. *J. Agric. Food Chem.* 48, 5476–5483. doi: 10.1021/jf0006123

Graça, J., and Santos, S. (2006a). Glycerol-derived ester oligomers from cork suberin. *Chem. Phys. Lipids* 144, 96–107. doi: 10.1016/j.chemphyslip.2006.08.001

Graça, J., and Santos, S. (2006b). Linear aliphatic dimeric esters from cork suberin. *Biomacromolecules* 7, 2003–2010. doi: 10.1021/bm060174u

Graça, J., and Santos, S. (2007). Suberin: a biopolyester of plants' skin. *Macromol. Biosci.* 7, 128–135. doi: 10.1002/mabi.200600218

Guillemonat, A. (1949). Le liége matière première d'une industrie chimique. *Revue du Bois* 4, 4–6.

Guillemonat, A. (1960). Progrès récents dans l'étude de la constitution chimique du liège. *Ann. Fac. Sci. Marseille* 30, 43–54.

Heinäemäeki, J., Halenius, A., Paavo, M., Alakurtti, S., Pitkäenen, P., Pirttimaa, M., et al. (2015). Suberin fatty acids isolated from outer birch bark improve moisture barrier properties of cellulose ether films intended for tablet coatings. *Int. J. Pharm.* 489, 91–99. doi: 10.1016/j.ijpharm.2015.04.066

Holloway, P. J. (1983). Some variations in the composition of suberin from the cork layers of higher-plants. *Phytochemistry* 22, 495–502. doi: 10.1016/0031-9422(83)83033-7

Huf, S., Kruegener, S., Hirth, T., Rupp, S., and Zibek, S. (2011). Biotechnological synthesis of long-chain dicarboxylic acids as building blocks for polymers. *Europ. J. Lipid Sci. Technol.* 113, 548–561. doi: 10.1002/ejlt.201000112

Jensen, W. (1952). Studies on suberin. IV. Isolation of phloionic acid from suberin of Quercus suber. *Paperi ja Puu* 34B, 467–479.

Koch, K., and Barthlott, W. (2009). Superhydrophobic and superhydrophilic plant surfaces: an inspiration for biomimetic materials. *Philos. Trans. R. Soc.* 367, 1487–1509. doi: 10.1098/rsta.2009.0022

Kolattukudy, P. (2001). "Polyesters in Higher Plants," in *Biopolyesters,* eds W. Babel and A. Steinbüchel (Berlin; Heidelberg: Springer), 1–49.

Kolattukudy, P. E. (2002). "Suberin from Plants," in *Biopolymers.Polyesters I.*, eds. Y. Doi and A. Steinbüchel (Weinheim: Wiley-VCH Verlag), 41–73.

Kolattukudy, P. E., and Espelie, K. E. (1989). "Chemistry, biochemistry, and function of suberin and associated waxes," in *Natural Products of Woody Plants,* ed J. Rowe (Berlin; Heidelberg: Springer), 304–367.

Kolattukudy, P. E., Kronman, K., and Poulose, A. J. (1975). Determination of structure and composition of suberin from roots of carrot, parsnip, rutabaga, turnip, red beet, and sweet-potato by combined gas-liquid-chromatography and mass-spectrometry. *Plant Physiol.* 55, 567–573. doi: 10.1104/pp.55.3.567

Krizková, L., Lopes, M. H., Polónyi, J., Belicová, A., Dobias, J., and Ebringer, L. (1999). Antimutagenicity of a suberin extract from Quercus suber cork. *Mut. Res. Genet. Toxicol. Environ. Mutagen.* 446, 225–230. doi: 10.1016/s1383-5718(99)00190-4

Lapierre, C., Pollet, B., and Negrel, J. (1996). The phenolic domain of potato suberin: structural comparison with lignins. *Phytochemistry* 42, 949–953. doi: 10.1016/0031-9422(96)00097-0

Lulai, E. C., and Corsini, D. L. (1998). Differential deposition of suberin phenolic and aliphatic domains and their roles in resistance to infection during potato tuber (*Solanum tuberosum* L.) wound-healing. *Physiol. Mol. Plant Pathol.* 53, 209–222. doi: 10.1006/pmpp.1998.0179

Lulai, E. C., and Orr, P. H. (1994). Techniques for detecting and measuring developmental and maturational changes in tuber native periderm. *Am. Potato J.* 71, 489–505. doi: 10.1007/bf02851322

Marques, A. V., and Pereira, H. (2013). Lignin monomeric composition of corks from the barks of Betula pendula, Quercus suber and Quercus cerris determined by Py-GC-MS/FID. *J. Anal. Appl. Pyrolysis* 100, 88–94. doi: 10.1016/j.jaap.2012.12.001

Mattinen, M. L., Filpponen, I., Järvinen, R., Li, B., Kallio, H., Lehtinen, P., et al. (2009). Structure of the Polyphenolic Component of Suberin Isolated from Potato (*Solanum tuberosum* var. *Nikola*). *J. Agric. Food Chem.* 57, 9747–9753. doi: 10.1021/jf9020834

Molina, I., Li-Beisson, Y., Beisson, F., Ohlrogge, J. B., and Pollard, M. (2009). Identification of an arabidopsis feruloyl-coenzyme a transferase required for suberin synthesis. *Plant Physiol.* 151, 1317–1328. doi: 10.1104/pp.109.144907

Negrel, J., Pollet, B., and Lapierre, C. (1996). Ether-linked ferulic acid amides in natural and wound periderms of potato tuber. *Phytochemistry* 43, 1195–1199. doi: 10.1016/s0031-9422(96)00500-6

Neto, C. P., Cordeiro, N., Seca, A., Domingues, F., Gandini, A., and Robert, D. (1996). Isolation and characterization of a lignin-like polymer of the cork of Quercus suber L. *Holzforschung* 50, 563–568. doi: 10.1515/hfsg.1996.50.6.563

Neto, C. P., Rocha, J., Gil, A., Cordeiro, N., Esculcas, A. P., Rocha, S., et al. (1995). C-13 solid-state nuclear-magnetic-resonance and fourier-transform infrared

studies of the thermal-decomposition of cork. *Solid State Nucl. Magn. Reson.* 4, 143–151. doi: 10.1016/0926-2040(94)00039-f

Neubauer, J. D., Lulai, E. C., Thompson, A. L., Suttle, J. C., Bolton, M. D., and Campbell, L. G. (2013). Molecular and cytological aspects of native periderm maturation in potato tubers. *J. Plant Physiol.* 170, 413–423. doi: 10.1016/j.jplph.2012.10.008

Olsson, A., Lindström, M., and Iversen, T. (2007). Lipase-catalyzed synthesis of an epoxy-functionalized polyester from the suberin monomer cis-9,10-epoxy-18-hydroxyoctadecanoic acid. *Biomacromolecules* 8, 757–760. doi: 10.1021/bm060965w

Pereira, H. (1988). Chemical-composition and variability of cork from quercus-suber L. *Wood Sci. Technol.* 22, 211–218.

Pereira, H. (2007). "Chapter 11—Cork products and uses," in *Cork,* ed H. Pereira (Amsterdam: Elsevier Science B.V.), 243–261.

Pinot, F., and Beisson, F. (2011). Cytochrome P450 metabolizing fatty acids in plants: characterization and physiological roles. *Febs J.* 278, 195–205. doi: 10.1111/j.1742-4658.2010.07948.x

Pinto, P., Sousa, A. R., Silvestre, A. J. D., Neto, C. P., Gandini, A., Eckerman, C., et al. (2009). Quercus suber and Betula pendula outer barks as renewable sources of oleochemicals: a comparative study. *Ind. Crops Prod.* 29, 126–132. doi: 10.1016/j.indcrop.2008.04.015

Pollard, M., Beisson, F., Li, Y., and Ohlrogge, J. B. (2008). Building lipid barriers: biosynthesis of cutin and suberin. *Trends Plant Sci.* 13, 236–246. doi: 10.1016/j.tplants.2008.03.003

Ribas, I. (1952). Étude sur la constitution chimique du liège. *Chim. Industr.* 68, 333–350.

Ribas, I., and Blasco, E. (1940). Investigaciones sobre el corcho. I. Sobre la existencia de glicerina. *Anal. Real Soc. Españ. Fís. Quím.* 36B, 141–147.

Riley, R. G., and Kolattukudy, P. E. (1975). Evidence for covalently attached para-coumaric acid and ferulic acid in cutins and suberins. *Plant Physiol.* 56, 650–654. doi: 10.1104/pp.56.5.650

Rios, P., Cabral, V., Santos, S., Mori, F., and Graça, J. (2014). The chemistry of Kielmeyera coriacea outer bark: a potential source for cork. *Europ. J. Wood Wood Prod.* 72, 509–519. doi: 10.1007/s00107-014-0811-y

Santos, S., Cabral, V., and Graça, J. (2013). Cork suberin molecular structure: stereochemistry of the C-18 Epoxy and vic-diol omega-hydroxyacids and alpha,omega-diacids analyzed by NMR. *J. Agric. Food Chem.* 61, 7038–7047. doi: 10.1021/jf400577k

Santos, S., and Graça, J. (2006). Glycerol-omega-hydroxyacid-ferulic acid oligomers in cork suberin structure. *Holzforschung* 60, 171–177. doi: 10.1515/hf.2006.028

Santos, S., and Graça, J. (2014). Stereochemistry of C-18 monounsaturated cork suberin acids determined by spectroscopic techniques including H-1-NMR multiplet analysis of olefinic protons. *Phytochem. Anal.* 25, 192–200. doi: 10.1002/pca.2491

Schmutz, A., Buchala, A. J., and Ryser, U. (1996). Changing the dimensions of suberin lamellae of green cotton fibers with a specific inhibitor of the endoplasmic reticulum-associated fatty acid elongases. *Plant Physiol.* 110, 403–411.

Schreiber, L. (2010). Transport barriers made of cutin, suberin and associated waxes. *Trends Plant Sci.* 15, 546–553. doi: 10.1016/j.tplants.2010.06.004

Schreiber, L., Franke, R., and Hartmann, K. (2005). Wax and suberin development of native and wound periderm of potato (*Solanum tuberosum* L.) and its relation to peridermal transpiration. *Planta* 220, 520–530. doi: 10.1007/s00425-004-1364-9

Serra, O., Soler, M., Hohn, C., Sauveplane, V., Pinot, F., Franke, R., et al. (2009). CYP86A33-Targeted gene silencing in potato tuber alters suberin composition, distorts suberin lamellae, and impairs the periderm's water barrier function. *Plant Physiol.* 149, 1050–1060. doi: 10.1104/pp.108.127183

Sitte, P. (1959). Mischkorperdoppelbrechung der kork-zellwande. *Naturwissenschaften* 46, 260–261.

Sitte, P. (1962). Zum feinbau der suberinschichten im flaschenkork. *Protoplasma* 54, 555–559. doi: 10.1007/bf01252642

Soliday, C. L., Kolattukudy, P. E., and Davis, R. W. (1979). Chemical and ultrastructural evidence that waxes associated with the suberin polymer constitute the major diffusion barrier to water-vapor in potato-tuber (*Solanum-Tuberosum*-L). *Planta* 146, 607–614. doi: 10.1007/bf00388840

Sousa, A. F., Gandini, A., Silvestre, A. J. D., Neto, C. P., Pinto, J., Eckerman, C., et al. (2011). Novel suberin-based biopolyesters: from synthesis to properties. *J. Pol. Sci. Part A Pol. Chem.* 49, 2281–2291. doi: 10.1002/pola.24661

Stark, R. E., and Garbow, J. R. (1992). Nuclear-magnetic-resonance relaxation studies of plant polyester dynamics.2. Suberized potato cell-wall. *Macromolecules* 25, 149–154. doi: 10.1021/ma00027a025

Teixeira, R. T., and Pereira, H. (2010). Suberized cell walls of cork from cork oak differ from other species. *Micros. Microanal.* 16, 569–575. doi: 10.1017/s1431927610093839

Torron, S., Semlitsch, S., Martinelle, M., and Johansson, M. (2014). Polymer thermosets from multifunctional polyester resins based on renewable monomers. *Macromol. Chem. Phys.* 215, 2198–2206. doi: 10.1002/macp.201400192

Vandoorn, W. G., and Stead, A. D. (1997). Abscission of flowers and floral parts. *J. Exp. Bot.* 48, 821–837. doi: 10.1093/jxb/48.4.821

Vanwisselingh, C. (1888). Sur la paroi des celules subéreuses. *Arch.Neérland. Sci. Exact. Natur.* 22, 253–298.

Wang, W., Tian, S., and Stark, R. E. (2010). Isolation and identification of triglycerides and ester oligomers from partial degradation of potato suberin. *J. Agric. Food Chem.* 58, 1040–1045. doi: 10.1021/jf902854y

Yan, B., and Stark, R. E. (1998). A WISE NMR approach to heterogeneous biopolymer mixtures: dynamics and domains in wounded potato tissues. *Macromolecules* 31, 2600–2605. doi: 10.1021/ma9714880

Yan, B., and Stark, R. E. (2000). Biosynthesis, molecular structure, and domain architecture of potato suberin: a C-13 NMR study using isotopically labeled precursors. *J. Agric. Food Chem.* 48, 3298–3304. doi: 10.1021/jf000155q

Yang, W., Pollard, M., Li-Beisson, Y., Beisson, F., Feig, M., and Ohlrogge, J. (2010). A distinct type of glycerol-3-phosphate acyltransferase with sn-2 preference and phosphatase activity producing 2-monoacylglycerol. *Proc. Natl. Acad. Sci. U.S.A.* 107, 12040–12045. doi: 10.1073/pnas.0914149107

Yokota, T., and Watanabe, A. (1990). *Process for producing omega-hydroxy fatty acids.* European patent EP0357865A3. Available online at: http://www.google.com/patents/EP0357865A3?cl=en

Polyhydroxyester films obtained by non-catalyzed melt-polycondensation of natural occurring fatty polyhydroxyacids

José Jesús Benítez[1]*, José Alejandro Heredia-Guerrero[2], Susana Guzmán-Puyol[2], Markus J. Barthel[3], Eva Domínguez[4] and Antonio Heredia[4]

[1] Instituto de Ciencia de Materiales de Sevilla (ICMS), Spanish Research Council (CSIC) and University of Seville, Seville, Spain, [2] Smart Materials, Nanophysics, Fondazione Istituto Italiano di Tecnologia (IIT), Genova, Italy, [3] Drug Discovery and Development Department, Fondazione Istituto Italiano di Tecnologia (IIT), Genova, Italy, [4] Instituto de Hortofruticultura Subtropical y Mediterránea (IHSM), Spanish Research Council (CSIC) and University of Malaga, Malaga, Spain

Free-standing polyesters films from mono and polyhydroxylated fatty acids (C_{16} and C_{18}) have been obtained by non-catalyzed melt-condensation polymerization in air at 150°C. Chemical characterization by Fourier transform infrared spectroscopy and ^{13}C Magic Angle Spinning Nuclear Magnetic Resonance (^{13}C MAS–NMR) has confirmed the formation of the corresponding esters and the occurrence of hydroxyl partial oxidation, which extent depends on the type of hydroxylation of the monomer (primary or secondary). Generally, polyester films obtained are hydrophobic, insoluble in common solvents, amorphous and infusible as revealed by X-ray diffraction and differential scanning calorimetry. In ω-polyhydroxy acids, esterification reaction with primary hydroxyls is preferential and, therefore, the structure can be defined as linear with variable branching depending on the amount of esterified secondary hydroxyls. The occurrence side oxidative reactions like the diol cleavage are responsible for chain cross-linking. Films are thermally stable up to 200–250°C though this limit can be extended up to 300°C in the absence of ester bonds involving secondary hydroxyls. By analogy with natural occurring fatty polyesters (i.e., cutin in higher plants), these polymers are proposed as biodegradable and non-toxic barrier films or coatings to be used, for instance, in food packing.

Keywords: biomimicry, polyhydroxyesters, non-toxic, coatings, waste, valorization

Introduction

The use of plastics in the packaging industry is massive and solidly implanted and, despite the increasing tendency to recycle, their disposal is causing a serious and global environmental problem. This is originated by the fact that, in contact with the soil, most of hydrocarbon-based materials have degradation periods of decades and beyond. Furthermore, in the case of food containers, the toxicity associated to the release of some additives like bisphenol A from the plastic matrix or the protective internal coating is becoming a notorious health concern (NPT-CERHR Monograph on the Potential Human Reproductive and Developmental Effects of Bisphenol A, 2008).

In Nature, higher plants have solved the "packing problem" by wrapping their fruits, leaves, stems, and seeds with a cuticle, a continuous extracellular protective membrane essentially composed of a

polymeric polyester skeleton supporting other components like external and embedded waxes, phenolic compounds, and polysaccharides (Pollard et al., 2008). In aerial parts, such polymeric framework is the cutin, and it constitutes an abundant renewable stock representing up to 1200 kg/crop hectare (Heredia, 2003). The inherent characteristics of biopolymer cutin (Domínguez et al., 2011), i.e., non-toxicity, biodegradability, and availability, are very attractive features to overcome the aforementioned drawbacks of current packaging materials and, consequently, the design and obtaining of cutin inspired polymers is proposed as an alternative. The insolubility and infusibility of natural cutin impedes its direct processing and, therefore, the strategy comprises the chemical degradation of the biopolymer, the isolation of the monomers, and the reconstruction of the polyester under synthetic conditions. Chemically, cutin can be described as an amorphous polymeric network of ester bonded C_{16} and C_{18} polyhydroxylated fatty acids (Baker and Holloway, 1970; Kolattukudy, 1981; Walton, 1990). Thus, the reaction involved is an esterification between the carboxylic acid and the alcohol groups that is typically performed by polycondensation in an organic media using an acidic surfactant as a promoter or a metallic catalyst (Bawn and Huglin, 1962; Saam, 1998; Heredia-Guerrero et al., 2009; Liu et al., 2011; Zhang et al., 2011). However, to avoid the use of organic solvents as well as aromatic and heavy metal catalysts jeopardizing the non-toxicity of the final product, we have used the direct, non-catalyzed synthesis from molten precursors in air. Conceptually, this is a quite simple method for preparing thin films or coatings that could be easily scaled up to large production processes at a very low cost. Particularly, and, if conceived as internal food container coatings, the preservation of the insolubility and infusibility of natural cutin is desirable to resist the sterilization protocols and the chemical attack of edible fluids.

Thus, the aim of this article is the characterization of the materials resulting from the non-catalyzed melt-polycondensation of cutin representative C_{16} monomers like 16-hydroxy, 10,16-dihydroxy and 9,10,16-trihydroxypalmitic acids, as well as other reference C_{18} polyhydroxyacids to state the effect of the hydroxylation degree in the physical and chemical properties of the polyhydroxyesters obtained. Results will constitute a reference for designing a synthesis of non-toxic and biodegradable protective films or coatings based on the valorization of residues like peels of large scale production fruits.

Materials and Methods

Products

16-Hydroxypalmitic acid (Aldrich, 98%) (HPA), 12-hydroxystearic acid (Aldrich, 99%) (HSA), 9,10-dihydroxystearic (Sigma-Aldrich, 99%) (diHSA), and aleuritic (DL-*threo*-9,10,16-trihydroxypalmitc, Fluka, 93.8%) (triHPA) were commercially available and used as received. The product named as 10,16-dihydroxyhexadecanoic acid (diHPA) actually refers to an extract obtained from tomato mature green cuticles (Luque et al., 1995). Cuticles were isolated by incubation for 5 days in a 2% pectinase/0.2% cellulose solution at pH = 3.6 and treated with chloroform:methanol (3/1, *v*/*v*) for 3 h to remove waxes. Dewaxed

cuticles were depolymerized by saponification in 1% KOH/methanol for 6 h under refluxing conditions. The filtrate was neutralized with HCl 1N and extracted with diethyl ether. The solid contains about 82% (*w*/*w*) of 10(9),16-dihydroxyhexadecanoic acids and minor amounts of other diacids and hydroxyacids (Baker and Holloway, 1970; del Río and Hatcher, 1998; Kosma et al., 2010). The chemical structure of monomers and polyester nomenclature used along this article are summarized in (**Figure 1**).

Polyester Synthesis by Non-Catalyzed Melt-Condensation Polymerization

For this procedure, about 150 mg of solid monomer were placed on open carbon doped Teflon molds (30 mm ×10 mm and 1 mm deep) and heated in air inside a natural air convention oven at 150°C for 16–24 h. After cooling for several hours at room conditions, pale yellow/brown rubbery free-standing films with a thickness of about 300–350 µm can be easily separated from the mold. In the case of poly HSA, a very viscous product is obtained. To prepare samples under reduced pressure, the oven was pumped for 12 h at 25 mbar.

Polymer Synthesis by DBSA Assisted Polycondensation

As a reference for the samples obtained by the previous method, polyesters of HPA, diHPA, and triHPA have been prepared by

FIGURE 1 | Chemical structure of monomers, nomenclature used and polyester appearance.
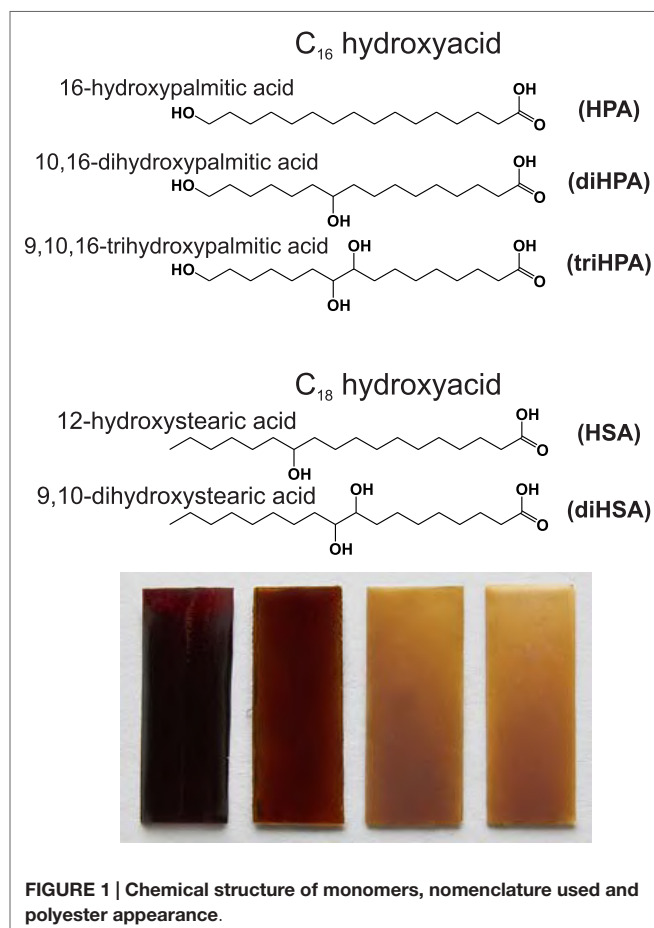
low-temperature polycondensation in similar conditions as those reported (Saam, 1998). Typically, about 200–250 mg of monomer, 80 mg of dodecylbenzenesulfonic acid (DBSA), and 5 mL of toluene were introduced in a 50-mL flask. The mixture was briefly heated to about 100°C under continuous stirring until solids were dissolved, and then cooled to 80°C. Minor losses of organic solvent by evaporation were corrected and, in these conditions, the product began to precipitate in about 20 min forming a solid phase at the bottom of the flask. After 3 h, the reaction was stopped and the solid was filtered, washed sequentially three times with toluene, chloroform, and methanol and dried at room temperature for 24 h. A continuous layer adapting to the bottom of the flask was obtained only when triHPA was used.

Independently on the preparation method, solids obtained are quite insoluble in common solvents such as water, chloroform, toluene, dimethyl sulfoxide (DMSO), and light alcohols. Only poly HPA and poly HSA were found to be soluble in some of these solvents.

Characterization

Transmission infrared spectra of samples were collected in a Fourier transform infrared spectroscopy (FTIR) spectrometer (FT/IR-6200, JASCO) equipped with a DTGS detector and using KBr pellets containing 1.5% (w/w) of sample. Spectra were recorded in the 4000–600 cm^{-1} range at 4 cm^{-1} resolution and accumulating 50 scans.

Solid state ^{13}C MAS–NMR proton decoupling single-pulse spectra of polymers were obtained with a Bruker Avance DRX-400 spectrometer using a magnetic field of 9.36 T and equipped with a multinuclear probe. Minced samples were packed in 4 mm Ø zirconia rotors and spun at 10 KHz. The spectra were acquired at a frequency of 100.61 MHz, using a π/6 pulse width of 2.5 μs and a pulse space of 10 s to ensure full relaxation and to allow quantitative analysis from peak areas. The chemical shifts are reported in ppm referenced to tetramethylsilane.

Differential scanning calorimetry thermograms were acquired with a DSC Q20 (TA Instruments) from −60 to 150°C under dry nitrogen flow (50 mL/min) at 10°C/min. Accurately weighed small pieces (about 3.5–4 mg) were cut from the films and stabilized at 55% RH in a glove box for 5 days. After stabilization, samples were packed in hermetic aluminum pans inside the glove box and a pin hole was made immediately before running the DSC experiment. Samples were first cooled to −60°C and then a heating–cooling–heating cycle was performed. The glass transition temperature (T_g) is obtained from the second heating using the inflection method.

Water uptake was calculated from the desorption peak in the first heating. With values well below 1% (w/w), this method was found to be more accurate than weighing.

X-ray diffraction (XRD) patterns were obtained at the CITIUS X-ray laboratory (University of Seville, Spain) using a Bruker D8 Advance instrument equipped with a Cu K$_α$ radiation source operating at 40 kV and 30 mA. XRD patterns were obtained in the 3–70° 2θ-range with a step size of 0.015° and a time step of 0.1° 2θ/min.

Thermal stability of polyesters was monitored with a SDT Q600 TGA/DSC analyzer (TA Instruments). Samples (about 6 mg) were heated from RT to 500°C at 5°C/min under N$_2$ flow (100 mL/min).

Tensile measurements were done with a MTS Criterion 42 machine equipped with a 10-N load cell. Rectangular uniform pieces (7 mm × 20 mm) and typically 300–350 μm thick were brought to rupture at a constant deformation rate of 0.2 mm/min at room environmental conditions. Stress values were calculated using the specimen cross-section under no applied load and the Young's modulus from the initial slope of the stress–strain curves. Experiments were repeated at least five times and values averaged.

Insoluble fraction was calculated considering the weight loss of minced samples (about 200 mg) placed inside a glass micro-fiber extraction thimbles and immersed in dimethyl sulfoxide (DMSO) at 90°C for 16 h under continuous magnetic stirring.

Gel-permeation chromatography (GPC) measurements were carried out on an Agilent 1260 Infinity quaternary LC system using two PLGel 5-μm MIXED-C columns at 25°C and a refractive index detector. Tetrahydrofuran (THF) was used as eluent at 1 mL/min flow rate. The system was calibrated with Agilent EasyVial PS standards. Due to the very low solubility of most of these polyhydroxyesters in THF, only consistent results can be obtained for poly HPA and poly HSA.

Results

Chemical Analysis of Polyhydroxyesters Obtained by Non-Catalyzed Melt Polycondensation in Air

In every case, ester formation is clearly stated from the carbonyl ^{13}C MAS–NMR peak around 174 ppm (Garbow and Stark, 1990; Zlotnik-Mazori and Stark, 1998; Ahmed et al., 2003; Pandey et al., 2010; Arrieta-Baez et al., 2011; Liu et al., 2011) (**Figure 2**) and the characteristic FTIR ν(C=O) around 1730 cm^{-1} and ν(OC–O–C) bands at 1240 and 1170 cm^{-1} (Bellamy, 1975) (**Figure 3**).

A detailed analysis of obtained polyesters is given below:

Poly HPA

In poly HPA (**Figure 2**), single ^{13}C MAS–NMR peaks at 174.0 ppm (–COO–CH_2–) and 65.3 ppm (–COO–CH_2–) reveal a very high esterification degree. This is confirmed by a very weak contribution of free acid at 9 ppm in the corresponding ^{1}H MAS–NMR spectrum (not shown). A residual non-reacted hydroxyl population can also be detected from the weak signal at 61.8 ppm (HO–CH_2–). On the other side, the quantitative analysis of the ^{13}C MAS–NMR data shows an excess of carbonyls and a deficiency of singly bonded (C–O) when compared to the nominal composition of the polyester (**Table 1**). This is the result of the partial oxidation of hydroxyl groups to ketones and –COOH species as presumed from a weak MAS–NMR signal at 43.4 ppm (–CH_2–COR) and confirmed from ^{13}C NMR in solution (Figure S1 in Supplementary Material). Such oxidation by-products are not observed in samples prepared under reduced pressure. ^{13}C NMR data also detect the absence of etherification and dehydration reactions in both preparation conditions.

FTIR data, (**Figure 3**), confirm the formation of the polyester by the characteristic peaks at 1732 and 1169 cm^{-1} (Liu et al., 2011)

FIGURE 2 | Solid state ^{13}C MAS-NMR spectra of polyesters. For clarity, the intensity of the 50–200 ppm region is multiplied by a factor of 3.
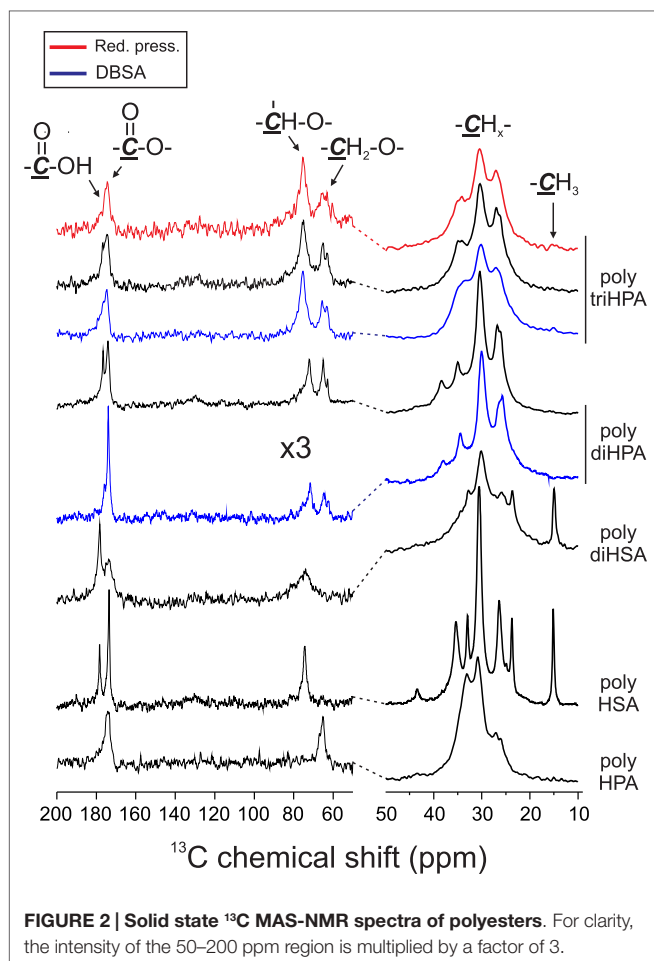
and the low intensity of hydroxyls (3600–3200 cm^{-1} band). The broad shoulder around 1715 cm^{-1} is assigned to carbonyls in a loosely packed polyester phase as well as to ester groups interacting with residual hydroxyls and to loosely associated carboxyls (Heredia-Guerrero et al., 2014). Additionally, a weak absorption at 1775 cm^{-1} is assigned to peroxyester (R–CO–O–O–R′) species (Davison, 1951) as an oxidation by-product.

When prepared under reduced pressure (red trace in **Figure 3**), the FTIR spectrum reveals a reduction of peroxy species due to the weaker exposure to oxygen.

Poly HSA

The esterification of the secondary hydroxyls is characterized by ^{13}C MAS–NMR peaks at 173.5 (–COO–CH<) and 74.4 ppm (–COO–CH<) (**Figure 2**). The presence of free acid (^{13}C 178.3 ppm and ^{1}H ~9 ppm) is notorious, and there is little indication of free hydroxyl groups (no appreciable contribution on the higher chemical shift side of the 74.4 ppm peak (–CH$_2$–CHOH–CH$_2$–) and no aliphatic signal at 38 ppm (–CH$_2$–CHOH–CH$_2$–). Based on the quantification of ^{13}C MAS–NMR spectra (**Table 1**), there is a clear deficiency of (C–O) and an excess of (C=O) species. These data reveal that secondary hydroxyl oxidation is noticeable. Indeed, the intermediate ketone is clearly detected by the 43.5 ppm ^{13}C MAS–NMR peak (–CH$_2$–CO–CH$_2$–) in the solid

and by the corresponding 211.9 ppm signal (–CH$_2$–CO-CH$_2$–) after dissolving in CDCl$_3$ (not shown).

In the FTIR spectrum, both the ester bands (1731, 1246 and 1175 cm^{-1}) and the low concentration of free hydroxyls are confirmed (**Figure 3**). The high concentration of free acid is characterized by the broadening on the lower wavenumber side (~1700 cm^{-1}) of the carbonyl stretching and by the definition of the peak at 1712 cm^{-1} (ester carbonyl perturbed by –COOH). As in poly HPA, a small amount of per-oxidation is evidenced by the weak band around 1775 cm^{-1}.

Gel-permeation chromatography results are consistent with the low polymerization degree of poly HSA and reveal the presence of oligomers containing few monomeric units ($n = 1–5$) (**Table 2**). However, esterification degree of hydroxyls is as high as in poly HPA (**Table 1**). The combination of both results, i.e., low M_w and high percentage of esterified hydroxyls suggest intra-esterification and the formation of cyclic oligomeric structures in poly HSA.

Poly diHSA

^{13}C MAS–NMR spectrum of poly diHSA (**Figure 2**) displays broad ester (173.6 ppm) and (C–O) peaks, which is interpreted as a variety of chemical configurations. Thus, vicinal –OH groups may remain free (~76 ppm) or esterify (one, doublet at 74 and 81 ppm; both, single peak at 76 ppm) and consequently no reliable quantitative chemical information can be directly extracted. However, the most relevant findings are the strong presence of free acid (sharp peak at 178.3 ppm, about 52% of carbonyls) and the intense reduction of (C–O) bonds (**Table 1**). As in the previous case, this is the consequence of hydroxyl oxidation to carboxylic acid.

FTIR data (**Figure 3**) support NMR information and detect the ester formation (bands at 1731, 1236 and 1166 cm^{-1}) and the reduced population of free hydroxyl groups (weak broad bands around 3500 and 3250 cm^{-1}). The broadening of the carbonyl stretching and the development of 1708 and 1690 cm^{-1} components are the consequence of the more heterogeneous chemical environment of carbonyl groups and the perturbation exerted by the considerable population of free acid.

Poly diHPA

Poly diHPA is the only polyester of the series that has been prepared from a hydroxyacid extract mostly composed of 10,16 dihydroxypalmitic acid but containing other acids and hydroxyacids from the C$_{18}$ and C$_{16}$ families. For that reason, data in **Table 1** are referenced to the monomeric mixture composition. Poly diHPA is slightly deficient in (C–O) and enriched in carbonyl groups, which suggests that hydroxyls are partially oxidized to acid.

The ^{13}C MAS–NMR spectrum (**Figure 2**) evidences the ester formation (174.1 ppm) and the presence (~15%) of free acid (^{13}C 176 ppm and ^{1}H 9.6 ppm). The (C–O) signal reveals that most of primary hydroxyls are esterified (Saam, 1998; Deshmukh et al., 2003, 2005) (65.1 ppm,–COO–CH$_2$–) and only about 11% of them remain as non-reacted (62.9 ppm, –CH$_2$OH). On the other side, the 72.2 ppm peak (–CH$_2$–CHOH–CH$_2$–) indicates that secondary hydroxyls are mostly intact. Indeed, by comparing the total amount of ester carbonyls and the esterified primary
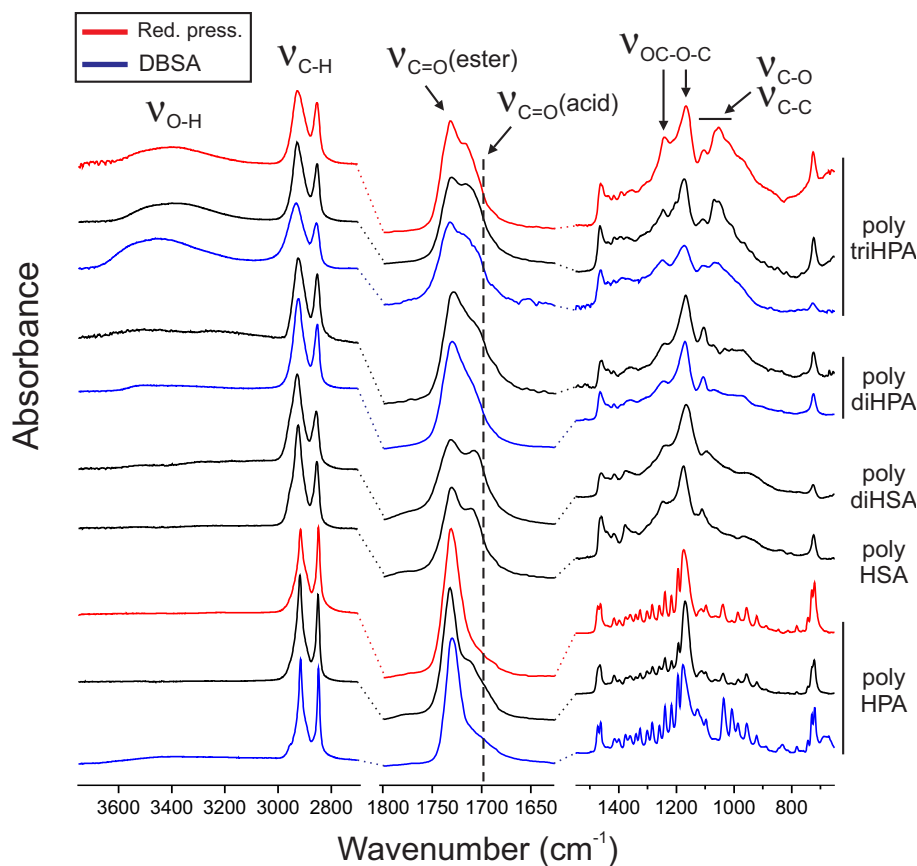
FIGURE 3 | FTIR spectra of polyhydroxyesters.

TABLE 1 | Chemical composition from ^{13}C MAS–NMR.

Monomer	Primary OH (%)		Secondary OH (%)		(C–O) ratio	(C=O) ratio	COOH (%)
	Free	Esterified	Free	Esterified			
Poly HPA	4	96	–	–	0.88	1.13	4
Poly HPA (red. press.)	0	100	–	–	1.01	1.02	0
Poly HSA	–	–	6	94	0.74	1.22	22
Poly diHSA	–	–	24	76	0.58	1.82	52
Poly diHPA (DBSA)	22	78	77	23	0.88	0.94	5
Poly diHPA	11	89	82	18	0.91	1.12	15
Poly triHPA (DBSA)	29	71	82	18	0.96	1.05	0
Poly triHPA	14	86	89	11	0.90	1.12	7
Poly triHPA (red. press.)	8	92	94	6	0.92	1.02	0

hydroxyls and by quantifying the aliphatic peak at 38.4 ppm ($-CH_2-CHOH-CH_2-$), we have calculated that only about 18% of secondary hydroxyls have reacted.

As in previous cases, FTIR confirms the formation of the ester by the characteristic (C=O) and (C–O–C) stretchings (**Figure 3**). It also detects the presence of non-reacted hydroxyl groups (broad bands around 3500 and 3250 cm^{-1}). The carbonyl peak (1729 cm^{-1}) is accompanied by a shoulder at 1712 cm^{-1} that gathers the contribution of both –COOH and –OH groups hydrogen bonding ester carbonyls.

Poly triHPA

Poly triHPA is obtained from the most hydroxylated acid (aleuritic acid) of the series and the ^{13}C MAS–NMR is displayed in **Figure 2**. The dominant ester peak (174.6 ppm) is accompanied by a free acid fraction ($-CH_2-COOH$, 176.7 ppm and $-CH_2-COOH$, 34.9 ppm) that it is estimated in about 7%. Esterification is mainly with primary hydroxyls (65.3 ppm) leaving a non-reacted (63.1 ppm) population of about 14%. Most of secondary hydroxyls (75.2 ppm) are preserved though a small peak ~84 ppm can be considered as the result of mono esterification of the vicinal diol

TABLE 2 | Physical parameters of polyhydroxyesters obtained.

Polymer	Young's Modulus (MPa)	UTS (MPa)	Elongation at break (%)	T_g (°C)	T_m (°C)	ΔH_m (J/g)	Water uptake (% w/w)[a]	δT_g (°C)	Insoluble fraction (% w/w)	M_w (g/mol)
Poly HPA (DBSA)	(n.m.)	(n.m.)	(n.m.)	−18	88	107	(n.m.)	(n.m.)	33	*
Poly HPA	123 ± 15	6.3 ± 0.4	11 ± 2	−20	86	95	(n.m.)	(n.m.)	89	59500
Poly HPA (red. press.)	196 ± 28	9 ± 2	6 ± 2	(n.m.)	94	134	(n.m.)	(n.m.)	96	(p.s.)
Poly HSA	(n.m.)	(n.m.)	(n.m.)	−44	−20	6	0.08	0.5	17	1400
Poly diHSA	1.5 ± 0.2	0.3 ± 0.1	18 ± 3	−19	–	–	0.30	3.8	76	(i)
Poly diHPA (DBSA)	(n.m.)	(n.m.)	(n.m.)	−7	–	–	0.14	0.9	86	(i)
Poly diHPA	4.5 ± 0.4	0.8 ± 0.1	24 ± 4	−13	–	–	0.25	3.0	92	(i)
Poly triHPA (DBSA)	17 ± 3	2.0 ± 0.5	33 ± 4	−8	–	–	1.00	8.7	67	(i)
Poly triHPA	4.1 ± 1.3	0.9 ± 0.3	33 ± 7	−6	–	–	0.62	5.0	94	(i)
Poly triHPA (red. press.)	6.9 ± 1.6	2.0 ± 0.6	25 ± 6	−5	–	–	0.68	6.5	88	(i)

[a]RH = 55%, (i) insoluble in THF, (p.s.) partially soluble in THF, (n.m.) cannot be measured, (–) does not exist, (*) not measured.

moiety. From the area of this peak, and the difference between the ester carbonyls and esterified primary hydroxyls, the fraction of esterified secondary –OH groups is calculated to be ~11%. As the others polyesters of the series, poly triHPA is enriched in (C = O) and deficient in (C–O) suggesting a small hydroxyl oxidation.

Fourier transform infrared spectroscopy (**Figure 3**) reveals the excess of non-reacted hydrogen bonded hydroxyls with broad $\nu_{(O-H)}$ bands at 3465 and 3375 cm^{-1}. Such hydroxyl surplus is also perturbing the carbonyl vibration causing a broad peak at 1717 cm^{-1} accompanying the ester vibration at 1731 cm^{-1}. In addition to the (C–O–C) stretching in ester group at 1173 cm^{-1}, there is a doublet (1069 and 1053 cm^{-1}) that we assign to the (C–O) stretching of vicinal secondary hydroxyls.

As a reference for the non-catalyzed polycondensation in air, the reaction has been performed under reduced pressure (25 mbar). The polyester obtained after 12 h (**Figures 2** and **3**, red traces) is chemically quite similar to the one prepared in air. ^{13}C MAS–NMR displays an ester peak at 174.4 ppm with some broadening at higher chemical shift but no evidence of free acid is detected. The lack of free acid is also confirmed from the absence of the aliphatic signal ~35 ppm (–CH_2–COOH) and the narrowing on the low wavenumber side of the carbonyl stretching. Most of primary (92%) and about 6% of secondary hydroxyls are esterified and the (C–O)/(C=O) signal ratio suggests no hydroxyl oxidation. The (C–O) ratio <1 is likely due to a very mild dehydration favored by pumping. The higher esterification degree is supported by both the weakening of both the hydroxyl band around 3400 cm^{-1} and the shoulder at 1717 cm^{-1}.

Chemical Analysis of Polyhydroxyesters Obtained by DBSA Promoted Polycondensation

As reference for the non-catalyzed process, the polycondensation reaction has also been performed in the presence of a hydrophilic acidic agent such as DBSA (dodecylbenzenesulfonic acid). The analysis is basically restricted to diHPA and triHPA because their potential technical interest considering the abundance of their natural sources.

DBSA Poly diHPA
^{13}C MAS–NMR spectrum of DBSA poly diHPA (**Figure 2**, blue trace) shows a very sharp peak of ester carbonyl at 174.0 ppm

with little contribution (~5%) of free acid (175.8 ppm). As in the non-catalyzed bulk polycondensation homologous, esterification is mostly with primary hydroxyls (64.7 ppm) leaving about 22% of non-reacted groups (62.6 ppm). Esterification with secondary hydroxyls is slightly more extended (23%) using DBSA, as deduced from the broadening of the 75.5 ppm peak at higher chemical shift. It is also visible when comparing the intensities of the 34.5 and 38.1 ppm corresponding to the aliphatic carbon in –CH_2–CHO(R)–CH_2– and –CH_2–CHOH–CH_2–, respectively (**Figure 2**). Though there is a small loss of (C–O) bonds upon formation of the polyester, this is not accompanied by an increment of (C=O). Consequently, the elimination of hydroxyls is not considered to be caused by oxidation but to the migration of the hydroxyl rich species of the monomeric mixture toward the solvent.

When compared to poly diHPA, FTIR of DBSA poly diHPA (**Figure 3**) shows a sharper carbonyl stretching region with an ester peak at 1733 cm^{-1} and a weaker shoulder at 1713 cm^{-1}. This is caused by a more reduced population of free acid groups perturbing the carbonyl vibration.

DBSA Poly triHPA
DBSA poly triHPA is characterized as an ester by the ^{13}C MAS–NMR signal at 174.7 ppm (**Figure 2**, blue trace). Compared to non-catalyzed poly triHPA, the carbonyl signal is broader on the higher chemical shift side but displays no distinctive peak of free acid. Such broadening is due to hydrogen bonding with hydroxyls, which are characterized by the IR band at 3450 cm^{-1} (**Figure 3**). Another indication of such hydrogen bonded phase is the shoulder around 1715 cm^{-1}. As in poly triHPA, esterification of primary hydroxyls is preferential (71%) while only 18% of secondary have reacted.

The Structure of Polyhydroxyesters
IR data, i.e., the low frequency and width of the (–CH_2–) stretching peaks (2917 and 2850 cm^{-1}), the splitting of the scissoring (1469 and 1465 cm^{-1}) and rocking (729 and 721 cm^{-1}) modes and the presence of progression bands in the 1400–1200 cm^{-1} (Stein and Sutherland, 1954; Casal et al., 1982) reveal that only poly HPA is crystalline. This is confirmed by
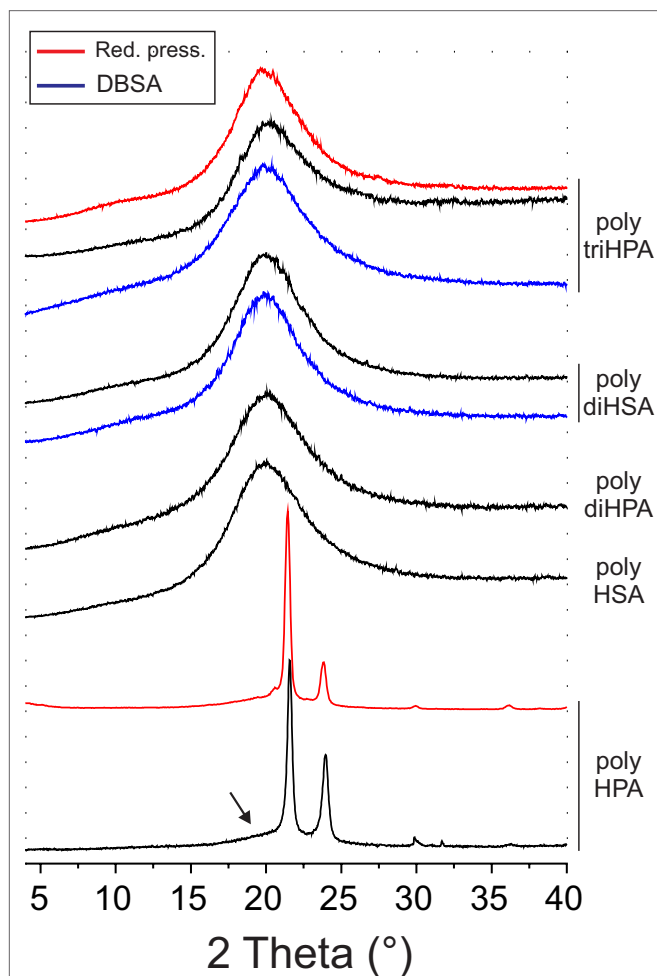
FIGURE 4 | XRD diagrams of polyesters. The broad peak around 20° is typical for amorphous solids. The arrow highlights the formation of an amorphous phase in poly-HPA prepared in air.

XRD (**Figure 4**) and DSC (**Figure 5**). Melting temperature (T_m) and enthalpy (ΔH_m) values (**Table 2**) are in good agreement with results reported for poly ω-hydroxyltetradecanoic acid (Liu et al., 2011).

The rest of the members of the series are amorphous at room temperature (Davison and Corish, 1955; Snyder et al., 1996) and DSC thermograms display clear vitreous transitions with T_g values generally increasing with the hydroxylation degree of the monomer (**Table 2**).

Mechanical Properties

Uniaxial tensile parameters of free-standing films obtained are compiled in **Table 2**. Within the series, crystalline poly HPA is the stiffest and displays a brittle fracture at quite low strain. If compared to values reported for the analogous poly ω-hydroxyl tetradecanoic acid (Liu et al., 2011), it can be deduced that this behavior is likely caused by a low molecular weight polymerization and by partial amorphization, as indicated by the broad peak around 20° in **Figure 4**. In this sense, self-polycondensation of

HPA under reduced pressure is more efficient and yields a higher molecular weight polyester.

The rest of polyesters prepared are amorphous and have quite low Young's modulus and rupture stress values, as well as moderate (20–30%) elongation at break. They can be defined as viscoelastic materials showing no strain softening or plastic flow regions. Among these polyhydroxyesters, poly triHPA (DBSA) displays the highest tensile parameters, particularly the Young's modulus. The self-polycondensation of aleuritic acid has been studied in detail in a previous work (Benítez et al., 2014) and it was found that tensile parameters experienced a sudden modification when achieving full esterification. Curiously, poly triHPA (DBSA) values do fit within this gap and we conclude that polycondensation in the organic medium was not completed in the experimental conditions used.

Water Uptake

Hydrophobicity is a desirable feature in barrier polymers to prevent, among others, mechanical modifications by swelling, chemical degradation, and material lixiviation. In this series of polyhydroxyacids, the nominal hydroxyl to acid ratio is equal or above 1 and, therefore, the excess of hydroxyl groups is expected to act as water absorbent sites. To comparatively estimate hydrophobicity, water uptake of films has been evaluated by DSC. *In situ* sample drying shows two events on the thermogram: the desorption peak around 70–80°C and the T_g shift (δT_g) (**Figure 5**). Both parameters increase with the monomer hydroxylation degree (**Table 2**). Their good correlation with the normalized area of the FTIR hydrogen bonded hydroxyls (inset in **Figure 5**, for instance) clearly states that surplus hydroxyls are the origin of polyhydroxyesters surface affinity for water.

Thermal Stability

The thermal stability of a polymer is a very important feature conditioning its potential applications. Moreover, TGA experiments of these polyesters under inert atmosphere were found to be structure sensitive (**Figure 6**). Thus, TGA patterns of reference monomers (primary HPA and secondary HSA) show two decomposition stages (dashed lines). The low temperature peak (240–250°C) is common and it is mostly associated to the dehydration and decarboxylation processes of the hydroxyacids. Its absence in the polyester series is consistent with spectroscopic data indicating high esterification degrees. On the other side, the second decomposition stage is specific for each type of monohydroxyacid: ~335°C for secondary and ~410°C for primary.

In poly HPA, poly HSA, and poly diHSA it is observed that the thermogravimetric patterns mostly depend on the type of monomer hydroxylation (primary or secondary). Thus, polyesters from exclusively secondary functionalized monomers (poly HSA and poly diHSA) are thermally decomposed at lower temperature (335–350°C) than the one obtained from an exclusively primary hydroxylated precursor (poly HPA) (410°C). The fact that the TGA profile of the polyhydroxyesters overlaps with those of the corresponding monomers, indicates that the primary thermal degradation mechanism in the polymers is the scission of the
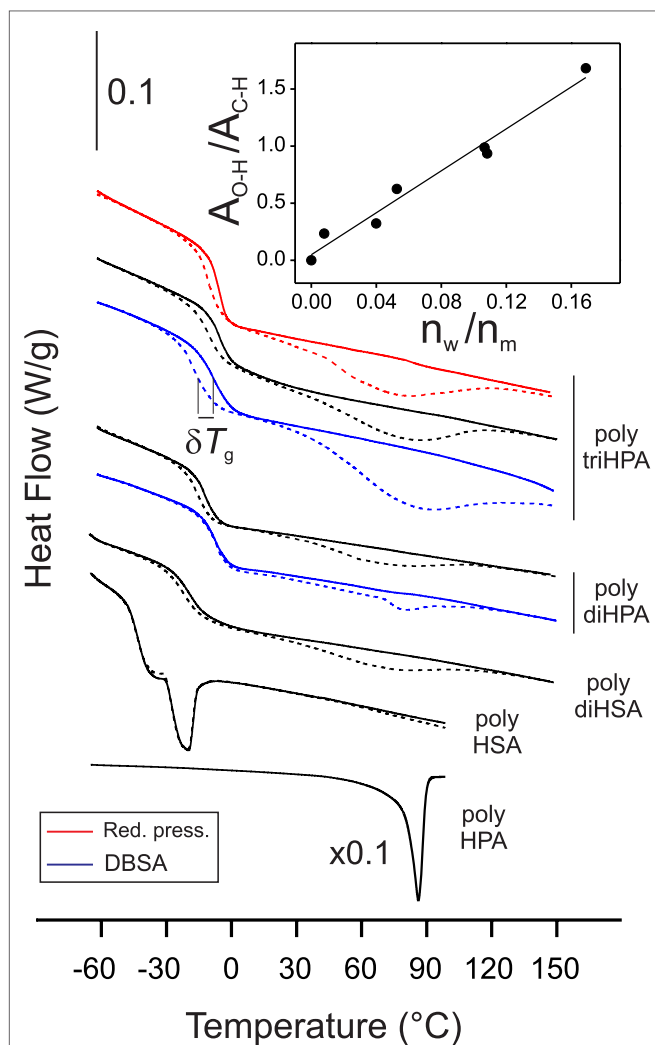
FIGURE 5 | DSC thermograms of polyesters under N_2 flow. Dashed lines correspond to samples stabilized at 55% RH and display the desorption of water around 80°C. Solid lines correspond to *in situ* dried samples. The inset in the upper right corner shows the correlation between the FTIR ν(O–H)/ν(C–H) band area ratio and the amount of adsorbed water (n_w) calculated from DSC and referred to the monomer content (n_m) (mol/mol).

FIGURE 6 | (up) TGA and (bottom) derivative curves of polyesters under N_2 flow.

Discussion

Experimental results have shown that free-standing polyesters films of C_{16} and C_{18} polyhydroxyacids can be prepared by non-catalyzed melt-polycondensation in air. In general, esterification degrees were quite high, particularly when the monomer contains a primary hydroxyl. However, the formation of minor amounts oxidation and dehydration by-products is associated to this preparation procedure. On the other side, the resolution of the ^{13}C MAS–NMR spectra, as well as the overlapping with the (C–O) region, prevents a reliable detection of ether formation. The absence of ether species was only confirmed in poly HPA prepared in air and under reduced pressure (Figure S1 in Supplementary Material).

Consistency of films obtained by non-catalyzed melt-polycondensation in air is found to depend on the type of hydroxylation of the monomer. Thus, products from those containing only secondary hydroxyls are very soft (poly diHSA) or even resinous (poly HSA). On the contrary, films obtained from the ω-hydroxyacid (poly HPA) are crystalline and, mechanically, the most robust within the series. Such a difference is likely due to the balance between inter and intra-estererifiction reactions, leading to the formation of low M_w cyclic structures from exclusively secondary hydroxylated monomers. Thus, free-standing polyesters are better prepared from long-chain hydroxyacids containing primary hydroxyls.

When primary and secondary hydroxyls coexist, experimental data have shown that the formation of the primary ester is

ester bond into an olefin and a carboxylic acid, followed by their subsequent decomposition (Goldfarb and McGuchan, 1968; Sutton and Tighe, 1973).

In polyhydroxyesters containing both primary and secondary hydroxyls (poly diHPA and poly triHPA), the decomposition peak is mostly displaced toward the high temperature side indicating that esterification with primary hydroxyls is preferential, as already pointed by ^{13}C MAS–NMR.

Poly triHPA (DBSA) is a particular case within the series and shows considerable decomposition starting at 200°C. Since there are no spectroscopic evidences of a significant acid phase responsible for such thermal lability, we consider the possibility of an impurity arising from the DBSA method catalyzing the scission reaction.
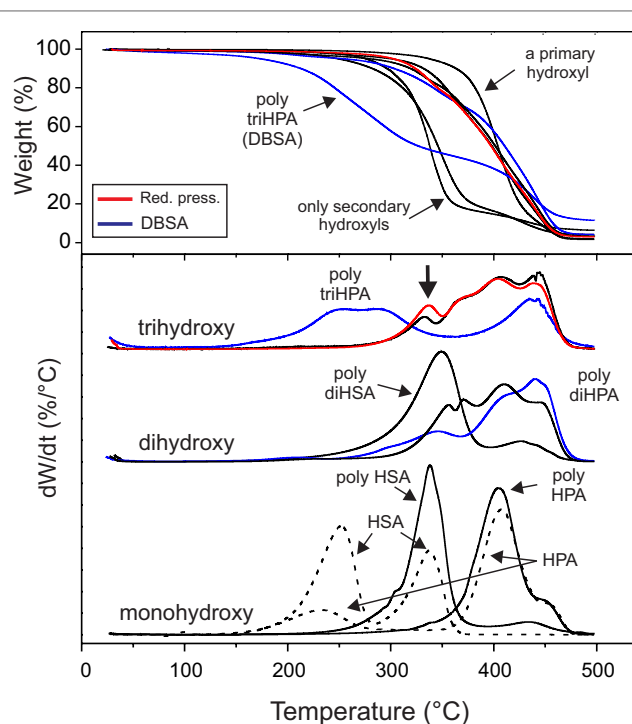
preferential. Consequently, their structure can be described as mostly linear with some degree of branching depending on the extent of the esterification with secondary –OH (**Figure 7**). However, and despite no cross-linking between chains is possible because of the AB (–COOH/–OH) stoichiometry, they are found to be quite insoluble thermosets.

Chemically, polyhydroxyesters obtained by non-catalyzed melt-polycondensation in air are generally deficient in (C–O) bonds and enriched in (C = O) linkages in the form of acid and/or ester. This is the result of hydroxyl oxidation to carbonyl species, which is more intense for secondary hydroxyls, particularly in vicinal configuration, where an oxidative diol cleavage reaction is feasible:

$$R - CH(OH) - (OH)HC - R' + 3/2\,O_2$$
$$\rightarrow R - COOH + HOOC - R' + H_2O \tag{1}$$
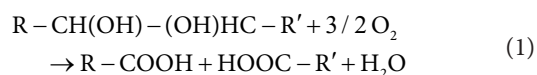
Newly formed carboxylic groups may undergo further esterification with available hydroxyls creating two ester bonds per broken C–C. One of the fragments is a dicarboxylic acid and it is susceptible of generating cross-linking between polymeric chains (**Figure 7**). This mechanism would explain, for instance, the better consistency of poly diHSA vs. poly HSA as well as its higher insoluble fraction (**Table 2**).

The same oxidative diol cleavage reaction can also be proposed for poly triHPA. However, the experimental (C=O/C–O) ratio

FIGURE 7 | Scheme representing chain propagation, branching, and cross-linking in the structure of a polyhydroxyester resulting from monomers bearing a primary and a secondary hydroxyl (poly diHPA, blue) and one primary and two vicinal secondary hydroxyls (poly triHPA, blue plus green). In this later case, the oxidative vicinal diol cleavage reaction is shown as an inset.

indicates that the oxidation is not as intense as in poly diHSA. The main difference between both monomers is the presence of a primary hydroxyl in the 9,10,16-trihydroxypalmitic acid and we have already confirmed the higher reactivity of primary hydroxyls. Consequently, we propose that the preferential esterification of primary hydroxyls progressively gives rise to a viscous polyester phase that impedes oxygen diffusion to the bulk and reduces the extent of the oxidative diol cleavage in poly triHPA when compared to poly diHSA. The association of cross-linking with the extent of the oxidative diol cleavage and further esterificacion in poly triHPA would explain the increment of the insoluble fraction values in the sense air > reduced pressure > DBSA assisted, as contact with oxygen is reduced.

Poly diHPA is by far the most interesting polyhydroxyester among the series. It has been obtained from a monomeric mixture extracted from tomato cuticles and may represent a stock of about 35,000 t considering only the dry wastes of tomato processing in Europe. The monomeric mixture is mostly composed of positional isomers of the ω-dihydroxyhexadecanoic acid, being the 10,16 the most abundant (Holloway and Deas, 1971). In this molecule, the oxidative cleavage is not possible because of the lack of vicinal diols. However, as biopolyester cutin, synthetic poly diHPA is infusible and quite insoluble, pointing to a cross-linked structure. Our hypothesis is that other minor components are responsible for such properties. The esterification of secondary hydroxyls of different polymeric chains with dioic acids is considered here as the source of cross-linking. Such dioic acid have been detected in the monomeric mixture (~2.5%) (del Río and Hatcher, 1998) or can also be *in situ* generated by the oxidative cleavage of the small amounts of 9,10,16-trihydroxyhexadecanoic and 9,10,18-trihydroxyoctadecanoic acids (~1.4%). Another option is a partial oxidation of the significant amount of the ω-hydroxyacid (~9.3%) to the dioic acid as observed for poly HPA.

Conclusion

Polycondensation of molten fatty polyhydroxyacids (C_{16}–C_{18}) in the absence of a catalyst is proven to yield generally amorphous, infusible and insoluble free-standing polyester films. The process is relatively slow, as conditioned by the effective elimination of generated water molecules. Esterification is observed to be preferential with primary hydroxyls and, therefore, their structure can be described as linear with variable branching, depending on the extent of the secondary hydroxyl esterification. When conducted in air, partial oxidation of hydroxyl groups takes place, but, despite the harsh preparation conditions used, the oxidation extent is found to be limited by the diminishment of the oxygen diffusion within the viscous bulk as the polyhydroxyester phase is being formed. Hydroxyl oxidation and acid formation is observed to be more intense for secondary groups, particularly, in vicinal diol configuration. Esterification of newly formed dicarboxylic acids with surplus secondary hydroxyls leads to chain cross-linking, which in turn is positive to obtain insoluble, infusible and thermally stable polyhydroxyester films or coatings.

The synthesis of a cutin inspired polyhydroxyester (poly diHPA) is of particular interest since it represents the valorization
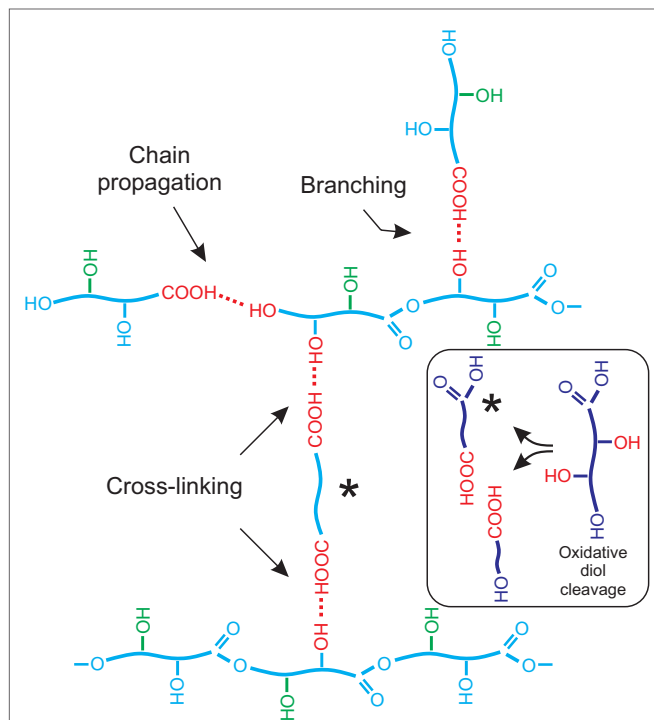
of the abundant waste coming from the processing of large scale production fruits like tomato.

Supplementary Material

The Supplementary Material for this article can be found online at http://journal.frontiersin.org/article/10.3389/fmats.2015.00059

References

Ahmed, A., Crawford, T., Gould, S., Ha, Y. S., Hollrah, M., Noor-E-Ain, F., et al. (2003). Synthesis of R- and (S)-10,16-dihydroxyhexadecanoic acid: cutin stereochemistry and fungal activation. *Phytochemistry* 63, 47–52. doi:10.1016/S0031-9422(03)00003-7

Arrieta-Baez, D., Cruz-Carrillo, M., Gómez-Patiño, M. B., and Zepeda-Vallejo, L. G. (2011). Derivatives of 10,16-dihydroxyhexadecanoic acid isolated from tomato (solanum lycopersicum) as potential material for aliphatic polyesters. *Molecules* 16, 4923–4936. doi:10.3390/molecules16064923

Baker, E. A., and Holloway, P. J. (1970). Constituent acids of angiosperm cutins. *Phytochemistry* 9, 1557–1562. doi:10.1016/S0031-9422(00)85275-9

Bawn, C. E. H., and Huglin, M. B. (1962). The kinetics of the polycondensation of 12-hydroxystearic acid. *Polymer* 3, 257–262. doi:10.1016/0032-3861(62)90086-1

Bellamy, L. J. (1975). *The Infrared Spectra of Complex Molecules*. New York: John Wiley and Sons.

Benítez, J. J., Heredia-Guerrero, J. A., Guzmán-Puyol, S., Domínguez, E., and Heredia, A. (2014). Polyester films obtained by noncatalyzed melt-condensation polymerization of aleuritic (9,10,16 trihydroxyhexadecanoic) acid in air. *J. Appl. Polym. Sci.* 132, 1060–1066. doi:10.1002/APP.41328

Casal, H. L., Mantsch, H. H., Cameron, D. G., and Snyder, R. G. (1982). Interchain vibrational coupling in phase II (hexagonal) n-alkanes. *J. Chem. Phys.* 77, 2825–2830. doi:10.1063/1.444173

Davison, W. H. T. (1951). Infra-red absorption of the carbonyl group. Part I. Diacyl peroxides, per-esters and per-acids. *J. Chem. Soc.* 2456–2461. doi:10.1039/jr9510002456

Davison, W. H. T., and Corish, P. J. (1955). Infrared spectra and crystallinity. 1. Polyesters. *J. Chem. Soc.* 2428–2431. doi:10.1039/jr9550002428

del Río, J. C., and Hatcher, P. G. (1998). Analysis of aliphatic biopolymers using thermochemolysis with tetramethylammonium hydroxide (TMAH) and gas chromatography-mass spectrometry. *Org. Geochem.* 29, 1441–1451. doi:10.1016/S0146-6380(98)00070-9

Deshmukh, A. P., Simpson, A. J., Hadad, C. M., and Hatcher, P. G. (2005). Insights into the structure of cutin and cutan from *Agave* americana leaf cuticle using HRMAS NMR spectroscopy. *Org. Geochem.* 36, 1072–1085. doi:10.1016/j.orggeochem.2005.02.005

Deshmukh, A. P., Simpson, A. J., and Hatcher, P. G. (2003). Evidence for cross-linking in tomato cutin using HR-MAS NMR spectroscopy. *Phytochemistry* 64, 1163–1170. doi:10.1016/S0031-9422(03)00505-3

Domínguez, E., Heredia-Guerrero, J. A., and Heredia, A. (2011). The biophysical design of plant cuticles: an overview. *New. Phytol.* 189, 938–949. doi:10.1111/j.1469-8137.2010.03553.x

Garbow, J. R., and Stark, R. E. (1990). Nuclear magnetic resonance relaxation studies of plant polyester dynamics. 1. Cutin from limes. *Macromolecules* 23, 2814–2819. doi:10.1021/ma00212a037

Goldfarb, I. J., and McGuchan, R. (1968). *Thermal Degradation of Polyesters. I. Aliphatic Polymers. Technical Report AFML-TR-68-182, Part I*. Ohio: Air Force Materials Laboratory, Wright-Patterson Air Force Base.

Heredia, A. (2003). Biophysical and biochemical characteristics of cutin, a plant barrier biopolymer. *Biochim. Biophys. Acta.* 1620, 1–7. doi:10.1016/S0304-4165(02)00510-X

Heredia-Guerrero, J. A., Benítez, J. J., Domínguez, E., Bayer, I. S., Cingolani, R., Athanassiou, A., et al. (2014). Infrared and Raman spectroscopic features of plant cuticles: a review. *Front Plant Sci.* 5:1–13. doi:10.3389/fpls.2014.00305

Heredia-Guerrero, J. A., Heredia, A., García-Segura, R., and Benítez, J. J. (2009). Synthesis and characterization of plant cutin mimetic polymer. *Polymer* 50, 5633–5637. doi:10.1016/j.polymer.2009.10.018

Holloway, P. J., and Deas, A. H. B. (1971). Occurrence of positional isomers of dihydroxyhexadecanoic acid in plant cutins and suberins. *Phytochemistry* 10, 2781–2785. doi:10.1016/S0031-9422(00)97279-0

Kolattukudy, P. E. (1981). Structure, biosynthesis and biodegradation of cutin and suberin. *Ann. Rev. Plant Physiol.* 32, 539–567. doi:10.1146/annurev.pp.32.060181.002543

Kosma, D. K., Parsons, E. P., Isaacson, T., Lü, S., Rose, J. K. C., and Jenks, M. A. (2010). Fruit cuticle lipid composition during development in tomato ripening mutants. *Physiol. Plant.* 139, 107–117. doi:10.1111/j.1399-3054.2009.01342.x

Liu, C., Liu, F., Cai, J., Xie, W., Long, T. E., Turner, S. R., et al. (2011). Polymers from fatty acids: poly(ω-hydroxyl tetradecanoic acid) synthesis and physico-mechanical studies. *Biomacromolecules* 12, 3291–3298. doi:10.1021/bm2007554

Luque, P., Bruque, S., and Heredia, A. (1995). Water permeability of isolated cuticular membranes: a structural analysis. *Arch. Biochem. Biophys.* 317, 417–422. doi:10.1006/abbi.1995.1183

NPT-CERHR Monograph on the Potential Human Reproductive and Developmental Effects of Bisphenol A. (2008). Center for the Evaluation of Risks to Human Reproduction, US Department of Health and Human Services, Pub. No. 08-5994.

Pandey, A. K., Nande, S. S., Selukar, B. S., and Garnaik, B. (2010). Synthesis and characterization of novel value added biodegradable poly(aleuritic acid) from renewable resources (shellac) and invertible amphyphilic behaviors in various solvents. *e-Polymers* 131, 1–12. doi:10.1515/epoly.2010.10.1.1476

Pollard, M., Beisson, F., Li, Y. H., and Ohlrogge, J. B. (2008). Building lipid barriers: biosynthesis of cutin and suberin. *Trends Plant Sci.* 13, 236–246. doi:10.1016/j.tplants.2008.03.003

Saam, J. C. (1998). Low-temperature polycondensation of carboxylic acids and carbinols in heterogeneous media. *J. Polym. Sci. A Polym. Chem.* 36, 341–356. doi:10.1002/(SICI)1099-0518(19980130)36:2<341::AID-POLA17>3.3.CO;2-0

Snyder, R. G., Liang, G. L., Strauss, H. J., and Mendelsohn, R. (1996). IR spectroscopy study of the structure and phase behavior of long-chain diacyl-phosphatidylcholines in the gel state. *Biophys. J.* 71, 3186–3198. doi:10.1016/S0006-3495(96)79512-7

Stein, R. S., and Sutherland, G. B. B. M. (1954). Effect of intermolecular interactions between CH frequencies on the infrared spectra of n-paraffins and polythene. *J. Chem. Phys.* 22, 1993–1999. doi:10.1063/1.1739980

Sutton, G. J., and Tighe, B. J. (1973). Poly-α-ester degradation studies. I. Introduction: design and construction of equipment. *J. Polym. Sci. A Polym. Chem.* 11, 1069–1077. doi:10.1002/pol.1973.170110513

Walton, T. J. (1990). Waxes, cutin and suberin. *Methods Plant Biochem.* 4, 105–158.

Zhang, S., Lefebvre, H., Tessier, M., and Fradet, A. (2011). Influence of Brønsted acid ionic liquid structure on hydroxyacid polyesterification. *Green Chem.* 13, 2786–2793. doi:10.1039/c1gc15241f

Zlotnik-Mazori, T., and Stark, R. E. (1998). Nuclear magnetic resonance studies of cutin, and insoluble plant polyester. *Macromolecules* 21, 2412–2417. doi:10.1021/ma00186a019

Polymerization of 10,16-Dihydroxyhexadecanoic Acid, Main Monomer of Tomato Cuticle, Using the Lewis Acidic Ionic Liquid Choline Chloride·2ZnCl₂

*Mayra Beatriz Gómez-Patiño[1,2], Diana Yaremy Gutiérrez-Salgado[3],
Edgar García-Hernández[3], Juan Vicente Mendez-Mendez[1], J. Alberto Andraca Adame[1],
José Campos-Terán[2] and Daniel Arrieta-Baez[1]**

[1] *Instituto Politécnico Nacional, Centro de Nanociencias y Micro y Nanotecnologías, Mexico City, Mexico,* [2] *Departamento de Procesos y Tecnología, DCNI, Universidad Autónoma Metropolitana, Unidad Cuajimalpa, Mexico City, Mexico,*
[3] *Departamento de Ingenierías Química y Bioquímica, Instituto Tecnológico de Zacatepec, Zacatepec de Hidalgo, Mexico*

10,16-Dihydroxyhexadecanoic acid, main monomer of the tomato cuticle obtained from agroresidual wastes, was polymerized using ionic liquid (choline chloride·2ZnCl₂) as catalyst at three different temperatures (80, 90, and 100°C). The resulting polyesters obtained under these conditions were insoluble in most of the organic solvents and showed different physicochemical properties. While at 80°C, polymers were obtained as powder, and at higher temperature, they were found in viscous consistency. According to the cross polarization magic angle spinning nuclear magnetic resonance and Fourier transform infrared spectroscopy attenuated total reflectance analysis, polymers showed a linear structure with an increasing degree of esterification in position C-10. Polyesters were analyzed by means of differential scanning calorimetry, atomic force microscopy, and X-ray diffraction (small- and wide-angle scattering) techniques.

Keywords: ionic liquids, long-chain aliphatic polyesters, tomato, 10,16-DHPA, choline chloride·2ZnCl₂

INTRODUCTION

Biodegradable polymers belong to one of the most attractive biomaterials because of their wide applications in biomedical fields. Most of the research on renewable and biodegradable materials based on polyesters has been concentrated on polylactide (PLA), polyglycolide (PGA), and their copolymer poly(lactide-*co*-glycolide) (PLGA), which are the most commonly used and extensively studied biodegradable polymers because of their good biocompatibility, low immunogenicity, and satisfactory mechanical properties (Albertsson and Varma, 2002; Chen and Wu, 2005; Nair and Laurencin, 2007; Philip et al., 2007). Although the application-relevant property profile of any polymeric material depends on numerous properties, one significant disadvantage of these aliphatic polyesters is their lower melting points (Yamamoto et al., 2002). Apart from the very short-chain aliphatic polyesters, melting points of polyesters based on common aliphatic monomers are too low for thermoplastic processing. Linear polyesters do not have strong interacting groups, so, the predominant factor affecting melting temperature is the number of conformations available in the

molten state, in other words chain flexibility. Higher flexibility leads to higher entropy of melting and lower melting temperature. For example, Tm of poly(alkylene adipates)s is different for poly(alkylene terephthalate)s, an aliphatic and aromatic polyesters (Tm 50 and 265°C, respectively). It has been demonstrated that the presence of functionalizable groups, such as hydroxyl and carboxylate, in polyesters can efficiently increase their hydrophilicity and degradability, plus modulate their mechanical, thermal, chemical, and biological properties (Lecomte et al., 2006; Parrish and Emrick, 2006; Williams, 2007). Within the new group of degradable polymers, various types of aliphatic polyesters films have been described (Bayer et al., 2004; Benitez et al., 2004; Olsson et al., 2007; Heredia-Guerrero et al., 2009; Quinzler and Mecking, 2010; Stempfle et al., 2014; Benítez et al., 2015). Between them, successful polycondensation reactions have been achieved using titanium alkoxides as catalyst to afford the corresponding long-chain aliphatic polyesters (Quinzler and Mecking, 2010; Stempfle et al., 2014).

Even when long-chain polyhydroxyesters (C16–C20) are present in nature in the form of the plant biopolymer cutin, its monomeric complexity makes difficult to get and use it as natural polyester for commercial source of "green" chemicals (Olsson et al., 2007).

We were able to isolate the main monomer of the tomato cutin, the 10,16-dihydroxyhexadecanoic acid (10,16-DHPA), from agroresidual wastes (Arrieta-Baez et al., 2011). These residuals represent approximately 20% of the crop losses and are a good source of this aliphatic long-chain acid, which could be used to get other monomers. 10,16-DHPA was successfully polymerized with *Candida antarctica* lipase-B (CAL-B) to get polyesters with Mw = 814 and Mn = 1,206 Da (Gómez-Patiño et al., 2013). The most prominent synthetic aliphatic polyesters are usually prepared by enzymatic ring-opening polymerization (ROP) of the respective cyclic monomers. This method provides sufficient polymerization control, resulting in polymers of the required molar masses and with the desired end groups. However, it has been very difficult to prepare aliphatic long-chain polyesters by direct polycondensation because of their thermal degradation at high temperature and low hydrolytic stability in one step (Akinori et al., 2003).

Most of the polymerization reactions are carried out in organic solvents of which some eventually end up polluting environment by evaporation or leakage. Recently, there have been intense research efforts to replace conventional organic solvents with novel solvent systems, which are recyclable and environmentally compatible and therefore reduce waste and hazard. Ionic liquids (ILs; Seddon, 1997; Welton, 1999) and other non-conventional solvent systems, such as choline chloride/oxalic acids (Abbott et al., 2004) and ZnCl$_2$, have drawn attention to the synthetic organic and polymer chemists worldwide, since they offer a potentially clean method to carry out chemical reactions or processes. They are non-volatile, while liquids over a wide range of temperatures, and offer benign alternatives to traditional organic solvents.

However, it is still a challenging subject to seek for other excellent catalysts in order to achieve in one-step synthesis long-chain aliphatic polyesters under milder conditions (lower temperature and short time). Polycondensations under mild conditions are very important from an environmental technology view point (Shu et al., 1994; Quinzler and Mecking, 2010; Stempfle et al., 2014).

The present work describes the synthesis of aliphatic polyesters from 10,16-hydroxyhexadecanoic acid obtained from agroresidual tomato wastes using an IL, such as choline chloride·2ZnCl$_2$, as a potent catalyst in the synthetic method for the synthesis of long-chain wax esters. These aliphatic polyesters obtained at different temperatures and times showed particular physicochemical characteristics. Although it has been reported that enzymatic lipase-mediated reactions give soluble oligomeric products (Gómez-Patiño et al., 2013), reactions with choline chloride yield insoluble polymers that were characterized by cross polarization magic angle spinning nuclear magnetic resonance (CPMAS ^{13}C NMR), Fourier transform infrared spectroscopy (FT-IR), and differential scanning calorimetry (DCS).

MATERIALS AND METHODS

Materials

Choline chloride, zinc chloride·toluene, hexane, dimethylformamide (DMF), and 2-methyl-2-butanol (2M2B) of reagent grade were purchased from Merck (Naucalpan de Juarez, Edo. de Mexico, Mexico) and used without further purification.

Isolation of 10,16-Dihydroxyhexadecanoic Acid (10,16-DHPA 1)

10,16-DHPA (1) was obtained by depolymerization of tomato cutin as described elsewhere (Osman et al., 1995, 1999). Identification of the monomer was done by nuclear magnetic resonance (NMR) spectrometry and mass spectrometry (MS) analysis, and the data were compared with those previously reported (Ahmed et al., 2003; Quinzler and Mecking, 2010).

10,16-DHPA (1). Yellow pale powder. ^{1}H-NMR (500 MHz, CH$_3$OD) δ ppm 3.63 (m, 4H) C(OH)H-10 and C(OH)H$_2$-16, 2.27 (t, J = 7.52 Hz, 2H) CH$_2$-2, 1.60–1.22 (m) CH$_2$-3-9 and CH$_2$-11-15. ^{13}C-NMR (CH$_3$OD) δ 177.68 (CO); 72.40 (C-10); 63.00 (C-16). EI-MS (m/z): 289 [M + H]$^{+}$, 271 [M-H$_2$O]$^{+}$, 253 [M-2H$_2$O]$^{+}$, 130 [C$_8$H$_{18}$O$_2$-OH]$^{+}$ (Quinzler and Mecking, 2010).

Preparation of Choline Chloride·2ZnCl$_2$

Choline chloride (20 mmol) was mixed with zinc chloride (40 mmol) and heated to 150°C with stirring until a clear colorless liquid was obtained (Sunitha et al., 2007).

General Procedure for Polyesterification Reaction

Polyesterification reactions were carried out under low vacuum reflux with two-necked round-bottom flask equipped with a magnetic stirrer, thermometer and fitted with a Dean Stark adapter and a condenser for reflux. These reactions were carried out at three different temperatures (80, 90, and 100°C) with different reaction times (2, 4, 6, 12, and 24 h) using IL, choline chloride·2ZnCl$_2$ as a catalyst. IL catalyst was used at molar ratio 1:1 to the reactant. Polymers were precipitated with cold methanol, extracted, and characterized by NMR, FT-IR, and DSC.

Methods

NMR Spectroscopy

Soluble products were characterized by ^{1}H- and ^{13}C-NMR (Varian NMR System, 500 MHz; Palo Alto, CA, USA). The NMR spectra were recorded in deuterated chloroform (CDCl$_3$) or methanol (CH$_3$OD).

Insoluble polymers were analyzed using standard CPMAS ^{13}C NMR experiments carried out on a Varian Instruments Unityplus 300 widebore spectrometer (Palo Alto, CA, USA) equipped for solid-state NMR. The resonance frequency was 74.443 MHz, with a customary acquisition time of 30 ms, a delay time of 2 s between successive acquisitions, and a cross polarization (CP) contact time of 1.5 ms. Typically, each 30-mg sample was packed into a 5-mm rotor and supersonic magical angle spinning (MAS) probe from Doty Scientific (Columbia, SC, USA), then spun at 6.00 (0.1 kHz and room temperature for approximately 10 h. No spinning side-bands were observed up- or downfield from the major carbonyl or aliphatic carbon peaks. The resulting data were processed with 50 Hz of exponential line broadening.

ATR FT-IR Spectroscopy

Attenuated total reflectance ATR) FT-IR spectra were recorded with a BOMEM 157 FTIR spectrometer equipped with a deuterated triglycine sulfate (DTGS) detector. The instrument was under continuous dry air purge to eliminate atmospheric water vapor. The spectra were recorded in the region of 4000–400 cm^{-1}.

AFM Analysis

The atomic force microscopy (AFM) image was obtained fixing the samples on a metallic disk with double face tape, using a MultiMode AFM V (Bruker, Santa Barbara, CA, USA) in air with a RTESP cantilever, the size of each image was $5 \times 5\,\mu m^2$ in taping mode. The roughness parameters Rq and Ra were determined using the expressions $Rq = \sqrt{\sum Z_1^2/N}$ and $Ra = 1/N \sum_{j=1}^{N} |Z_j|$, where Rq is the root mean square average of the height deviations, Ra is the arithmetic average of the absolute values of the surface height deviations, Z is the height value, and N is the number of the number of the data, these parameters were obtain using the nanoscope analysis image Software.

X-Ray Diffraction (Small- and Wide-Angle Scattering) Study

The X-ray patterns were measured from 1.5° to 30°. It is possible to do SAXS and WAXS in a single run [small- and wide-angle scattering (SWAXS)] with the equipment used. X Pert PRO MRD Diffractometer from PANalytical in Bragg-Brentano geometry was used with Cu radiation (K$\alpha = 1.54\,\text{Å}$) at 45 kV and 40 mA tube power. The step size was 0.03 and 500 s for each step. X-ray mirror with 1/32 divergence slit and Soller slit (0.04 rad) were used in incident optic for parallel beam and measurements in small angle. PIXcel ultrafast X-ray detector for diffracted optic was used.

DSC Analyses

Differential scanning calorimetry was performed with a TA Instrument 2010 Modulated DSC (New Castle, DE, USA). Sample of about 10 mg was encapsulated in aluminum pan and heated from 30 to 220°C at a heating rate of 5°C min^{-1} under 50 mL min^{-1} nitrogen purge.

RESULTS AND DISCUSSION

Polymerization Reaction

Polyesters (**Scheme 1**) derived from 10,16-DHPA (1) were synthesized via IL, using choline chloride·2ZnCl$_2$ as a catalyst. When compared with enzymatic reactions as previously reported (Gómez-Patiño et al., 2013), the obtained polyesters were completely different, they were waxes, with ILs were powders and materials with viscous consistence.

After reaction, polyesters were precipitated with methanol and separated from the IL. Subsequently, they were washed with water, methanol, and chloroform and dried to characterize them by NMR, FT-IR, and DSC techniques. The IL was subject to an extraction with ethyl acetate to recover the unreacted monomer and after that was heated at 150°C to evaporate remained solvents. After this, the IL was used at least four times without any significant loss of activity. The synthesis data are shown in **Table 1**.

Polyesters obtained were insoluble in chloroform, methanol, water, DMSO, and DMF, which made them difficult to analyze by means of MS in order to get their molecular weight.
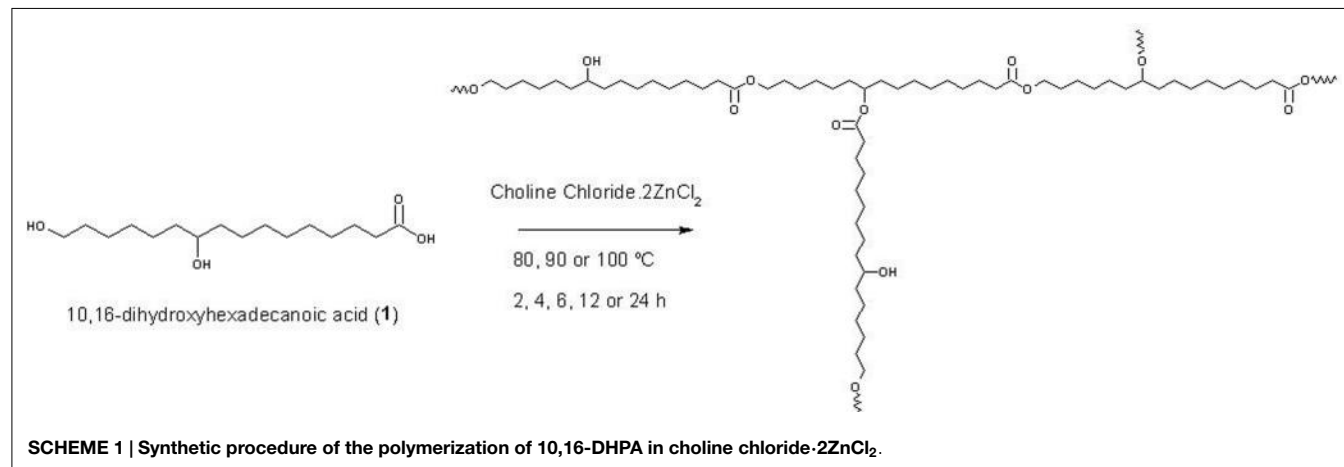

SCHEME 1 | Synthetic procedure of the polymerization of 10,16-DHPA in choline chloride·2ZnCl$_2$.

TABLE 1 | The result of synthesis of 10,16-DHPA under different temperatures at different times in choline chloride·2ZnCl2.

Entry	Temperature (°C)	Time (h)	Isolated yield (%)
1	80	2	95.6
2	80	4	90
3	80	6	78.75
4	80	12	65.6
5	80	24	45.6
6	90	2	78.1
7	90	4	80
8	90	6	63.75
9	90	12	48.1
10	90	24	40
11	100	2	68.75
12	100	4	63.1
13	100	6	41.2
14	100	12	35.6
15	100	24	29.3

Characterization of the Polymers

Polymers obtained from IL, choline chloride·2ZnCl$_2$, at different temperatures and different times showed different physical characteristics (**Figure 1**). Polymers obtained in reactions at 80°C were mainly powder; those obtained at 90°C were solid whiles those obtained at 100°C were essentially viscous, completely different from those obtained from enzymatic reactions, which were like waxes (Gómez-Patiño et al., 2013). However, all of them were insoluble in most of the solvents.

ATR-FT-IR Spectroscopy

We have found that polyesters obtained from enzymatic reactions are mainly linear (Gómez-Patiño et al., 2013). Polyesters obtained from CAL-B with 10,16-DHPA (Mw = 982 and Mn = 860 Da) showed a band at 3365 cm^{-1} attributed to the presence of residual OH and an intense band at 1738 cm^{-1} attributed to C = O stretching in ester groups, and the asymmetric stretching vibration of the C–CO–O at 1172 cm^{-1} which confirm the presence of a linear polyester group (Gómez-Patiño et al., 2013). For the polymers obtained in choline chloride·2ZnCl$_2$, the IR spectra (**Figures 2A,B**) spectra are very similar, and the majority of the bands correspond to an ester functional group stated by the νC = O around 1735 cm^{-1} and the (OC–O–C) stretching at 1177 and 1247 cm^{-1} (Quinzler and Mecking, 2010; Gómez-Patiño et al., 2013) and the weak contribution of the free acid IR peak around 1700 cm^{-1}, that was not present, confirm that polymers are mainly linear. At longer reaction time (24 h), there is a reduction in the intensities of these signals, which maybe due to the polyesterifications with the secondary OH.

CPMAS ^{13}C NMR Analysis

To further characterize the polyesters, solid-state CPMAS ^{13}C NMR spectra have been acquired (**Figure 3**). The main carbonyl peak at 174.2 ppm evidences the formation of the corresponding esters. The ester peak should be accompanied by a decreasing component of free –COOH groups at −177 ppm. However, we could not see the presence of this peak, which indicates the complete consumption of the monomer. As we can see in **Figures 1–3**, a single peak at 174.2 ppm was observed in the reaction at 80°C.

FIGURE 1 | Purified polymers obtained from the reaction of 10,16-DHPA in choline chloride·2ZnCl$_2$.

This is in agreement for a linear polymer such as those obtained with enzymatic reactions (Gómez-Patiño et al., 2013) and in agreement with the FT-IR analysis. However, from reaction at 90°C (**Figures 2** and **3**), a peak at 172 ppm showed up and this signal increased in reaction at 100°C (**Figure 3**). This could be due to the esterification with the secondary OH's at position 10.

According to our previous NMR analysis of polyesters obtained from enzymatic reactions, the signals for esterified carbons of primary –OH are at ≈63–64 ppm and carbons of secondary −OH are at ≈72–74 ppm (Gómez-Patiño et al., 2013). The analysis in the C–O region shows that most of the primary hydroxyls are esterified (intense peak at 65.0 ppm, –CH$_2$–CO–O–CH$_2$– versus the weak contribution at 63 ppm, HO–CH$_2$–). Consequently, the esterification of secondary hydroxyls has to be a minority because of the COOH/OH imbalance in the monomer mixtures. The peak at 75.0 ppm (**Figures 2** and **3**) is then probably due to free secondary hydroxyl groups, and the weak signals around 73 and 72 ppm reveal the minor formation of esters in this position. This confirms that most of the polymers have a linear structure.

AFM Analysis

The topography of bulk polymers was analyzed by AFM. The roughness study showed that polyesters obtained at 90°C (24 h) has the highest values with an Rq 200 nm and an Ra 159 nm, while those obtained at 100°C (24 h) showed values of Rq 196 nm and Ra 157 nm, which resulted very similar. However, the polyester obtained at 80°C (24 h) presented the lowest roughness with an Rq 146 nm and an Ra 113 nm. The roughness analysis did not show a clear difference between the analyzed polyesters.

However, the AFM amplitude error images showed clear differences. In **Figure 4B**, agglomerates of particles sizing about 100 nm can be observed, while in **Figure 4D,** it is possible to observe also the agglomeration of particles and some well-defined islands with sizes about 150 nm, and finally in **Figure 4F,** an amorphous structure conformation is clearly observed and individual particles were not found.

The image analysis may suggest that reactions at 80°C could produce polymeric chains with different molecular weights that could have partial conformation and crystallinity. Most of this sample looks amorphous (**Figure 4B**). The increasing polyesterification could lead to the presence of isolated particles in
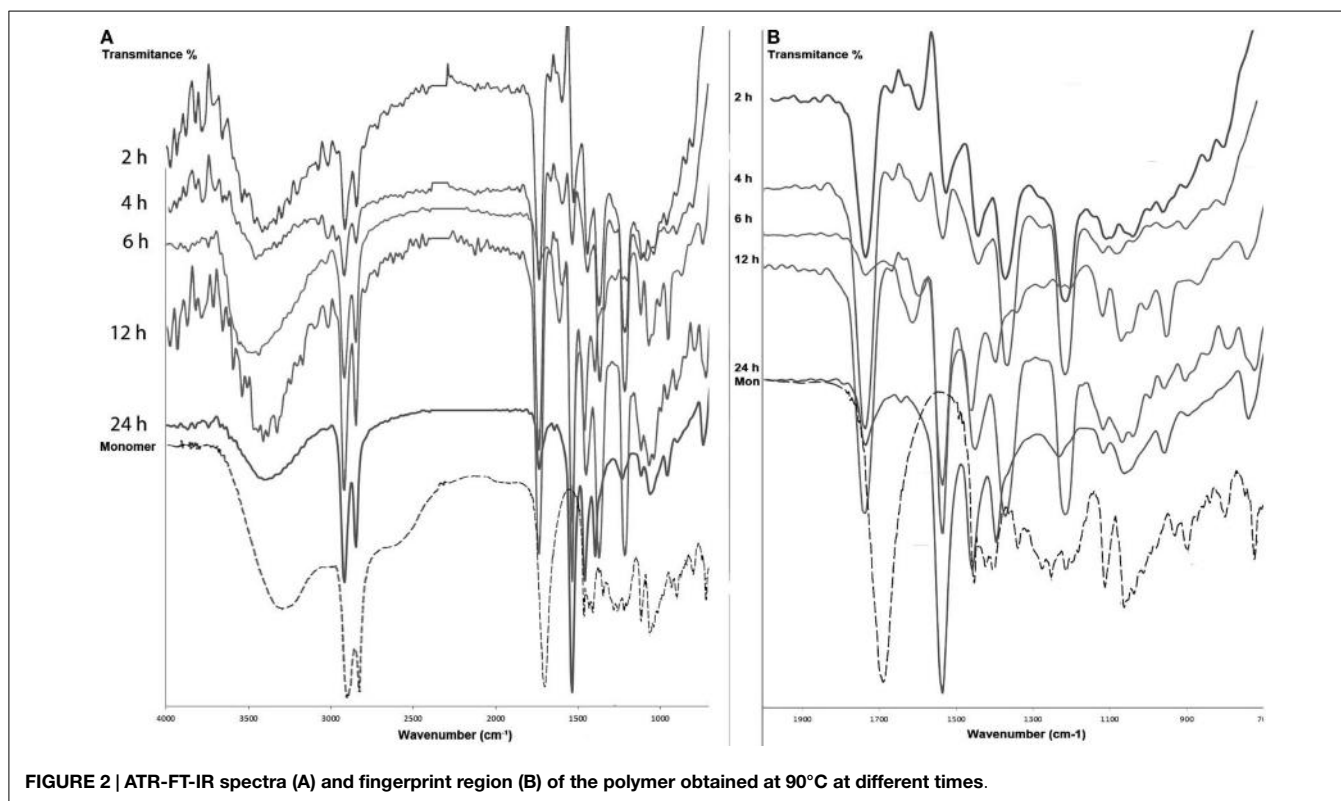
FIGURE 2 | ATR-FT-IR spectra (A) and fingerprint region (B) of the polymer obtained at 90°C at different times.
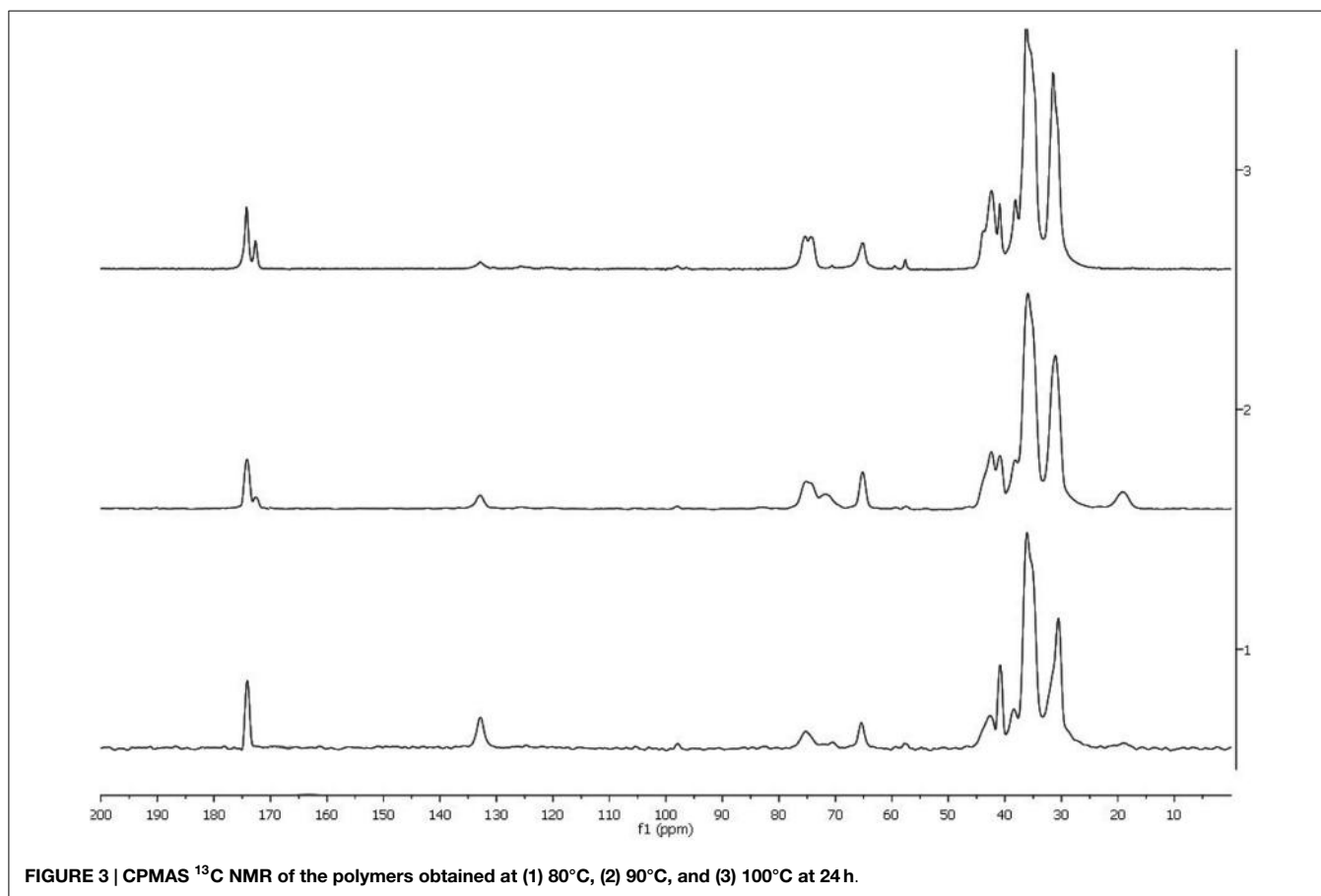

FIGURE 3 | CPMAS ^{13}C NMR of the polymers obtained at (1) 80°C, (2) 90°C, and (3) 100°C at 24 h.
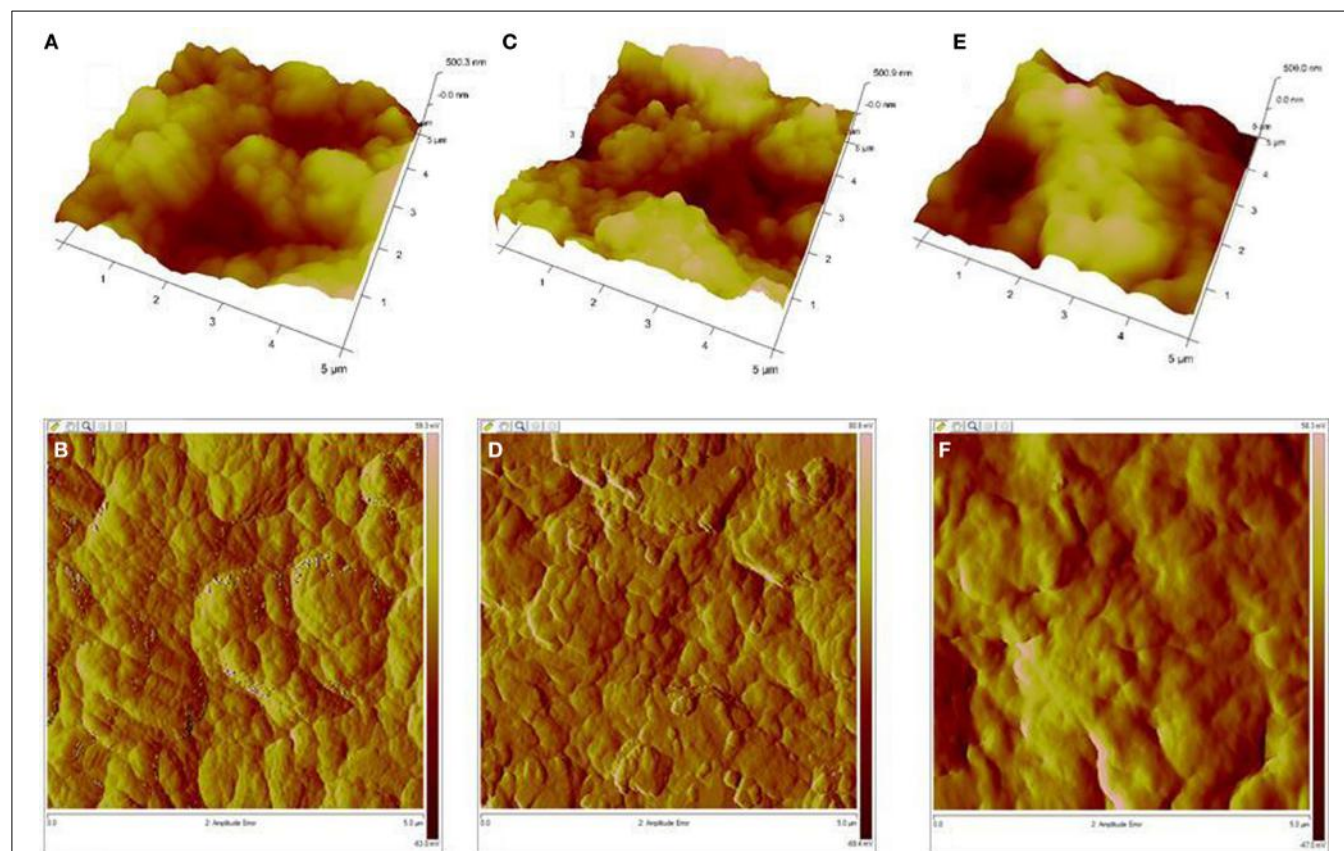
FIGURE 4 | Topographical images obtained using an atomic force microscope from polyesters of 10,16-dihydroxyhexadecanoic acid at (A) 80°C, (B) 90°C, and (C) 100°C and their amplitude error images (B,D,F).

Figure 4D (90°C), and finally the topography shown in **Figure 4F** (100°C) may be related to the higher degree of polyesterification at this temperature.

X-Ray Diffraction Analysis (Small- and Wide-Angle Scattering)

The X-ray patterns from the polyester obtained from 10,16-dihydroxyhexadecanoic at 80, 90, and 100°C at 12 and 24 h were measured with small- and wide-angle X-ray scattering (SWAXS) in a conventional diffractometer with adequate optics as explained in Section "Methods." The results were surprising since the polyesters looks like the crystalline structure of the potassium palmitate ($C_{16}H_{31}KO_2$) with PDF # 00-007-0730 (black lines in **Figure 5**). Unfortunately, there are no polymer data to correlate the X-ray patterns with this kind of polyesters, and we are working with the analysis of different long-chain polyesters to understand this behavior. However, semicrystallinity has been reported in polyesters with long-chain hydrocarbon segments derived of oleic and erucic acid (Stempfle et al., 2014).

Figure 5 shows the X-ray patterns from polyesters obtained at 80, 90, and 100°C for 12 h of reaction. There is a small glide for the peak in the position 4.0 for sample at 80°C to 4.3 for sample at 90°C and back to 4.15 for sample at 100°C. The effect is due to changes in the interplanar distance at 2.207, 2.053, and 2.127 nm, respectively. Also, it can be observed that the peak at 6.11 moves

to 6.66° and the peak at 8.1 changes to 8.71° in the samples at 80 and 100°C, respectively, with both contributions in the sample at 90°C. This observation indicates that the interplanar distance of the polyesters change from 14.48 to 13.51 nm and from 10.9 to 10.1 nm with the change in reaction temperature of 80–100°C, respectively, according to Bragg's law. However, both structures with the same parameters are present in the polymer obtained at 90°C. Another displacement is observed with the peak at 18.4° that changes when temperature increases. However, it disappears in the polyester obtained at 100°C.

Figure 6 shows the X-ray patterns from polyesters obtained at 80, 90, and 100°C for 24 h of reaction. The changes observed in the peaks are similar to those seen in the samples obtained at 12 h for the different temperatures. The best crystalline structure is observed in the sample at 90°C for 24 h. In this case, the peaks are more defined and they have more intensity. More comprehensive studies are underway to understand and explain the changes in the structure of these new polymers.

Thermal Properties of Polymers

DSC analysis was essential to analyze the polymerization homogeneity in the reactions at different times. While reactions obtained in the first hours and lower temperatures showed more than two endothermic transitions, reactions at longer times and higher temperatures showed only one, indicating that polymers
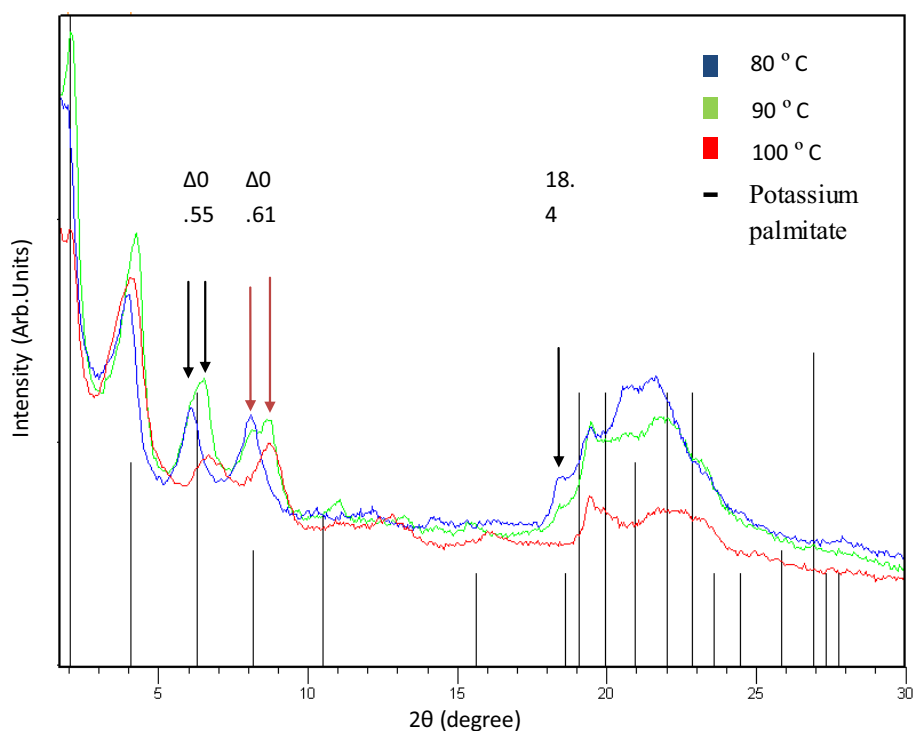
FIGURE 5 | X-ray patterns from polyesters obtained at 80, 90, and 100°C with 12 h of reaction (Cu Kα = 1.54 Å). Black lines correspond to potassium palmitate (C16H31KO2) PDF # 00-007-0730 crystalline structure.
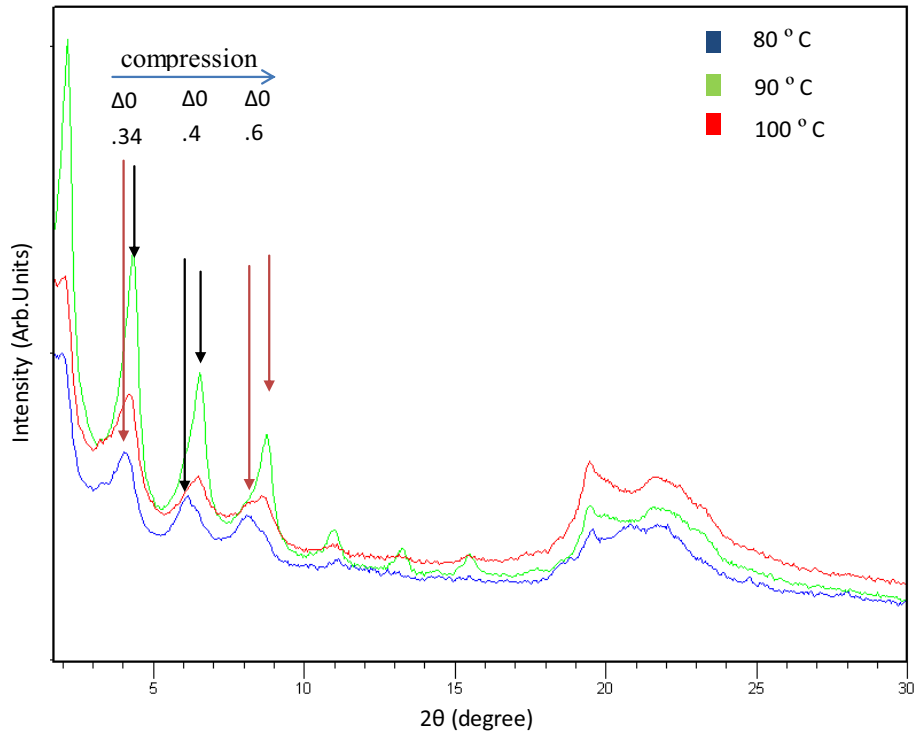

FIGURE 6 | X-ray patterns from polyesters obtained at 80, 90, and 100°C with 24 h of reaction (Cu Kα = 1.54 Å).
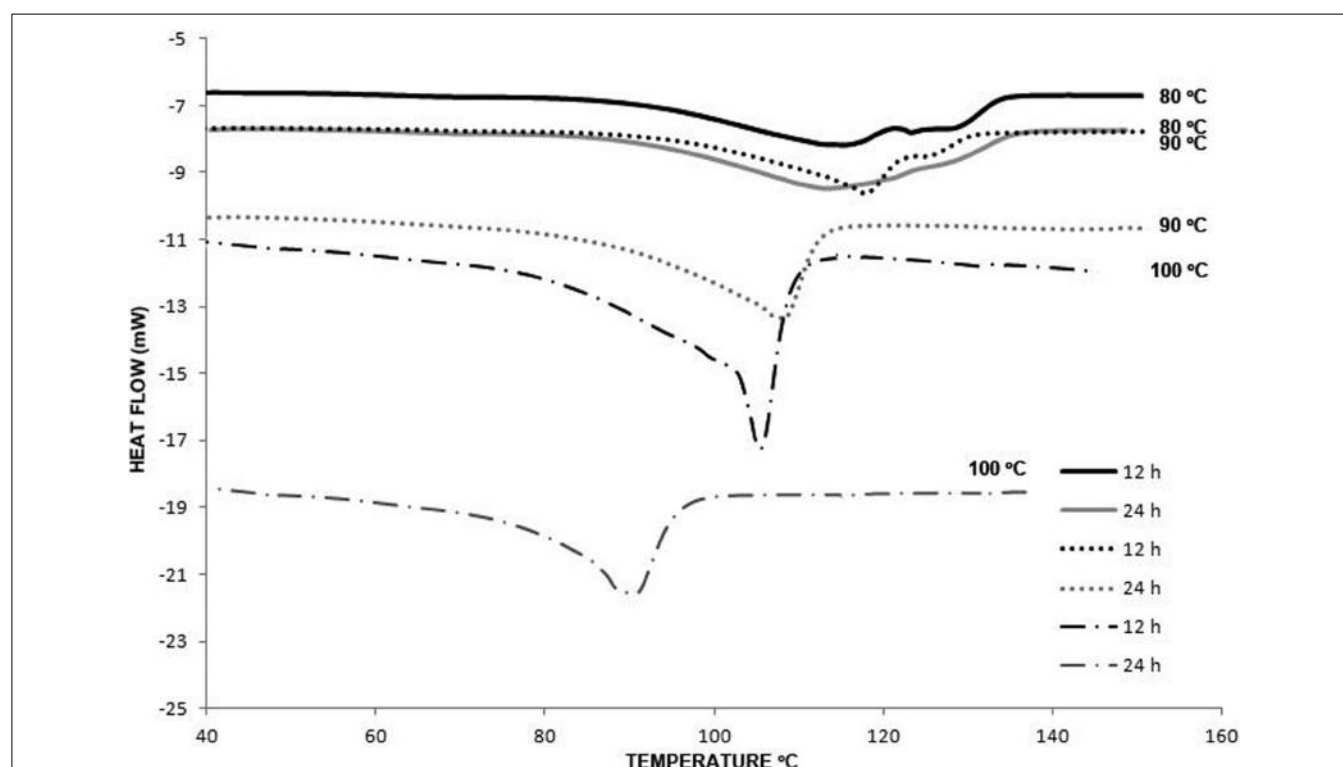
FIGURE 7 | DSC thermograms of the polyesters obtained at 80, 90, and 100°C at 12 and 24 h. Endothermal transitions (Tm) are detected in the polymers (see text for description).

obtained at these times (12 and 24 h) could have more homogenous physicochemical characteristics. The DSC thermograms of polymers obtained at 80, 90, and 100°C at 12 and 24 h of reaction are shown in **Figure 7**. For the polymers at 12 h of reaction at 80 and 90°C, two endothermic transitions (Tm) can be observed at around 115 and 122°C. Meanwhile for the same reaction time but at 100°C, only one endothermic transition is observed at 105°C. At longer reaction times, 24 h, only one endothermic transition at 109 and 90°C was detected for reaction temperatures of 90 and 100°C, respectively. For the case of the polymers obtained at 80°C for 24 h, two endothermic transitions are still observed at almost the same temperature that the ones observed at 12 h of reaction.

The fact that two endothermic transitions are observed after 12 h of reaction could be attributed to high-molecular-weight dispersion, due to the presence of different chain sizes (larger short-range ordered domains), since it has been described that in polymerization by polycondensation reactions, the chain length is not completely controlled (Okada, 2002; Albertsson and Srivastava, 2008; You et al., 2010). Also SWAXS results demonstrated that all the polymers showed crystallinity that could explain the relatively high temperature of the transitions observed. Above these temperatures, the vibrational energy of the polymer chain is sufficient to overcome secondary bonds between the chains and allow for translational chain motion.

In this sense, the sample obtained at 90°C for 24 h is the one with the highest crystalline structure since the peak and the temperature of transition at its thermogram are the most defined, in agreement with what is observed in SWAXS.

One interesting observation is that the transition temperatures for the samples at 90 and 100°C for 24 h reaction are reduced compared with the ones obtained after 12 h. A possible explanation could be that some polymers present branching that reduces the percentage of crystallinity. In this case, the transition temperatures decrease since the molecules are less densely packed and therefore cannot form Van der Waals interactions or hydrogen bonds as easily.

CONCLUSION

We have used the IL, choline chloride·2ZnCl₂, to polymerize efficiently the main monomer of tomato cuticle. The 10,16-DHPA was obtained from tomato residual wastes and used to produce polymers at different times and temperatures. According to the FT-IR and CPMAS ^{13}C NMR analysis, the reaction produces polymers that are mainly linear. The best experimental conditions to get these polymers were 90°C at 24 h and 100°C at 12 h. However, at longer times and higher temperatures, polymers show branched structures with esterification in the −OH-10. The high polymerization and the branching present in the polymers could be the reason for the insolubility observed in different solvents. The use of choline chloride·2ZnCl₂ in the polymerization of 10,16-DHPA could be more efficient than those common process used to esterify long-chain fatty acids, like the DCC/DMAP reaction. Beside, it is cheap, very easy to prepare, and can be reused for at least six cycles without any pretreatment or significant loss of activity. Polymers obtained from these reactions have potential use for a wide range of biomedical applications.

ACKNOWLEDGMENTS

REFERENCES

Abbott, A. P., Boothby, D., Capper, G., Davies, D. L., and Rasheed, R. K. (2004). Deep eutectic solvents formed between choline chloride and carboxylic acids: versatile alternatives to ionic liquids. *JACS* 126, 9142. doi:10.1021/ja048266j

Ahmed, A., Crawford, T., Gould, S., Ha, Y. S., Hollrah, M., Noor-E-Ain, F., et al. (2003). Synthesis of (R)- and (S)-10,16-dihydroxyhexadecanoic acid: cutin stereochemistry and fungal activation. *Phytochemistry* 63, 47–52. doi:10.1016/S0031-9422(03)00003-7

Akinori, T., Yoshika, O., Yoshitaka, I., Yoshihito, I., and Tadamichi, H. (2003). Synthesis of aliphatic polyesters by direct polyesterification of dicarboxylic acids with diols under mild conditions catalyzed by reusable rare-earth triflate. *Macromolecules* 36, 1772–1774. doi:10.1021/ma021462v

Albertsson, A. C., and Varma, I. K. (2002). "Aliphatic polyesters: synthesis, properties and applications" in *Degradable Aliphatic Polyesters*, ed. A. C. Albertsson (Berlin: Springer-Verlag), 1–40.

Albertsson, A. Ch, and Srivastava, K. R. (2008). Recent developments in enzyme-catalyzed ring-opening polymerization. *Adv. Drug Deliv. Rev.* 60, 1077–1093. doi:10.1016/j.addr.2008.02.007

Arrieta-Baez, D., Cruz-Carrillo, M., Gómez-Patiño, M. B., and Zepeda-Vallejo, L. G. (2011). Derivatives of 10,16-dihydroxyhexadecanoic acid isolated from tomato (*Solanum lycopersicum*) as potential material for aliphatic polyesters. *Molecules* 16, 4923–4936. doi:10.3390/molecules16064923

Bayer, I. S., Guzman-Puyol, S., Heredia-Guerrero, J. A., Ceseracciu, L., Pignatelli, F., Ruffilli, R., et al. (2004). Direct transformation of edible vegetable waste into bioplastics. *Macromolecules* 47, 5135–5143. doi:10.1021/ma5008557

Benitez, J. J., García-Segura, R., and Heredia, A. (2004). Plant biopolyester cutin: a tough way to its chemical synthesis. *Biochim. Biophys. Acta* 1674, 1–3. doi:10.1016/j.bbagen.2004.06.012

Benítez, J. J., Heredia-Guerrero, J. A., Guzmán-Puyol, S., Domínguez, E., and Heredia, A. (2015). Long-chain polyhydroxyesters from natural occurring aleuritic acid as potential material for food packaging. *Soft Mater.* 13, 5–11. doi:10.1080/1539445X.2014.993476

Chen, G. Q., and Wu, Q. (2005). The application of polyhydroxyalkanoates as tissue engineering materials. *Biomaterials* 26, 6565–6578. doi:10.1016/j.biomaterials.2005.04.036

Gómez-Patiño, M. B., Cassani, J., Jaramillo-Flores, M. E., Zepeda-Vallejo, L. G., Sandoval, G., Jimenez-Estrada, M., et al. (2013). Oligomerization of 10,16-dihydroxyhexadecanoic acid and methyl-10,16-dihydroxyhexadecanoate catalyzed by lipases. *Molecules* 18, 9317–9333. doi:10.3390/molecules18089317

Heredia-Guerrero, J. A., Heredia, A., García-Segura, R., and Benitez, J. J. (2009). Synthesis and characterization of a plant cutin mimetic polymer. *Polymer* 50, 5633–5637. doi:10.1016/j.polymer.2009.10.018

Lecomte, P., Riva, R., Schmeits, S., Rieger, J., Van Butsele, K., and Jerome, C. (2006). New prospects for the grafting of functional groups onto aliphatic polyesters. Ring opening polymerization of alpha- or gamma-substituted epsilon-caprolactone followed by chemical derivatization of the substituents. *Macromol. Symp.* 240, 157–165. doi:10.1002/masy.200650820

Nair, L. S., and Laurencin, C. T. (2007). Biodegradable polymers as biomaterials. *Prog. Polym. Sci.* 32, 762–798. doi:10.1016/j.progpolymsci.2007.05.017

Okada, M. (2002). Chemical synthesis of biodegradable polymers. *Prog. Polym. Sci.* 27, 87–133. doi:10.1016/S0079-6700(01)00039-9

Olsson, A., Lindstrom, M., and Iversen, T. (2007). Lipase-catalyzed synthesis of an epoxy-functionalized polyester from the suberin monomer cis-9,10-Epoxy-18-hydroxyoctadecanoic acid. *Biomacromolecules* 8, 757–760. doi:10.1021/bm060965w

Osman, S. F., Gerard, H. C., Fett, W. F., Moreau, R. A., and Dudley, R. L. (1995). Method for the production and characterization of tomato cutin oligomers. *J. Agric. Food Chem.* 43, 2134–2137. doi:10.1021/jf00056a033

Osman, S. F., Irwin, P., Fett, W. F., O'Connor, J. V., and Parris, N. (1999). Preparation, isolation, and characterization of cutin monomers and oligomers from tomato peels. *J. Agric. Food Chem.* 47, 799–802. doi:10.1021/jf980693r

Parrish, B., and Emrick, T. (2006). Strategies in aliphatic polyester synthesis for biomaterial and drug delivery applications. *ACS Symp. Ser.* 939, 248–266. doi:10.1021/bk-2006-0939.ch016

Philip, S., Keshavarz, T., and Roy, I. (2007). Polyhydroxyalkanoates: biodegradable polymers with a range of applications. *J. Chem. Technol. Biotechnol.* 82, 233–247. doi:10.1002/jctb.1667

Quinzler, D., and Mecking, S. (2010). Linear semicrystalline polyesters from fatty acids by complete feedstock molecule utilization. *Angew. Chem. Int. Ed.* 49, 4306. doi:10.1002/anie.201001510

Seddon, K. R. (1997). Ionic liquids for clean technology. *J. Chem. Tech. Biotechnol.* 68, 351. doi:10.1002/(SICI)1097-4660(199704)68

Shu, K., Iwao, K., and Yoshinori, Y. (1994). Repeated use of the catalyst in Ln(OTf)3-catalyzed aldol and allylation reactions. *J. Chem. Soc. Jpn.* 67, 2342–2344. doi:10.1246/bcsj.67.2342

Stempfle, F., Ritter, B. S., Mülhaupt, R., and Mecking, S. (2014). Long-chain aliphatic polyesters from plant oils for injection molding, film extrusion and electrospinning. *Green Chem.* 16, 2008–2014. doi:10.1039/c4gc00114a

Sunitha, S., Kanjilal, S., Reddy, P. S., and Prasad, R. B. N. (2007). Liquid–liquid biphasic synthesis of long chain wax esters using the Lewis acidic ionic liquid choline chloride·2ZnCl$_2$. *Tetrahedron Lett.* 48, 6962–6965. doi:10.1016/j.tetlet.2007.07.159

Welton, T. (1999). Room-temperature ionic liquids. Solvents for synthesis and catalysis. *Chem. Rev.* 99, 2071. doi:10.1021/cr980032t

Williams, C. K. (2007). Synthesis of functionalized biodegradable polyesters. *Chem. Soc. Rev.* 36, 1573–1580. doi:10.1039/b614342n

Yamamoto, M., Witt, U., Skupin, G., Beimborn, D., and Muller, R.-J. (2002). "Biodegradable aliphatic-aromatic polyesters: "Ecoflex®," in *Biopolymers, Polyesters III*, Chap. 11. Vol. 4, eds A. Steinbuchel and Y. Doi (Weinheim: Wiley-VCH), 299–311.

You, Z., Cao, H., Gao, J., Shin, P. H., Day, B. W., and Wang, Y. (2010). A functionalizable polyester with free hydroxyl groups and tunable physiochemical and biological properties. *Biomaterials* 31, 3129–3138. doi:10.1016/j.biomaterials.2010.01.023

Waterproofing in Arabidopsis: Following Phenolics and Lipids *In situ* by Confocal Raman Microscopy

Batirtze Prats Mateu[1], Marie Theres Hauser[2], Antonio Heredia[3] and Notburga Gierlinger[1, 4, 5]*

[1] Department of Material Sciences and Process Engineering, University of Natural Resources and Life Sciences, Vienna, Austria, [2] Department of Applied Genetics and Cell Biology, University of Natural Resources and Life Sciences, Vienna, Austria, [3] Department of Molecular Biology and Biochemistry, University of Malaga, Malaga, Spain, [4] Institute for Building Materials, Eidgenössische Technische Hochschule Zurich, Zurich, Switzerland, [5] Applied Wood Research Laboratory, Empa-Swiss Federal Laboratories for Material Testing and Research, Dübendorf, Switzerland

Waterproofing of the aerial organs of plants imposed a big evolutionary step during the colonization of the terrestrial environment. The main plant polymers responsible of water repelling are lipids and lignin, which play also important roles in the protection against biotic/abiotic stresses, regulation of flux of gases and solutes, and mechanical stability against negative pressure, among others. While the lipids, non-polymerized cuticular waxes together with the polymerized cutin, protect the outer surface, lignin is confined to the secondary cell wall within mechanical important tissues. In the present work a micro cross-section of the stem of *Arabidopsis thaliana* was used to track *in situ* the distribution of these non-carbohydrate polymers by Confocal Raman Microscopy. Raman hyperspectral imaging gives a molecular fingerprint of the native waterproofing tissues and cells with diffraction limited spatial resolution ($\sim$300 nm) at relatively high speed and without any tedious sample preparation. Lipids and lignified tissues as well as their effect on water content was directly visualized by integrating the 1299, 1600, and 3400 cm^{-1} band, respectively. For detailed insights into compositional changes of these polymers vertex component analysis was performed on selected sample positions. Changes have been elucidated in the composition of lignin within the lignified tissues and between interfascicular fibers and xylem vessels. Hydrophobizing changes were revealed from the epidermal layer to the cuticle as well as a change in the aromatic composition within the cuticle of trichomes. To verify Raman signatures of different waterproofing polymers additionally Raman spectra of the cuticle and cutin monomer from tomato (*Solanum lycopersicum*) as well as aromatic model polymers (milled wood lignin and dehydrogenation polymer of coniferyl alcohol) and phenolic acids were acquired.

Keywords: lignin, cutin, wax, Raman, cuticle, secondary cell wall, trichomes

INTRODUCTION

Arabidopsis thaliana is the model organism for plant genetics and biology due to, among other reasons, the small genome size, its short generation time, the knowledge of its whole genomic sequence, the large amount of genetic resources (i.e., mutants), and simple genetic transformation and cultivation protocols (Kaul et al., 2000). Arabidopsis has been extensively used to reveal the

genetic basis and study the different plant polymers e.g., cellulose, hemicellulose, pectin, lignin, cutin, wax, and suberin (Beisson et al., 2012; Atmodjo et al., 2013; Pauly et al., 2013; McFarlane et al., 2014; Barros et al., 2015). The non-polysaccharide polymers, lignin, cutin, and suberin played an evolutionary important role during the transition from water to land by conferring waterproofing properties and mechanical strength. The need for mechanical support and the intensified water demand due to plant architectural changes such as branching and increasing height triggered the occurrence of the aforementioned polymers (Langdale and Harrison, 2008).

Lignin is a branched heterogeneous phenolic polymer originating from the oxidation of precursors called monolignols (p-coumaryl, coniferyl, and sinapyl alcohols) and subsequent radical coupling (Boerjan et al., 2003). It is known to act as an embedding media (together with the hemicelluloses) for the cellulose fibrils during secondary cell wall formation (Carpita et al., 1993). The hierarchical nature of biomaterials— the optimization at different length scales (levels of hierarchy)—is responsible for the achieved macroscopic properties (Bergander and Salmen, 2000). The reinforced bio-composite (Fratzl et al., 2004) has elevated resistance to compression failure and superior hardness (Gindl et al., 2004; de Borst et al., 2012; Burgert and Keplinger, 2013). Lignin stiffens the cell wall (Jones et al., 2001) and confers waterproofness and resistance to the negative pressure generated during water transport in the xylem as well as to biotic and abiotic stresses (Sarkanen and Ludwig, 1971). Arabidopsis has been used to study the secondary xylem development as model for wood formation (Chaffey et al., 2002) and lignification (Dima et al., 2015).

Cutin and wax form a lipid barrier called cuticle, which covers all aerial parts of land plants. The cuticle appeared in early plants around 450 million years ago and has been preserved because of its essential role during the colonization of land (Edwards, 1993) challenging gravity, desiccation, and brusque changes in temperature (Waters, 2003). The cuticle has further functions including abiotic and biotic stress protection (e.g., against pathogens or insects), the regulation of the flux of water, gases, and solutes and the sealing of aerial organs of leaves, fruits, petals, and non-lignified stems of the outer plant cell wall (Kerstiens, 1996; Pollard et al., 2008). It offers also mechanical rigidity to the plant (Dominguez et al., 2011). It consists of intracuticular waxes embedded in cutin and an epicuticular layer of crystalline wax at the outer part. In minor amounts it also includes triterpenoids, phenolic compounds including cinnamic acid, flavonoids, and secondary metabolites (Hunt and Baker, 1980). This wax is composed mainly of long chain aliphatic molecules (alkanes) derived from long chain fatty acids, and alcohols. Cutin can be described as a polyester matrix (mainly primary ester bonds) of hydroxy fatty acids and hydroxy-epoxy fatty acids C16 and C18 (Heredia, 2003; Pollard et al., 2008). The cuticle is a variable membrane depending on the function and necessity and environmental conditions (Macherius et al., 2011; Domínguez et al., 2015).

Confocal Raman Microscopy (CRM) has shown a high potential for *in situ* chemical characterization of plants due to its non-destructive nature (Agarwal, 2006; Gierlinger and Schwanninger, 2006, 2007; Gierlinger et al., 2012). The inelastic Raman scattering, recorded as an energy shift by the CCD camera, reflects the molecular vibrations (e.g., bond stretching, rotation, torsion) of the sample and thus the nature of its components (Mueller et al., 2003). The advantage of CRM is that position-resolved molecular fingerprints can be generated with a lateral resolution of 300 nm and a z resolution of ~700 nm (532 nm, NA 1.4). A Raman image is composed of thousands of spectra in which each local position carries its own chemical information and each spectral position has its own molecular identity (Smith and Dent, 2005). The large amount of data generated by Raman imaging can be overcome with the use of multivariate methods that help in the management and interpretation of the data. A blind source of unmixing is helpful since a spectrum can be comprised of many overlapping bands in which the human-eye assignment can be tedious and in many cases impossible. Several multivariate methods have been applied in Chemometrics (Geladi et al., 2010) and also on Raman images of plant cell walls (Gierlinger, 2014). Vertex Component Analysis (VCA) is an iterative method that finds the most pure spectra on the sample by projecting the endmembers in an orthogonal space (the endmembers are independent of each other; Nascimento and Dias, 2005). VCA is a fast, powerful, and reliable algorithm that is able to detect and extrapolate the hypothetical end members using the raw data without any need of dimensionality reduction.

In this work, CRM was used to generate Raman images on a stem microsection of Arabidopsis. The hyperspectral data were analyzed by a univariate method (band integration) and VCA to reveal new insights into the topochemistry of the plant polymers. The correspondent average and endmembers spectra were extracted for a detailed analysis and compared with reference spectra of non-polysaccharide plant polymers.

MATERIALS AND METHODS
Plant Material and Micro-Sectioning

The stem of a 3 week old Arabidopsis (accession Columbia) was transversally cut above ground/the rosette leaves for embedding in polyethylenglycol (PEG) 2000 (Sigma, Austria) following the protocol described in Gierlinger et al. (2012). The embedded blocks were cut in 2 μm thick cross sections using a rotary microtome (RM2235, Leica Biosystems Nussloch GmbH, Germany). The sections were washed with distilled water to remove the PEG. For Raman imaging single sections were put on a glass slide with a drop of water, covered with a coverslip (0.17 mm thick) and sealed with nail polish to avoid water evaporation.

Cuticles from green tomato (*Solanum lycopersicum* L., var. *Casacada*) fruits were isolated by incubation for 5 days in a 2% pectinase/0.2% cellulose solution at pH = 3.6 and treated with chloroform:methanol (3/1, v/v) for 3 h to remove waxes. Dewaxed cuticles were depolymerized by saponification in 1% KOH/methanol for 6 h under refluxing conditions. The filtrate was neutralized with HCl 1N and extracted with diethyl ether. The solid contains about 82% (w/w) of 10(9), 16-dihydroxyhexadecanoic acids and minor amounts of other

hydroxyacids and phenolics as *p*-coumaric acid (Heredia-Guerrero et al., 2014). This mixture will be considered as cutin monomer sample in the present work.

To help in band assignment of lignin structures Raman spectra were acquired from milled wood lignin (MWL) of spruce and beech. MWL is a preparation procedure (extraction with a dioxane–water mixture) widely used for structure studies of lignin and was compared to an artificial lignin dehydrogenation polymer (DHP) preparation based on coniferyl alcohol treated with H_2O_2 in the presence of the enzyme peroxidase. All lignin preparations have been provided by the group of Antje Potthast (University of Natural Resources and Life Sciences, BOKU, Vienna).

Confocal Raman Microscopy and Data Analysis

Raman spectra from the native Arabidopsis cross sections were acquired using a confocal Raman microscope (alpha300RA, WITec GmbH, Germany) with a 100x oil immersion objective (NA 1.4, 0.17 mm coverslip correction; Carl Zeiss, Germany). The sample was excited with a linear polarized (0°) coherent compass sapphire green laser $\lambda_{ex} = 532$ nm (WITec, Germany). The scattered Raman signal was detected with an optic multifiber (50 µm diameter) directed to a spectrometer UHTS 300 (WITec, Germany; 600 g mm^{-1} grating) and finally to the CCD camera DU401A BV (Andor, Belfast, North Ireland). The Control Four (WITec) acquisition software was used for the Raman imaging set up. The laser power was set at 30 mW and a short integration time between 0.1 and 0.5 s was chosen in order to ensure fast mapping and avoid changes in the components structure. One spectrum was taken every 0.3 µm to reach the maximum possible diffraction limited spatial resolution ($r = 0.6 \times \lambda/NA$).

Single Raman spectra of the cutin monomer and the milled wood reference samples were performed with a 100x objective (NA 0.9) and the $\lambda_{ex} = 785$ nm laser (optic multifiber with a 100 µm diameter) using an integration time of 1 s and 20 accumulations. The grating used was the same (600 gmm^{-1}) and the CCD camera corresponded to the model DU401A BR DD (Andor, Belfast, North Ireland). For the isolated tomato fruit cuticle the same instrument configuration was used and stack scans (x–y–z) performed with a z step size of $\Delta z = 0.350$ nm. Average spectra of the total scanned area were extracted and averaged for the first 2 µm from the outer cuticle surface (including the very thick epicuticular wax layer).

Cosmic ray removal was carried out before any further analysis in all cases using the WITec Project Plus 4.0 software (WITec, Germany). Raman images of the cross-sections of Arabidopsis were generated with the same software by using a sum spectral filter which allows specific band integration. This provides chemical images based on the specific bands attributed to different plant components e.g., lignin, water, and cutin plus waxes. Furthermore, based on the integration images, average spectra were extracted by setting an intensity threshold in order to obtain the characteristic Raman signature of the cuticle and the lignified tissues, separately.

Detailed analysis on lignified tissues and cuticles of Arabidopsis were done by Vertex Component Analysis (VCA)

in Cytospec (v.2.00.01) using different number of endmembers and areas within the spectral region of 300–3050 cm^{-1}. All calculated endmember spectra were exported into OPUS 7.0 (Bruker, Germany) for direct comparison. All the reference spectra (including milled wood lignins, cutin monomer, tomato cuticle, ferulic, and coumaric acid) were min–max normalized on the aromatic band at 1600 cm^{-1} for better comparison.

RESULTS

Waterproofing Polymers at the Micron-Level

To present an overview of the distribution of waterproofing polymers in the Arabidopsis stem Raman images were first calculated through integration over specific marker bands (**Figures 1A,B**). Integration over the broad water band around 3400 cm^{-1} visualizes directly the distribution of water within the investigated microsection (**Figure 1A**). High water content is represented by the white areas, whereas the dark areas point to low water content and thus impregnation of waterproofing polymers. The lumina of the cells appear white as they are almost completely water filled, except a few dark deposits are found. The parenchyma cell walls are colored in gray representing a high water content within the thin cell walls. On the contrary the thick walled sclerenchyma and xylem cells are almost black and thus represent low water content. Furthermore, a very thin black layer, the cuticle, is visualized at the outer waterproof surface (**Figure 1A**). The visualized hydrophobicity is due to the impregnation of non-polysaccharide polymers as proofed by integrating the marker bands of lignin (1550–1700 cm^{-1}) and cuticular lipids (1297 cm^{-1}, green), respectively. The red coloration represents impregnation with lignin and is restricted to the xylem and sclerenchyma cells, whereas cuticular lipids (waxes and cutin; green color) are confined to the epidermal outer cell wall surface, the cuticle (**Figure 1B**).

By setting an intensity threshold on the two different integration images, average spectra of the cuticle and the lignified tissues were extracted individually and compared (**Figure 1C**). The average spectrum of the lignified tissues (**Figure 1Ca**) is a combination of cellulose (bands at 380 and 1096 cm^{-1}, (Wiley and Atalla, 1987a,b), probably hemicelluloses (although the bands are not distinguishable at first sight) and lignin with typical bands at 1602 and 1658 cm^{-1} (see assignments in **Table 1**; Agarwal, 1999). The average spectrum of the outer cuticle (**Figure 1Cb**) has also a high intensity in the CH stretching region (~2800 cm^{-1}) due to the abundance of methylene CH2 in both aliphatic waxes and cutin, almost no carbohydrate contribution, but a small characteristic band of pectin at (855 cm^{-1}). The cuticle spectrum is characterized by clear bands at 1439, 1297, and 1602 cm^{-1}.

Figure 2 summarizes the reference spectra used in this study for comparison. Spectra of a cutin monomer mixture (**Figure 2a**), isolated green tomato cuticle (**Figure 2b**), and p-coumaric acid (**Figure 2c**) and ferulic acid (**Figure 2d**) were used for comparison with the stem cuticle of Arabidopsis. Cutin monomer mixture is composed of non-esterified polyhydroxy
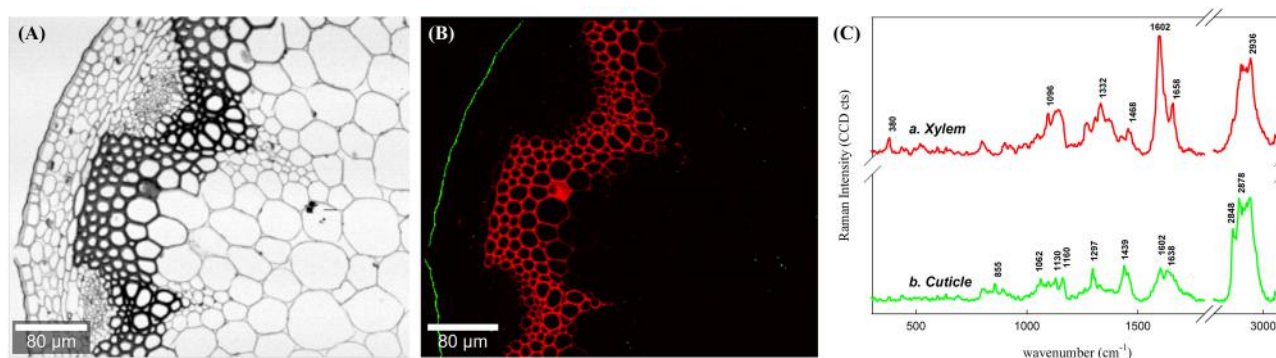
FIGURE 1 | Raman images of a cross section of an Arabidopsis stem by univariate data analysis. Figure captions correspond to images generated by integrating over the **(A)** water main band at around 3400 cm^{-1} and **(B)** lignin around the spectral area 1550–1700 cm^{-1} (in red) together with lipids (in green) at 1299 cm^{-1}. **(C)** Average spectra of calculated by setting an intensity thresold over the image **(B)** for lignin and cuticle in the stem, separetely. Note that the minimal water content in the section matches the areas covered by lignin and cuticle.
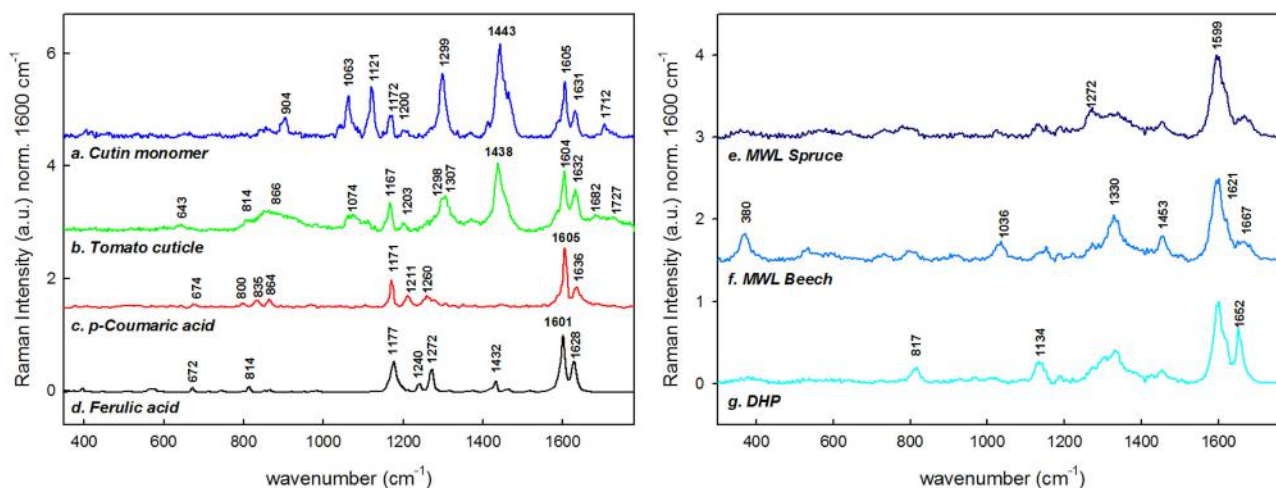
FIGURE 2 | Reference Raman spectra of lipids and phenolics. The spectra were cut (300–1800 cm^{-1}), base line corrected and normalized over the main aromatic stretching band at 1600 cm^{-1}. **(a)** Cutin monomer, **(b)** average spectra of the outer part of the tomato cuticle, **(c)** p-coumaric acid, **(d)** ferulic acid, **(e)** milled wood lignin from Spruce (*Picea abies*), **(f)** milled wood lignin of Beech (*Fagus sylvatica*), and **(g)** synthethized dehydrogenation polymer of lignin (DHP). The spectra are base line corrected and normalized over the 1600 cm^{-1} band.

fatty acids and low amount of phenolics, whereas the outer part of the native tomato cuticle used for the reference measurements is mainly constituted of waxes. If the two spectra are compared the two sharp bands at 1063 and 1121 cm^{-1} are only found in the cutin monomer, whereas bands around 1170, 1299, and 1440 cm^{-1} are found in both samples. The bands characteristic for p-coumaric acid at 1605, 1636, and 1171 cm^{-1} are found in the cutin monomer mixture as well as in the tomato cuticle. Additionally, spectra of milled wood lignin (MWL) of softwood (spruce, **Figure 2e**) and hardwood (beech, **Figure 2f**) and of the dehydrogenation polymer of coniferyl alcohol (DHP; **Figure 2g**) are shown: having all together the typical strong aromatic ring stretching band around 1600 cm^{-1}. The band typical for guaicyl units at 1272 cm^{-1} is seen more pronounced in MWL of spruce, whereas the typical syringyl unit bands at 370, 1036 and 1330, and 1453 cm^{-1} are only clearly seen in MWL of beech. In DHP

the bands at 1134 and 1652 cm^{-1} are more pronounced than in MWL. All characteristic band positions and possible assignments are resumed in **Table 1**.

Phenolic Barriers: Lignin in Cell Wall, Cell Corners, and Compound Middle Lamella

A selected area of the Arabidopsis scan comprising sclerenchyma fibers and xylem elements was analyzed in detail, using vertex component analysis (VCA) with a total of six endmembers and the spectral region 1000–1800 cm^{-1}. In order to compare univariate vs. multivariate statistical approaches, **Figure 3A** shows first the false color image generated by integration over the main lignin band at 1600 cm^{-1} (univariate approach). The lignin amount is higher in cell corner and compound middle lamella indicated by the darker color. Furthermore, it can be seen that the cell walls of xylem vessels (X) contain more

TABLE 1 | Assignments of the reference spectra summarized in Figure 2.

Wavenumber	Assignment (Literature)	Lignin and phenolic acids					Cuticle	
		DHP	MWL Spruce	MWL Beech	p-Coumaric acid	Ferulic acid	Cutin monomer	Tomato cuticle
370	Lignin of sugarcane pith (Agarwal unpublished cited in [1]). Syringyl unit in hardwoods [18]	370	370	371				
531	Skeletal deformation [1]			531				
	Lignin of sugarcane pith (Agarwal unpublished cited in [1])							
815	Out of plane bending C–OH [16]	817				814		814
833					835			
850–862	α-Glycosidic bond in pectin [16]						856	866
	Skeletal vibration pyranoid ring				864			
1033	C–O of aryl-O–CH3 and aryl-OH [2]			1039				
1037	Heavy atom (CC and CO) stretching [11]							
1061	ν C–C in cuticular wax [3, 4, 6, 15]						1063	
1136	Coniferyl/Sinapilaldehyde [1]	1134						
1170–1178	Ring δ ip (CH), ν(C–O–C) ester [3, 17]				1177	1177	1172	1167
	ν (C–O) [10]							
1266	δ ip (=C-H) *cis* of lipids [7, 8]		1272		1260	1272		
1272	Aryl-O stretching of aryl-OH and aryl-O–CH3 (G unit) [1]							
1274	ν(C–C) [10]							
1295	δ (CH2) twisting saturated wax [9]						1299	1298
1303	τ (CH2) lipids [4]							1307
1331–1334	Aliphatic O–H bend [1]	1331		1330				
	Syringyl lignin [5]							
1434	δ CH3 asym. sym. [10]					1432		
1441	δ (CH2) Lipids [7]						1443	1438
1453	CH3 bending in OCH3 [1, 2]	1453	1453	1463				
1588	Aromatic ν (C–C) phenolic compound [4]						1590 sh	
1607	Aromatic ν (C=C) Phenolic compound [3] e.g., Lignin [2]	1602	1599	1601	1605	1601	1605	1604
1621	ν C=C of coniferylaldehyde/sinapaldehyde [1]			1621				
1632	Unsaturated ν C=C of phenolic compound [3]				1636	1628	1631	1632
	ν C=C of coniferyl aldehyde [1, 12, 13, 14]							
1657–1660	C=O coniferyl aldehyde [1], C=C coniferyl alcohol [12]	1652	1667	1667				1662
1640–1680	Sym. ν C=O of carboxylic acid dimer							1682
1720	ν (C=O) cuticular wax [4]							1727

All values are given in wavenumbers (cm^{-1}). ip, in plane; δ, deformation; τ, torsion; ν, stretching; sh, shoulder; sym, symmetric; asym, asymmetric.

[1], (Agarwal et al., 2011); [2], (Agarwal and Ralph, 1997); [3], (Prinsloo et al., 2004); [4], (Trebolazabala et al., 2013); [5], (Sun et al., 2012); [6], (Yu et al., 2008); [7], (Schulz and Baranska, 2007); [8], (Da Silva et al., 2008); [9], (Edwards and Falk, 1997); [10], (Ram et al., 2003); [11], (Wiley and Atalla, 1987a); [12], (Agarwal and Ralph, 2008); [13], (Stewart et al., 1997); [14], (Hanninen et al., 2011); [15], (Wu et al., 2011); [16], (Synytsya et al., 2003); [17], (Heredia-Guerrero et al., 2014); [18], (Agarwal et al., 2015).

lignin (darker gray) than the cell walls of the interfascicular fibers (IF). **Figures 3B–F** display the abundance maps of the endmembers (EM) spectra shown in **Figure 3G** and after baseline correction and min–max normalization over the 1600 cm^{-1} band in **Figure 3H** (fifth EM not shown as no contribution at 1600 cm^{-1}). The sixth EM corresponding to the lumen (water) is not shown. The EM 1 differentiates the upper cell corners near the vessel elements (X), middle lamella, and the tangential cell wall of the vessels. The correspondent EM 1 (red spectrum

Figures 3G,H) shows the highest lignin band (1600 cm^{-1}) and almost no carbohydrate contribution. The EM 2 depicts an inner layer toward the lumen and the cell corners between the IF (**Figure 3C**). The spectrum (in blue) shows lower lignin contribution at 1600 cm^{-1}, a shoulder at 1623 cm^{-1} and the lowest intensity of the 1660 cm^{-1} peak relatively to the other EMs (**Figure 3H**), pointing to a change in lignin composition. The next abundance map in **Figure 3D** (EM 3) accentuates cell wall regions along the horizontal axis of the image, which
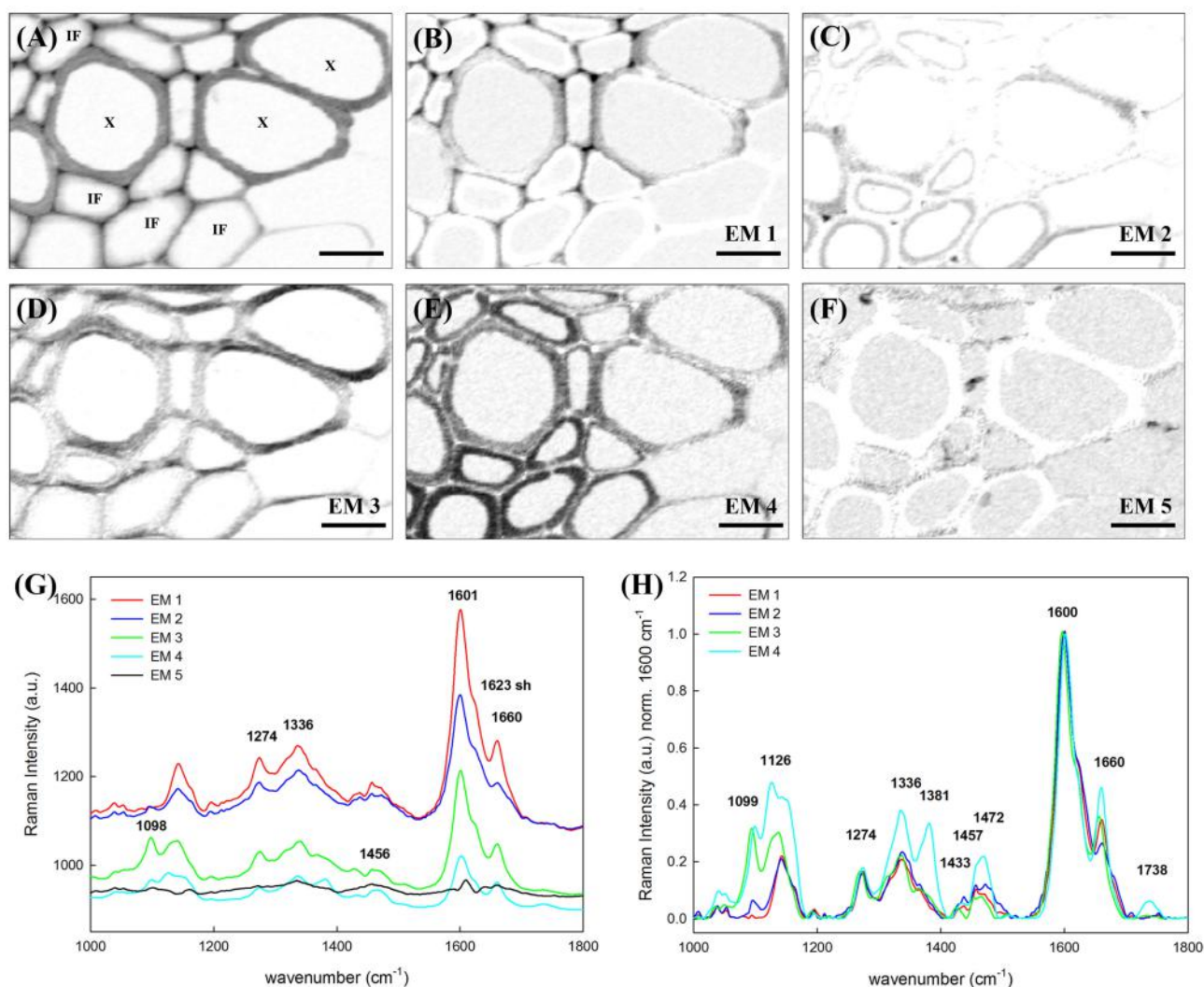
FIGURE 3 | Vertex component analysis of lignified tissue within an Arabidopsis stem. Scale bar: 8 μm. **(A)** Image generated by integrating over the lignin main band at 1600 cm^{-1}. The X is pointing to the vessel elements in xylem. IF stands for interfascicular fiber. **(B–F)** Abundance maps of the endmembers generated by VCA (the intensity profiles of abundance maps are scaled 0–1): **(B)** EM 1 depicts the cell corners and middle lamella together with the tangential walls of the vessel element, **(C)** EM 2 points to the inner cell wall of the IFs whereas **(D)** EM 3 highlights mostly the radial cell walls of the vessel. **(E)** EM 4 is characteristic of the IFs cell wall and **(F)** EM 5 depicts a high angle (and parallel to laser polarization) orientation of the cellulose microfibrils respect to the longitudinal axis. **(G)** Endmembers corresponding to the abundance maps above. EM 1–4 endmember spectra were normalized over the lignin main band at 1600 cm^{-1} and plotted in **(H)**.

points to an effect of the laser polarization direction. A high band at 1098 cm^{-1} in the EM spectrum (green) explains this effect due to an enhancement of this band in regions where the cellulose microfibril is aligned with a high angle with respect to the plant axis. Thus, a higher angle is observed in the vessel wall than in the IF, where the high intensity is restricted to a very small S1 layer. EM 4 (**Figure 3E**) highlights the cell wall of IFs and to less extent the vessel cell wall. This EM spectrum shows after normalization clearly the highest proportion of cellulose (**Figure 3H**, turquoise spectrum high at 1126, 1381 cm^{-1}). Besides, the pronounced band at 1336 cm^{-1}, which was seen as a marker band in beech MWL due to higher amount of incorporated syringyl units (**Figures 2e,f**), points to a

higher incorporation of syringyl units in the secondary cell wall of the IF. The last EM (**Figure 3F**) pictures several deposits in the lumen and the interfaces between cells. The EM spectrum (black spectrum) shows a broad band at 1456 cm^{-1} and other characteristics for a mixture of lipids and proteins. To summarize up VCA is not only able to detect changes in lignin amount, but also to reveal topochemical changes in the heterogenous lignin polymer composition.

Lipid Barriers: Wax and Cutin in the Cuticle

Epidermis and cuticle of the Arabidopsis cross-section was also object of VCA with a total of six EMs. The abundance maps of EM 1–5 (EM 6 corresponded to background and
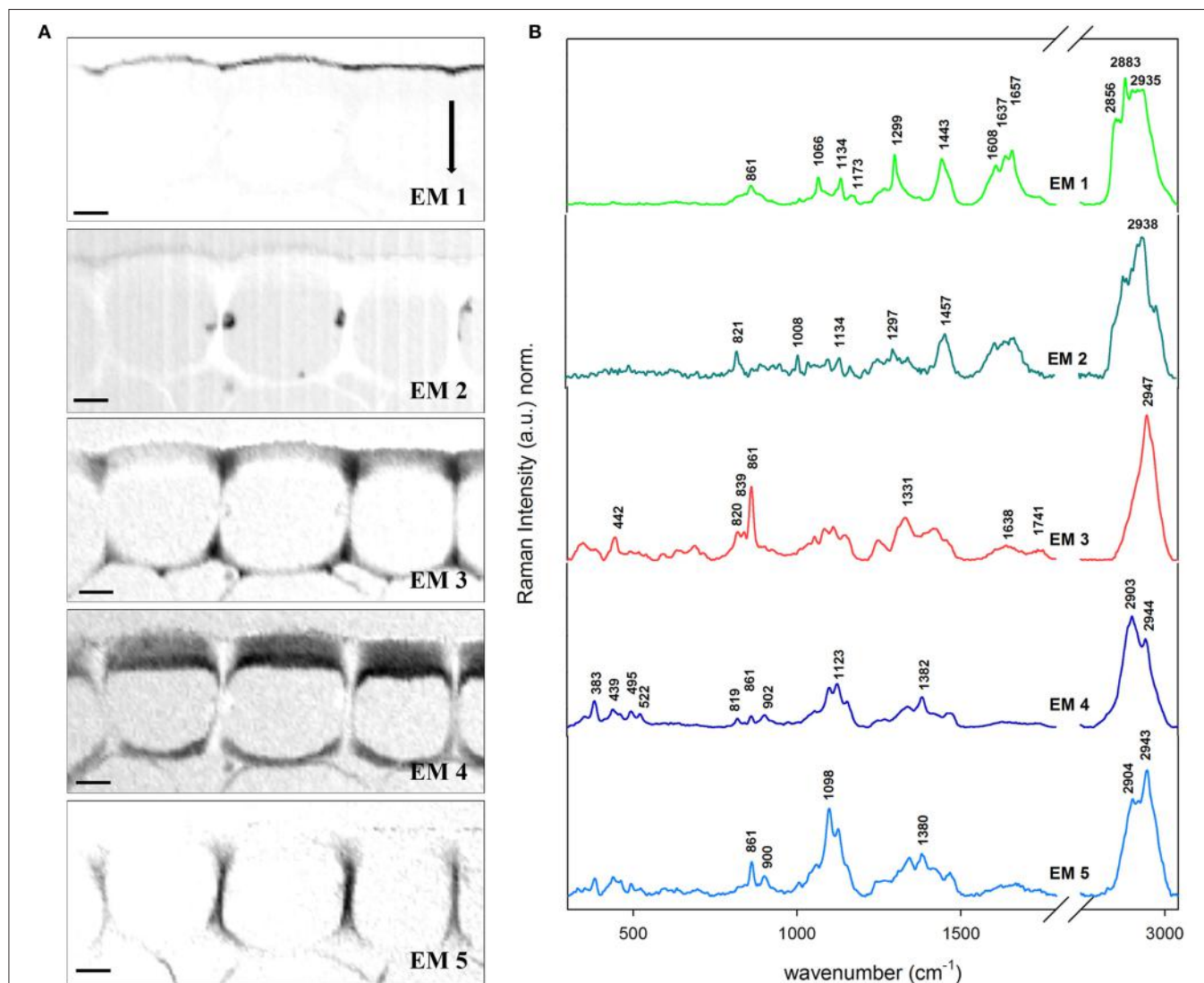
FIGURE 4 | Vertex component analysis on the cuticle of Arabidopsis stem. Scale bar: 4 μm. The number of endmembers chosen for initialization was six. **(A)** Endmember's abundance maps (endmember 6 corresponding to the background is not displayed). The intenisty profiles of abundance maps are scaled 0–1. **(B)** Endmember spectra corresponding to the abundance maps showed in **(A)**. EM 1 describes the cuticle and EM 2 deposits in the lumen and pectin near the cuticle. Contrarely, EM 3 is distinguising pectin accumulated in the epidermis while EM 4 is typical for cellulose parallel to the longitudinal axis. EM 5 is peculiar for high angle cellulose orientation. Each spectrum is baseline corrected and is scaled differently in order to facilitate the observation of minor bands. The arrow indicates the laser polarization direction.

represents just water and is therefore not shown) are displayed together with the related EM spectra (**Figures 4A,B**). The EM 1 abundance map depicts the cuticle (around 2 μm thick) which is characterized by the presence of pectin (855 cm^{-1}), lipids (1299, 1441, and 2883 cm^{-1}) including cuticular waxes (1066, 1299, and 1720 cm^{-1}) and phenolic compounds (1608, 1637, and 1657 cm^{-1}). EM 2 displays the cytoplasm in the lumen and partly the cuticle as well. The spectra again reveal the presence of pectin at 839 cm^{-1}, proteins and lipids (1003 and 1457 cm^{-1}) and phenolic compounds in the 1540–1670 cm^{-1} region. However, most of the pectin signal (839, 861, and unique band at 2947 cm^{-1}) is observed in the cell corners of the epidermis with a

triangular distribution (EM 3). Cellulose contribution is mainly restricted to the epidermis, and separated in EM 4 (tangential wall) and EM 5 (radial wall) due to high angle of the cellulose microfibrils with respect to the stem axis. The thick outer tangential wall displayed by EM 4 shows a gradient structure with higher cellulose intensity near the cytoplasm and less toward the cuticle, where the pectin (EM3) is more dominating. In EM 4 distinctive bands at lower wavenumber region appear which are attributed to both cellulose and hemicelluloses (383, 495, and 522 cm^{-1}) and pectin (439 cm^{-1}). In fact this data show that the cuticle is a modification of the outer cell wall of the epidermal cells.
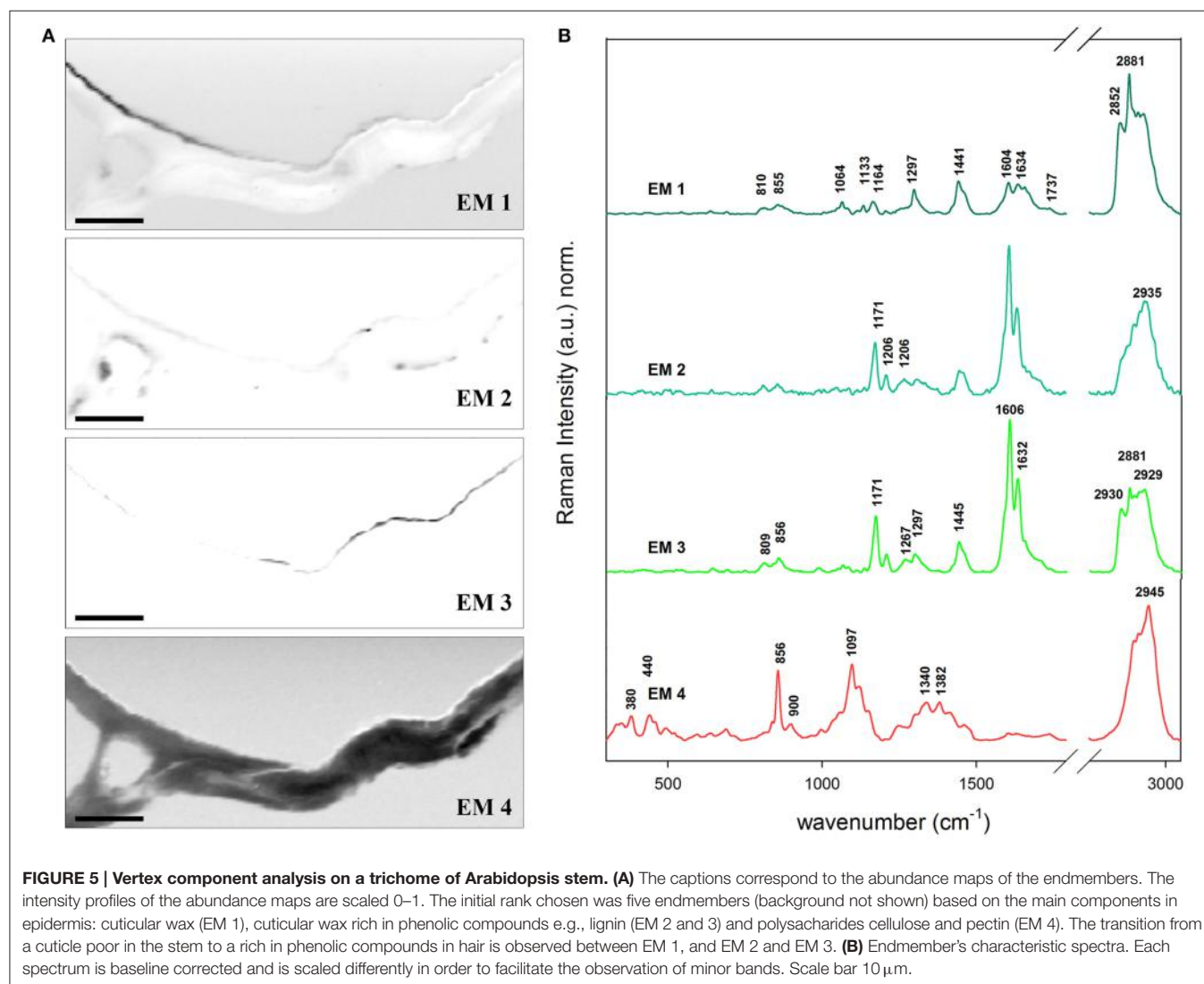
Arabidopsis Dries its Hair

Additionally a non-branched trichome of the stem of *Arabidopsis* was analyzed in detail by Confocal Raman Microscopy and VCA (**Figure 5**). The transition between a lipid-rich (near the stem) to a high-phenolic-containing cuticle (in the outermost extreme of the hair) is observed: the abundance maps of EM 1, EM 2, and EM 3 depict clearly three kinds of cuticle in regard of the phenolic components (1170 and 1560–1700 cm^{-1}) and the lipidic and cuticular wax content (1297 cm^{-1}). The polysaccharide polymers are gathered in EM 4 which shows peaks for pectin (856 cm^{-1}), cellulose (380 and 1097 cm^{-1}), and hemicelluloses (bands at lower region of the spectrum). EM 1 has the characteristic peaks for cuticular lipids. EM 3 as well but additionally higher intensities at the positions 1171 (ring CH deformation), 1606 and 1632 cm^{-1} (ring C=C and C=O stretching) typical for p-coumaric acid (see spectrum c of **Figure 2**). On the contrary, the band at 2881 cm^{-1} (anti-symmetric CH2 stretching of lipids and proteins) is higher in EM 1 when compared to EM 3 meaning that the relative lipid content in the hair cuticle (EM 3) is lower

than in the stem (EM 1). The EM 2 represents several deposits in the cytoplasm of the epidermal cell on the left side of the image and contributes slightly to the cuticle. The size of the lipid chains at these positions drops since the bands in the endmember spectra accounting for the CH2 stretching decrease tremendously, while the phenolic content is also similar high like in the before described hair cuticle. Actually, the band at 2935 cm^{-1} that is characteristic of the symmetric CH3 stretching of lipids but also of the O–CH3 stretching in lignin increases in relation to the others. VCA reveals that for hydrophobizing the stem cuticle and the trichome cuticle different strategies have evolved.

DISCUSSION

It is amazing to observe how plants have evolved to overcome "most" of their enemies and to optimize their living conditions even under dry conditions. Most of the physiological functions

FIGURE 5 | Vertex component analysis on a trichome of Arabidopsis stem. (A) The captions correspond to the abundance maps of the endmembers. The intensity profiles of the abundance maps are scaled 0–1. The initial rank chosen was five endmembers (background not shown) based on the main components in epidermis: cuticular wax (EM 1), cuticular wax rich in phenolic compounds e.g., lignin (EM 2 and 3) and polysacharides cellulose and pectin (EM 4). The transition from a cuticle poor in the stem to a rich in phenolic compounds in hair is observed between EM 1, and EM 2 and EM 3. **(B)** Endmember's characteristic spectra. Each spectrum is baseline corrected and is scaled differently in order to facilitate the observation of minor bands. Scale bar 10 μm.

of the cuticle are a consequence of the physical and chemical properties of cutin, its interaction with the cell wall components and the subtle regulation of other minor compounds. These key physical properties, belonging to three basic areas of physics—thermodynamics, hydrodynamics, and mechanics—are not isolated but they largely influence each other's performance. The design requirements of each property can be incompatible with the properties needed for the others to maximize their functions, leading to a necessary compromise (Dominguez et al., 2011). Thus, the biological role of waterproofing polymers is clear since plants have to keep their feet wet and avoid simultaneously plasmolysis due to out-of-equilibrium medium as well as to keep clean and be protected against new enemies. The characterization of waterproofing lipid and phenolic barriers is of great interest in plant science due to the mentioned biological relevance but also for their use as feedstock for long chain components and biodiesel production (Tsubaki and Azuma, 2013). Lately, different approaches in genetic engineering have been proposed to increase the yield of wax esters in tobacco plants (Aslan et al., 2015). In the same way, lignin has been recognized for its potential as renewable raw material for producing alkylated phenolic compounds, fuels and renewable chemicals (Kleinert and Barth, 2008; Bugg and Rahmanpour, 2015).

Imaging Waterproofing Polymers and also Their Effect on Water Content

The ability of *in situ* clustering and detecting polymers involved in a process such as waterproofing of the plant is essential to know more about the responsible mechanisms behind (Altartouri and Geitmann, 2015). In this study the topochemical distributions of non-polysaccharide polymers and water content were elucidated with a resolution of about 300 nm based on Raman imaging using univariate as well as advanced multivariate data analysis. The univariate analysis of the 2D Raman hyperspectral data revealed an immediate overview about changes in chemical composition between the main structural parts of the plant stem (Agarwal and Atalla, 1986; Agarwal, 2006; Gierlinger and Schwanninger, 2006, 2007) (**Figure 1B**): the cuticle was separated by integrating over the main lipid band around 1300 cm^{-1} (Wu et al., 2011), and the xylem was highlighted by integrating over the aromatic lignin band from 1540 to 1700 cm^{-1} (Agarwal and Ralph, 1997; Prats-Mateu et al., 2014). The water image (**Figure 1A**) showed directly the effect of the waterproofing polymers by an opposite hand picture with low water content in the regions where the non-polysaccharide polymers have been detected.

Representative average spectra of the lignified tissues and cuticle could be extracted through integration images and set intensity thresholds (**Figure 1C**). The spectrum of the lignified tissue (a) is a combination of cellulose (bands at 380 and 1096, Wiley and Atalla, 1987a,b, 2936 cm^{-1}), hemicelluloses (not distinguishable from the first), and lignin with bands at 1270, 1332, 1602, 1658 (see assignments in **Table 1**), and 2936 cm^{-1} due to the antisymmetric C–H stretching in O–CH3 (Agarwal,

1999). The absence of pectin at position 855 cm^{-1} (α-1,4-glycosidic bond; Synytsya et al., 2003) and the presence of lignin together with a thickening of the cell wall in these lignified tissues is an indication of a mature developmental stage of the tracheary elements (vessels and fibers) and their (ongoing) dead stage (Bollhöner et al., 2012). The cuticle by contrary was strongly defined by the presence of lipid components and slightly pectin (855 cm^{-1}) due to the close vicinity of the pectin rich epidermis. The lipidic part is defined mainly by an increase in the C–H and C–C groups due the large aliphatic chains characteristics of waxes and hydroxy fatty acids from cutin. This is visible in the spectrum at the positions 1062, 1297, 1441, and 2848 (symmetric) and 2878 cm^{-1} (asymmetric CH2 stretching vibration) (Weissflog et al., 2010; Littlejohn et al., 2015). The last two bands can be used to determine the crystallinity of the cuticle (Ho and Pemberton, 1998; Greene and Bain, 2005; Littlejohn et al., 2015) which differs in its inner (intracuticular wax) and outer parts (epicuticular wax; Heredia-Guerrero et al., 2014).

The univariate methods i.e., band integration is very suitable for bands, which are not (or only slightly overlapping) with others, to give a fast overview. Nevertheless, this approach is powerless regarding the splitting of the pure components or to separate changes in polymer amount from changes in polymer composition (side chains, crystallinity), which might go hand in hand. Furthermore, due to the multicomponent nature of biological materials we almost always have to deal with overlapping bands, which can lead to misleading conclusions or hide important changes.

Necessity of Multivariate Methods to Track Subtle Changes in Lignin Composition

Lignin is a heterogeneous phenolic compound which complexity is still puzzling scientist around the world (Voxeur et al., 2015). The diversity of the monomer (oligomer) coupling and polymerization mechanisms makes the study of this polymer a difficult task (Boerjan et al., 2003). The breaking pathways of lignin (Mar et al., 2015) are of great interest since it has been found as one of the principal responsible for biomass recalcitrance in biofuel production (Batalha et al., 2015). Lignin varies between species and also between cellular types inside the same tree/plant (Campbell and Sederoff, 1996; Neutelings, 2011).

The potential of Raman imaging combined with multivariate methods (e.g., VCA) to differentiate also subtle changes in lignin composition was shown in spruce wood (Gierlinger, 2014) and in this study on a Raman map of Arabidopsis including xylem vessels and sclerenchyma fibers (**Figure 3**). The calculated endmember spectra proofed that the lignin in the cell corners gluing together the sclerenchyma fibers has more similarity to the lignin in the xylem vessel than in the fibers itself (EM 1). Besides also changes in the matrix have been observed depending if cells are connected in the vascular tissue (EM 1) or in the mechanical stabilizing sclerenchymatic tissue (EM 2). Especially the band at 1660 cm^{-1} changes between secondary cell walls of fibers and xylem and cell corners (**Figure 3H**).

In comparison to the reference spectra of milled wood lignin (MWL) in **Figure 2**, also a higher band at $1660\,cm^{-1}$ assigned to the aromatic ring conjugated C=C bonds and to the C=O group (of coniferaldehyde and/or sinapaldehyde units in lignin; Agarwal and Ralph, 2008; Agarwal et al., 2011) was observed in Arabidopsis compared to MWL. Here more similarity was found with the artificial polymerized DHP, which showed also a higher band at $1652\,cm^{-1}$ band and also the band at $1132\,cm^{-1}$, assigned to coniferaldehyde/sinapaldehyde (Agarwal and Ralph, 2008; Agarwal et al., 2011), similarly pronounced like in EM spectra of Arabidopsis. The lignin most typical for the sclerenchyma fibers (**Figure 3**, EM 4), showed a higher band at 1336 and $1457\,cm^{-1}$, which were also clearly seen in MWL of beech (**Figure 2**, spectrum **f**) and are reported to be typically for syringyl units in lignin (Agarwal and Terashima, 2003; Sun et al., 2012). The presence of higher amounts of guaicyl lignin in vessel elements and higher proportion of syringyl in fibers has been reported for wood samples (Saito et al., 2012) and is now proofed for *Arabidopsis*. Syringyl and guaiacyl units differ in their degree of methylation of the phenylpropane units having the first one methyl group more. During evolution syringyl lignin appear first in angiosperms involving two more steps in the metabolic grid whereas guiacyl lignin is typical for conifers and derives directly from coniferyl alcohol (Eckardt, 2002). CRM gives the value of S/G ratios non-destructively (Sun et al., 2012) and assesses locally differences in xylem maturation and development.

Revealing *In situ* Changes in Cuticle Composition on the Micron-Level

The cuticle covers all aerial organs in the plant and its major characteristic, hydrophobicity, is given by the nature of its composition. Poly-hydroxy and epoxy fatty acids are crosslinked by ester bonds to cutin, which is combined with a variable, generally low amount, of waxes. The disposition of the main polymers in the epidermal cells matches the one suggested in literature (Dominguez et al., 2011) with a triangular area rich in pectin (EM 3) below the cuticle (EM 1) and a half moon formed cellulose layer (EM 4). The cellulose part was divided in two parts being the upper part a mixture of pectin and cellulose (as given by the endmembers 3 and 4) whereas the inner part toward the lumen was richer in cellulose. The presence of hemicelluloses is depicted by the low frequency band at $495\,cm^{-1}$ (Agarwal and Ralph, 1997). Comparing the cuticle EM spectrum (**Figure 4**, EM 1) of Arabidopsis with the acquired reference spectra of cutin monomer and tomato cuticle showed that the main lipid bands at 1443 and within $1299–1307\,cm^{-1}$ were present in all three. The peaks at $1063\,cm^{-1}$ (cuticular wax) and $1712\,cm^{-1}$ (ester bond) observed in EM 1 were only in common with the insoluble cutin reference monomer (**Figure 2a**; for assignments see **Table 1**) which indicated an esterification of the latter. Tomato cuticle and cutin had the band $1172\,cm^{-1}$ in common (characteristic for cuticular wax and/or p-coumaric acid (see Discussion below), which was not strongly visible in Arabidopsis (low intensity). This could mean that the cuticle of Arabidopsis consists mainly of cutin and only small amounts of cuticular waxes. The typical

phenolic bands ($1540–1680\,cm^{-1}$ region) showed less intensity in the cuticle of the Arabidopsis stem, whereas it was clearly seen in the spectra of both isolated cutin and native tomato cuticle. In fact, the main waxes and polyesters found in Arabidopsis are alkanes (and ketones) and dicarboxylic acids, respectively (Suh et al., 2005).

The amount and nature of the lipids and phenolics can also vary due to biotic/abiotic stresses and or tissue specialization i.e., trichomes. It has been found that the fraction of phenolics in the cutin/cuticle matrix is high in gymnosperms and appears in the form of lignin (up to ~26% of the isolated cuticle; Reina et al., 2001). However, the investigation of this feature in angiosperms remains to be done. Marks et al. (2008) found that isolated leaf trichomes of Arabidopsis had a fraction of lignin which they addressed to be in the cell wall after performing the Mäule reaction on detached trichomes. In **Figure 5** the VCA of a stem trichome of Arabidopsis shows the transition from a cuticle rich in lipids near the stem (EM 1) to a cuticle rich in phenolics (EM 3) since the bands at 1600 and $1630\,cm^{-1}$, similar to the ones in coumaric acid (**Figure 2**, spectrum **c** in red), are prominent in the more distant part of the trichome. Ferulic acid and p-coumaric acid have been also found covalently attached to cutin and suberin in apples, peach, pear, and tomato by mass spectrometry and gas chromatography (Riley and Kolattukudy, 1975). Furthermore, ferulic acid has been found not only in fruits but also in primary cell walls of gymnosperms by UV fluorescence microscopy and treatment with NaOH (Carnachan and Harris, 2000) and ferulate makes up to 1% of the cutin polymer (Pollard et al., 2008).

It seems then that phenolic compounds are common for both cell walls and cuticles. They are precursors of lignin and can also be incorporated in lignin of angiosperms (Ralph et al., 2008) and grasses (Lam et al., 2001). In *Brachypodium* contributions of ferulic acid have been found not only in the cell wall but also in cell corners (Gierlinger et al., 2013). We found that p-coumaric and/or ferulic acid were part of the cuticle at the hair but not of the epidermal cell wall by the presence of the peaks at 1171, 1266, and the doublet at 1606 and $1632\,cm^{-1}$ (Piot et al., 2001; Ram et al., 2003). The extracted cutin monomer and the native tomato cuticle (**Figures 2a,b** spectra, respectively) were also characterized by the doublet and the band at $1171–1177\,cm^{-1}$ indicating p-coumaric acid in these reference samples. The presence of phenolic compounds is related to an increase in the rigidity of the cutin matrix (López-Casado et al., 2007). The cutin monomer spectrum (mainly non-esterified hydroxy fatty acids) was more similar to the EM 1 in **Figure 5B** due to the presence of the peaks at 1064 and $1133\,cm^{-1}$ attributed to the C–C stretching of wax and cutin matrix (Prinsloo et al., 2004; Yu et al., 2007, 2008; Trebolazabala et al., 2013).

The potential of the Raman imaging approach in studying non-polysaccharide components is clearly seen in this study by revealing a molecular fingerprint on the micro-level. By this detailed information is gained on: (1) where are the components within the plant cells and (2) what is the chemical nature of the components. If combined with VCA even subtle changes in chemical compositions can be tracked. The advantage of VCA falls on the fact that it extracts the most pure components in

the pixel matrix and reveals the correspondent abundance or distribution maps.

AUTHOR CONTRIBUTIONS

NG: research idea and experiment design, data analysis, and writing of the manuscript; BP: Raman experiments, data analysis, and writing of the manuscript; AH: preparation of cutin monomer, and tomato cuticle, scientific input regarding all aspects of cuticles in the manuscript; MH: providing the Arabidopsis sample and English corrections.

REFERENCES

Agarwal, U. P. (1999). "An overview of Raman spectroscopy as applied to lignocellulosic materials," in *Advances in Lignocellulosics Characterization*, ed D. S. Argyropoulos (Atlanta, GA: TAPPI Press), 201–225.

Agarwal, U. P. (2006). Raman imaging to investigate ultrastructure and composition of plant cell walls: distribution of lignin and cellulose in black spruce wood (*Picea mariana*). *Planta* 224, 1141–1153. doi: 10.1007/s00425-006-0295-z

Agarwal, U. P., and Atalla, R. H. (1986). *In situ* Raman microprobe studies of plant-cell walls – macromolecular organization and compositional variability in the secondary wall of *Picea-mariana* (mill) bsp. *Planta* 169, 325–332. doi: 10.1007/BF00392127

Agarwal, U. P., McSweeny, J. D., and Ralph, S. A. (2011). FT-Raman investigation of milled-wood lignins: softwood, hardwood, and chemically modified black spruce lignins. *J. Wood Chem. Technol.* 31, 324–344. doi: 10.1080/02773813.2011.562338

Agarwal, U. P., and Ralph, S. A. (1997). FT-Raman spectroscopy of wood: identifying contributions of lignin and carbohydrate polymers in the spectrum of black spruce (*Picea mariana*). *Appl. Spectrosc.* 51, 1648–1655. doi: 10.1366/0003702971939316

Agarwal, U. P., and Ralph, S. A. (2008). Determination of ethylenic residues in wood and TMP of spruce by FT-Raman spectroscopy. *Holzforschung* 62, 667–675. doi: 10.1515/HF.2008.112

Agarwal, U. P., Ralph, S. A., Padmakshan, D., Liu, S., Karlen, S. D., Foster, C., et al. (2015). "Estimation of S/G ratio in woods using 1064 nm FT-Raman spectroscopy," in *Proceedings of the 18th ISWFPC* (Vienna), 333–336.

Agarwal, U. P., and Terashima, N. (2003). "FT-Raman study of dehydrogenation polymer (DHP) lignins," in *Proceedings of the 12th International Symposium on Wood, Fiber and Pulping Chemistry, Vol. 3* (Madison, WI: Department of Forest Ecology and Management; University of Wisconsin), 123–126.

Altartouri, B., and Geitmann, A. (2015). Understanding plant cell morphogenesis requires real-time monitoring of cell wall polymers. *Curr. Opin. Plant Biol.* 23, 76–82. doi: 10.1016/j.pbi.2014.11.007

Aslan, S., Hofvander, P., Dutta, P., Sun, C., and Sitbon, F. (2015). Increased production of wax esters in transgenic tobacco plants by expression of a fatty acid reductase: wax synthase gene fusion. *Transgenic Res.* 24, 945–953. doi: 10.1007/s11248-015-9893-5

Atmodjo, M. A., Hao, Z. Y., and Mohnen, D. (2013). Evolving views of pectin biosynthesis. *Ann. Rev. Plant Biol.* 64, 747–779. doi: 10.1146/annurev-arplant-042811-105534

Barros, J., Serk, H., Granlund, I., and Pesquet, E. (2015). The cell biology of lignification in higher plants. *Ann. Bot.* 115, 1053–1074. doi: 10.1093/aob/mcv046

Batalha, L. A. R., Han, Q., Jameel, H., Chang, H. M., Colodette, J. L., and Gomes, F. J. B. (2015). Production of fermentable sugars from sugarcane bagasse by enzymatic hydrolysis after autohydrolysis and mechanical refining. *Bioresour. Technol.* 180, 97–105. doi: 10.1016/j.biortech.2014.12.060

Beisson, F., Li-Beisson, Y., and Pollard, M. (2012). Solving the puzzles of cutin and suberin polymer biosynthesis. *Curr. Opin. Plant Biol.* 15, 329–337. doi: 10.1016/j.pbi.2012.03.003

Bergander, A., and Salmen, L. (2000). Variations in transverse fibre wall properties: relations between elastic properties and structure. *Holzforschung* 54, 654–660. doi: 10.1515/HF.2000.110

Boerjan, W., Ralph, J., and Baucher, M. (2003). Lignin biosynthesis. *Annu. Rev. Plant Biol.* 54, 519–546. doi: 10.1146/annurev.arplant.54.031902.134938

Bollhöner, B., Prestele, J., and Tuominen, H. (2012). Xylem cell death: emerging understanding of regulation and function. *J. Exp. Bot.* 63, 1081–1094. doi: 10.1093/jxb/err438

Bugg, T. D. H., and Rahmanpour, R. (2015). Enzymatic conversion of lignin into renewable chemicals. *Curr. Opin. Chem. Biol.* 29, 10–17. doi: 10.1016/j.cbpa.2015.06.009

Burgert, I., and Keplinger, T. (2013). Plant micro- and nanomechanics: experimental techniques for plant cell-wall analysis. *J. Exp. Bot.* 64, 4635–4649. doi: 10.1093/jxb/ert255

Campbell, M. M., and Sederoff, R. R. (1996). Variation in lignin content and composition – mechanism of control and implications for the genetic improvement of plants. *Plant Physiol.* 110, 3–13.

Carnachan, S. M., and Harris, P. J. (2000). Ferulic acid is bound to the primary cell walls of all gymnosperm families. *Biochem. Syst. Ecol.* 28, 865–879. doi: 10.1016/S0305-1978(00)00009-0

Carpita, N. C., Gibeaut, D. M., and Kim, J. B. (1993). Structural dynamics of the cell-wall during development. *J. Cell. Biochem.* 5, 5.

Chaffey, N., Cholewa, E., Regan, S., and Sundberg, B. (2002). Secondary xylem development in Arabidopsis: a model for wood formation. *Physiol. Plant.* 114, 594–600. doi: 10.1034/j.1399-3054.2002.1140413.x

Da Silva, C. E., Vandenabeele, P., Edwards, H. G. M., and De Oliveira, L. F. C. (2008). NIR-FT-Raman spectroscopic analytical characterization of the fruits, seeds, and phytotherapeutic oils from rosehips. *Anal. Bioanal. Chem.* 392, 1489–1496. doi: 10.1007/s00216-008-2459-0

de Borst, K., Bader, T. K., and Wikete, C. (2012). Microstructure-stiffness relationships of ten European and tropical hardwood species. *J. Struct. Biol.* 177, 532–542. doi: 10.1016/j.jsb.2011.10.010

Dima, O., Morreel, K., Vanholme, B., Kim, H., Ralph, J., and Boerjan, W. (2015). Small glycosylated lignin oligomers are stored in Arabidopsis leaf vacuoles. *Plant Cell* 27, 695–710. doi: 10.1105/tpc.114.134643

Dominguez, E., Cuartero, J., and Heredia, A. (2011). An overview on plant cuticle biomechanics. *Plant Sci.* 181, 77–84. doi: 10.1016/j.plantsci.2011.04.016

Domínguez, E., Heredia-Guerrero, J. A., and Heredia, A. (2015). Plant cutin genesis: unanswered questions. *Trends Plant Sci.* 20, 551–558. doi: 10.1016/j.tplants.2015.05.009

Eckardt, N. A. (2002). Probing the mysteries of lignin biosynthesis: the crystal structure of caffeic acid/5-hydroxyferulic acid 3/5-O-methyltransferase provides new insights. *Plant Cell* 14, 1185–1189. doi: 10.1105/tpc.140610

Edwards, D. (1993). Cells and tissues in the vegetative sporophytes of early land plants. *New Phytol.* 125, 225–247. doi: 10.1111/j.1469-8137.1993.tb03879.x

Edwards, H. G. M., and Falk, M. J. P. (1997). Fourier-transform Raman spectroscopic study of unsaturated and saturated waxes. *Spectrochim. Acta A Mol. Biomol. Spectrosc.* 53, 2685–2694. doi: 10.1016/S1386-1425(97)00161-3

Fratzl, P., Burgert, I., and Gupta, H. S. (2004). On the role of interface polymers for the mechanics of natural polymeric composites. *Phys. Chem. Chem. Phys.* 6, 5575–5579. doi: 10.1039/b411986j

Geladi, P., Grahn, H., and Manley, M. (2010). "Data analysis and chemometrics for hyperspectral imaging," in *Raman, Infrared, and Near-Infrared Chemical Imaging*, eds S. Šašić and Y. Ozaki (Hoboken, NJ: John Wiley & Sons, Inc.), 93–107. doi: 10.1002/9780470768150.ch5

Gierlinger, N. (2014). Revealing changes in molecular composition of plant cell walls on the micron-level by Raman mapping and vertex component analysis (VCA). *Front. Plant Sci.* 5:306. doi: 10.3389/fpls.2014.00306

Gierlinger, N., Keplinger, T., and Harrington, M. (2012). Imaging of plant cell walls by confocal Raman microscopy. *Nat. Protoc.* 7, 1694–1708. doi: 10.1038/nprot.2012.092

Gierlinger, N., Keplinger, T., Harrington, M., and Schwanninger, M. (2013). "Raman imaging of lignocellulosic feedstock," in *Cellulose – Biomass Conversion*, ed P. J. Kadla (InTech), 159–192.

Gierlinger, N., and Schwanninger, M. (2006). Chemical imaging of poplar wood cell walls by confocal Raman microscopy. *Plant Physiol.* 140, 1246–1254. doi: 10.1104/pp.105.066993

Gierlinger, N., and Schwanninger, M. (2007). The potential of Raman microscopy and Raman imaging in plant research. *Spectrosc. Int. J.* 21, 69–89. doi: 10.1155/2007/498206

Gindl, W., Gupta, H. S., Schoberl, T., Lichtenegger, H. C., and Fratzl, P. (2004). Mechanical properties of spruce wood cell walls by nanoindentation. *Appl. Phys. Mater. Sci. Process.* 79, 2069–2073. doi: 10.1007/s00339-004-2864-y

Greene, P. R., and Bain, C. D. (2005). Total internal reflection Raman spectroscopy of barley leaf epicuticular waxes *in vivo*. *Colloid. Surf. B Biointerfaces* 45, 174–180. doi: 10.1016/j.colsurfb.2005.08.010

Hanninen, T., Kontturi, E., and Vuorinen, T. (2011). Distribution of lignin and its coniferyl alcohol and coniferyl aldehyde groups in *Picea abies* and *Pinus sylvestris* as observed by Raman imaging. *Phytochemistry* 72, 1889–1895. doi: 10.1016/j.phytochem.2011.05.005

Heredia, A. (2003). Biophysical and biochemical characteristics of cutin, a plant barrier biopolymer. *Biochim. Biophys. Acta Gen. Subj.* 1620, 1–7. doi: 10.1016/S0304-4165(02)00510-X

Heredia-Guerrero, J. A., Benitez, J. J., Dominguez, E., Bayer, I. S., Cingolani, R., Athanassiou, A., et al. (2014). Infrared and Raman spectroscopic features of plant cuticles: a review. *Front. Plant Sci.* 5:305. doi: 10.3389/fpls.2014.00305

Ho, M., and Pemberton, J. E. (1998). Alkyl chain conformation of octadecylsilane stationary phases by Raman spectroscopy. 1. Temperature dependence. *Anal. Chem.* 70, 4915–4920. doi: 10.1021/ac980471s

Hunt, G. M., and Baker, E. A. (1980). Phenolic constituents of tomato fruit cuticles. *Phytochemistry* 19, 1415–1419. doi: 10.1016/0031-9422(80)80185-3

Jones, L., Ennos, A. R., and Turner, S. R. (2001). Cloning and characterization of irregular xylem4 (irx4): a severely lignin-deficient mutant of Arabidopsis. *Plant J.* 26, 205–216. doi: 10.1046/j.1365-313x.2001.01021.x

Kaul, S., Koo, H. L., Jenkins, J., Rizzo, M., Rooney, T., Tallon, L. J., et al. (2000). Analysis of the genome sequence of the flowering plant *Arabidopsis thaliana*. *Nature* 408, 796–815. doi: 10.1038/35048692

Kerstiens, G. (1996). Signalling across the divide: a wider perspective of cuticular structure-function relationships. *Trends Plant Sci.* 1, 125–129. doi: 10.1016/S1360-1385(96)90007-2

Kleinert, M., and Barth, T. (2008). Phenols from Lignin. *Chem. Eng. Technol.* 31, 736–745. doi: 10.1002/ceat.200800073

Lam, T. B. T., Kadoya, K., and Iiyama, K. (2001). Bonding of hydroxycinnamic acids to lignin: ferulic and p-coumaric acids are predominantly linked at the benzyl position of lignin, not the β-position, in grass cell walls. *Phytochemistry* 57, 987–992. doi: 10.1016/S0031-9422(01)00052-8

Langdale, J. A., and Harrison, C. J. (2008). "Developmental transitions during the evolution of plant form," in *Evolving Pathways Key Themes in Evolutionary Developmental Biology* ed A. Minelli (Cambridge, MA: Cambridge University Press), 299–316. doi: 10.1017/CBO9780511541582.021

Littlejohn, G. R., Mansfield, J. C., Parker, D., Lind, R., Perfect, S., Seymour, M., et al. (2015). *In vivo* chemical and structural analysis of plant cuticular waxes using stimulated raman scattering (srs) microscopy. *Plant Physiol.* 168, 18–28. doi: 10.1104/pp.15.00119

López-Casado, G., Matas, A. J., Domínguez, E., Cuartero, J., and Heredia, A. (2007). Biomechanics of isolated tomato (*Solanum lycopersicum* L.) fruit cuticles: the role of the cutin matrix and polysaccharides. *J. Exp. Bot.* 58, 3875–3883. doi: 10.1093/jxb/erm233

Macherius, A., Kuschk, P., Haertig, C., Moeder, M., Shtemenko, N. I., Bayona, A. H., et al. (2011). Composition changes in the cuticular surface lipids of the helophytes *Phragmites australis* and *Juncus effusus* as result of pollutant exposure. *Environ. Sci. Pollut. Res.* 18, 727–733. doi: 10.1007/s11356-010-0416-x

Mar, B. D., Qi, H. W., Liu, F., and Kulik, H. J. (2015). Ab Initio screening approach for the discovery of lignin polymer breaking pathways. *J. Phys. Chem. A* 119, 6551–6562. doi: 10.1021/acs.jpca.5b03503

Marks, M. D., Betancur, L., Gilding, E., Chen, F., Bauer, S., Wenger, J. P., et al. (2008). A new method for isolating large quantities of *Arabidopsis trichomes* for transcriptome, cell wall and other types of analyses. *Plant J.* 56, 483–492. doi: 10.1111/j.1365-313X.2008.03611.x

McFarlane, H. E., Döring, A., and Persson, S. (2014). The cell biology of cellulose synthesis. *Ann. Rev. Plant Biol.* 65, 69–94. doi: 10.1146/annurev-arplant-050213-040240

Mueller, J., Ibach, W., Weishaupt, K., and Hollricher, O. (2003). Confocal Raman Microscopy. *Microsc. Microanal.* 9, 1084–1085.

Nascimento, J. M., and Dias, J. M. B. (2005). Vertex component analysis: a fast algorithm to unmix hyperspectral data. *IEEE Trans. Geosci. Remote Sens.* 43, 898–910. doi: 10.1109/TGRS.2005.844293

Neutelings, G. (2011). Lignin variability in plant cell walls: contribution of new models. *Plant Sci.* 181, 379–386. doi: 10.1016/j.plantsci.2011.06.012

Pauly, M., Gille, S., Liu, L. F., Mansoori, N., De Souza, A., Schultink, A., et al. (2013). Hemicellulose biosynthesis. *Planta* 238, 627–642. doi: 10.1007/s00425-013-1921-1

Piot, O., Autran, J. C., and Manfait, M. (2001). Investigation by confocal Raman microspectroscopy of the molecular factors responsible for grain cohesion in thetriticum aestivum bread wheat. Role of the cell walls in the starchy endosperm. *J. Cereal Sci.* 34, 191–205. doi: 10.1006/jcrs.2001.0391

Pollard, M., Beisson, F., Li, Y. H., and Ohlrogge, J. B. (2008). Building lipid barriers: biosynthesis of cutin and suberin. *Trends Plant Sci.* 13, 236–246. doi: 10.1016/j.tplants.2008.03.003

Prats-Mateu, B., Stefke, B., Hauser, M. T., and Gierlinger, N. (2014). Elucidating structural and compositional changes in plant tissues and single cells by Raman spectroscopic imaging. *Spectrosc. Eur.* 26, 11–14.

Prinsloo, L. C., Du Plooy, W., and Van Der Merwe, C. (2004). Raman spectroscopic study of the epicuticular wax layer of mature mango (*Mangifera indica*) fruit. *J. Raman Spectrosc.* 35, 561–567. doi: 10.1002/jrs.1185

Ralph, J., Kim, H., Lu, F., Grabber, J. H., Leple, J. C., Berrio-Sierra, J., et al. (2008). Identification of the structure and origin of a thioacidolysis marker compound for ferulic acid incorporation into angiosperm lignins (and an indicator for cinnamoyl CoA reductase deficiency). *Plant J.* 53, 368–379. doi: 10.1111/j.1365-313X.2007.03345.x

Ram, M. S., Dowell, F. E., and Seitz, L. M. (2003). FT-Raman spectra of unsoaked and NaOH-soaked wheat kernels, bran, and ferulic acid. *Cereal Chem.* 80, 188–192. doi: 10.1094/CCHEM.2003.80.2.188

Reina, J. J., Dominguez, E., and Heredia, A. (2001). Water sorption-desorption in conifer cuticles: the role of lignin. *Physiol. Plant.* 112, 372–378. doi: 10.1034/j.1399-3054.2001.1120310.x

Riley, R. G., and Kolattukudy, P. E. (1975). Evidence for covalently attached para-coumaric acid and ferulic acid in cutins and suberins. *Plant Physiol.* 56, 650–654. doi: 10.1104/pp.56.5.650

Saito, K., Watanabe, Y., Shirakawa, M., Matsushita, Y., Imai, T., Koike, T., et al. (2012). Direct mapping of morphological distribution of syringyl and guaiacyl lignin in the xylem of maple by time-of-flight secondary ion mass spectrometry. *Plant J.* 69, 542–552. doi: 10.1111/j.1365-313X.2011.04811.x

Sarkanen, K. V., and Ludwig, C. H. (1971). *Lignins: Occurrence, Foramtion, Structure, and Reactions*. New York, NY: Wiley-Intersciences.

Schulz, H., and Baranska, M. (2007). Identification and quantification of valuable plant substances by IR and Raman spectroscopy. *Vibrational Spectrosc.* 43, 13–25. doi: 10.1016/j.vibspec.2006.06.001

Smith, E., and Dent, G. (2005). "The Raman experiment-Raman instrumentation, sample preparation, data handling and practical aspects of interpretation," in *Modern Raman Spectroscopy-A Practical Approach* (Chichester: John Wiley & Sons Ltd.), 21–67.

Stewart, D., Yahiaoui, N., McDougall, G. J., Myton, K., Marque, C., Boudet, A. M., et al. (1997). Fourier-transform infrared and Raman spectroscopic evidence for the incorporation of cinnamaldehydes into the lignin of transgenic tobacco (*Nicotiana tabacum* L.) plants with reduced expression of cinnamyl alcohol dehydrogenase. *Planta* 201, 311–318. doi: 10.1007/s0042500 50072

Suh, M. C., Samuels, A. L., Jetter, R., Kunst, L., Pollard, M., Ohlrogge, J., et al. (2005). Cuticular lipid composition, surface structure, and gene expression in Arabidopsis stem epidermis. *Plant Physiol.* 139, 1649–1665. doi: 10.1104/pp.105.070805

Sun, L., Varanasi, P., Yang, F., Loque, D., Simmons, B. A., and Singh, S. (2012). Rapid determination of syringyl: guaiacyl ratios using FT-Raman spectroscopy. *Biotechnol. Bioeng.* 109, 647–656. doi: 10.1002/bit.24348

Synytsya, A., Copikova, J., Matejka, P., and Machovic, V. (2003). Fourier transform Raman and infrared spectroscopy of pectins. *Carbohydr. Polym.* 54, 97–106. doi: 10.1016/S0144-8617(03)00158-9

Trebolazabala, J., Maguregui, M., Morillas, H., De Diego, A., and Madariaga, J. M. (2013). Use of portable devices and confocal Raman spectrometers at different wavelength to obtain the spectral information of the main organic components in tomato.(*Solanum lycopersicum*) fruits. *Spectrochim. Acta A Mol. Biomol. Spectrosc.* 105, 391–399. doi: 10.1016/j.saa.2012.12.047

Tsubaki, S., and Azuma, J. (2013). Total fractionation of green tea residue by microwave-assisted alkaline pretreatment and enzymatic hydrolysis. *Bioresour. Technol.* 131, 485–491. doi: 10.1016/j.biortech.2013.01.001

Voxeur, A., Wang, Y., and Sibout, R. (2015). Lignification: different mechanisms for a versatile polymer. *Curr. Opin. Plant Biol.* 23, 83–90. doi: 10.1016/j.pbi.2014.11.006

Waters, E. R. (2003). Molecular adaptation and the origin of land plants. *Mol. Phylogenet. Evol.* 29, 456–463. doi: 10.1016/j.ympev.2003. 07.018

Weissflog, I., Vogler, N., Akimov, D., Dellith, A., Schachtschabel, D., Svatos, A., et al. (2010). Toward *in vivo* chemical imaging of epicuticular waxes. *Plant Physiol.* 154, 604–610. doi: 10.1104/pp.110.161786

Wiley, J. H., and Atalla, R. H. (1987a). Band assignments in the Raman-spectra of celluloses. *Carbohydr. Res.* 160, 113–129. doi: 10.1016/0008-6215(87)80306-3

Wiley, J. H., and Atalla, R. H. (1987b). "Raman-spectra of celluloses," in *The Structure of Cellulose*, Vol. 340, ed R. H. Atalla (Washington, DC: ACS Symposium Series, American Chemical Society), 151–168.

Wu, H. W., Volponi, J. V., Oliver, A. E., Parikh, A. N., Simmons, B. A., and Singh, S. (2011). *In vivo* lipidomics using single-cell Raman spectroscopy. *Proc. Natl. Acad. Sci. U.S.A.* 108, 3809–3814. doi: 10.1073/pnas.1009043108

Yu, M. M. L., Konorov, S. O., Schulze, H. G., Blades, M. W., Turner, R. F. B., and Jetter, R. (2008). *In situ* analysis by microspectroscopy reveals triterpenoid compositional patterns within leaf cuticles of *Prunus laurocerasus*. *Planta* 227, 823–834. doi: 10.1007/s00425-007-0659-z

Yu, M. M. L., Schulze, H. G., Jetter, R., Blades, M. W., and Turner, R. F. B. (2007). Raman microspectroscopic analysis of triterpenoids found in plant cuticles. *Appl. Spectrosc.* 61, 32–37. doi: 10.1366/000370207779701352

Plant biopolymer–geopolymer: organic diagenesis and kerogen formation

*Neal S. Gupta**

Department of Science and Technology, Bryant University, Smithfield, RI, USA

Sedimentary organic matter is formed by diagenesis (reactions in sediments up to 60°C, Tegelaar et al., 1989) and catagenesis (those >100°C induced by thermal cracking, Tissot and Welte, 1984) of biological material introduced during deposition from primary producers. Over 90% of this sedimentary organic matter is a non-hydrolyzable (i.e., immune to acid–base hydrolysis) macropolymer called kerogen (de Leeuw and Largeau, 1993) that does not dissolve in organic solvents and produces petroleum upon catagenesis (Tissot and Welte, 1984). The composition and type of kerogen is heavily dependent on the nature of the biological input (de Leeuw et al., 2006), the environment of deposition (Goth et al., 1998), and the preservation pathway (diagenesis, Briggs, 1999). Both diagenesis and catagenesis can be simulated in the laboratory using P-t apparatus (Stankiewicz et al., 2000) and environmental decay experiments (Briggs, 1999; Gupta et al., 2009).

Kerogen formation is generally attributed to neogenesis (Tissot and Welte, 1984), in which sedimentary organic matter is formed by random intermolecular polymerization and polycondensation of biological residues (e.g., amino acids, sugars, and lipids) including melanoidins or the Selective Preservation of resistant biosynthesized macromolecules that undergo limited chemical change during diagenesis (i.e., they remain morphologically and chemically recognizable as organic remains in the sedimentary rock; Goth et al., 1998). Selective preservation which has gained widespread acceptance as a counter thesis to neogenesis since the mid-1980s posits that aliphatics in fossil organic matter are derived from highly aliphatic and resistant (insoluble and non-hydrolyzable) biopolymers in living organisms, such as algaenan (present in algae; Goth et al., 1998), cutan (present in plant leaves; Mösle et al., 1998), and suberan (present in suberinized vascular tissue, de Leeuw and Largeau, 1993). These survive decay more readily than labile biopolymers such as polysaccharides, proteins, and nucleic acids (Tegelaar et al., 1989). A thorough geochemical analysis of organic fossil matter using high-resolution spectroscopy in conjunction with mass spectrometry [such as in Goth et al. (1998)] and laboratory analytical chemistry methods (de Leeuw and Largeau, 1993) establishes the diagenetic pathway degree of biological preservation (Briggs, 1999) and insights into geochemical transformation of biomolecules to geomolecules (Gupta et al., 2009). Organic sulfurization (Kok et al., 2000) and oxidative reticulation of unsaturated cross-linkages in reacting molecules (Riboulleau et al., 2001) offer mechanistic insights through analysis and case study of modern (extant) and fossil material (discrete) or those disseminated in sediment as kerogen. In light of this, this synthesis opinion article focuses on complimentary and conflicting arguments from plant fossil analysis, their widespread relevance, the biochemical description of contributors, insights from controlled laboratory experiments (decay), and simulated autoclave experiments in pressure–temperature regimes from 270 to 350°C (Stankiewicz et al., 2000).

Morphology and chemical structure of fossil leaves from the Ardèche diatomite (Late Miocene, from southeast France) were detected using pyrolysis–gas chromatography–mass spectrometry, tetramethylammoniumhydroxide (TMAH)-assisted pyrolysis, micro-FTIR, and solid-state ^{13}C NMR spectroscopy to improve understanding of these questions (Gupta et al., 2007a).

These revealed the presence of benzene derivatives, lignin, pristenes, fatty acids, and an aliphatic geopolymer (insoluble in organic solvents, hence recalcitrant) similar in composition to kerogen. Modern leaves failed to reveal the presence of cutan (the aliphatic biopolymer that has been posited to be the direct source of aliphatics in leaf fossils), thereby precluding selective preservation of cutan as the source (Gupta et al., 2007a). TMAH-assisted pyrolysis (an online hydrolysis method) supported this argument by releasing incorporated fatty acyl moieties ranging in C number from C_8 to C_{32} from the macromolecule. The C_{10} to C_{32} acid units are characteristic of the free fatty acid from epicuticular waxes in modern leaves and also phospholipid fatty acid (PLFA) fraction of cell membranes (Gupta et al., 2007a) indicating their direct chemical incorporation in the fossil leaf geopolymer. Such lipid cross-linking is seen in fossil dinoflagellates as well (Versteegh et al., 2004). Cutan, the resistant non-hydrolyzable aliphatic biopolymer present in modern leaves (Mösle et al., 1998), was first reported in the cuticle of *Agave americana* and has generally been considered ubiquitous in leaf cuticles along with the biopolyester cutin. Because leaves and cuticles in the fossil record almost always have an aliphatic composition (Mösle et al., 1998), cutan has been argued as the source biopolymer, especially for the aliphatic component $>C_{20}$. However, Gupta et al. (2006a) analyzed modern leaves using chemical degradation techniques to test for the presence of cutan in multiple taxa concluding its absence in 16 out of 19 taxa analyzed (including gymnosperms and angiosperms). Cutin that forms the protective biopolymer-polyester in modern leaf cuticles (with C_{16} and C_{18} hydroxy fatty acids as abundant components) also acts as a possible source in fossils (Mösle et al., 1998; Gupta et al., 2007a). Other studies that offer similar examples of geopolymer formation in fossils include insects (Briggs, 1999; Stankiewicz et al., 2000), graptolites (Gupta et al., 2006b), kerogen (showing oxidative cross-linking with less selective preservation; Riboulleau et al., 2001), sporopollenin (Watson et al., 2012), and fossil algae (Versteegh et al., 2004).

Degradation of polysaccharides by microbes is dictated by the presence of polysaccharide utilization loci (PUL) in genomes of microbes that dictates which sugars can be utilized by the microbial consortia for energy. Hence, studies have been conducted to understand the relative rate of decay of plant biopolymers (Gupta et al., 2009 and references therein), e.g., by analysis of modern (decaying) and fossil *Metasequoia* leaves. These revealed the presence of structural polyester cutin, guaiacyl lignin units (typical of gymnosperms), and polysaccharides. Analysis of environmentally decayed leaves revealed that the lignin units and cellulose were degraded more relative to cutin, suggesting that cutin is likely more stable than lignin and cellulose in this environmental setting. This is supported by electron microscopy of changes in the
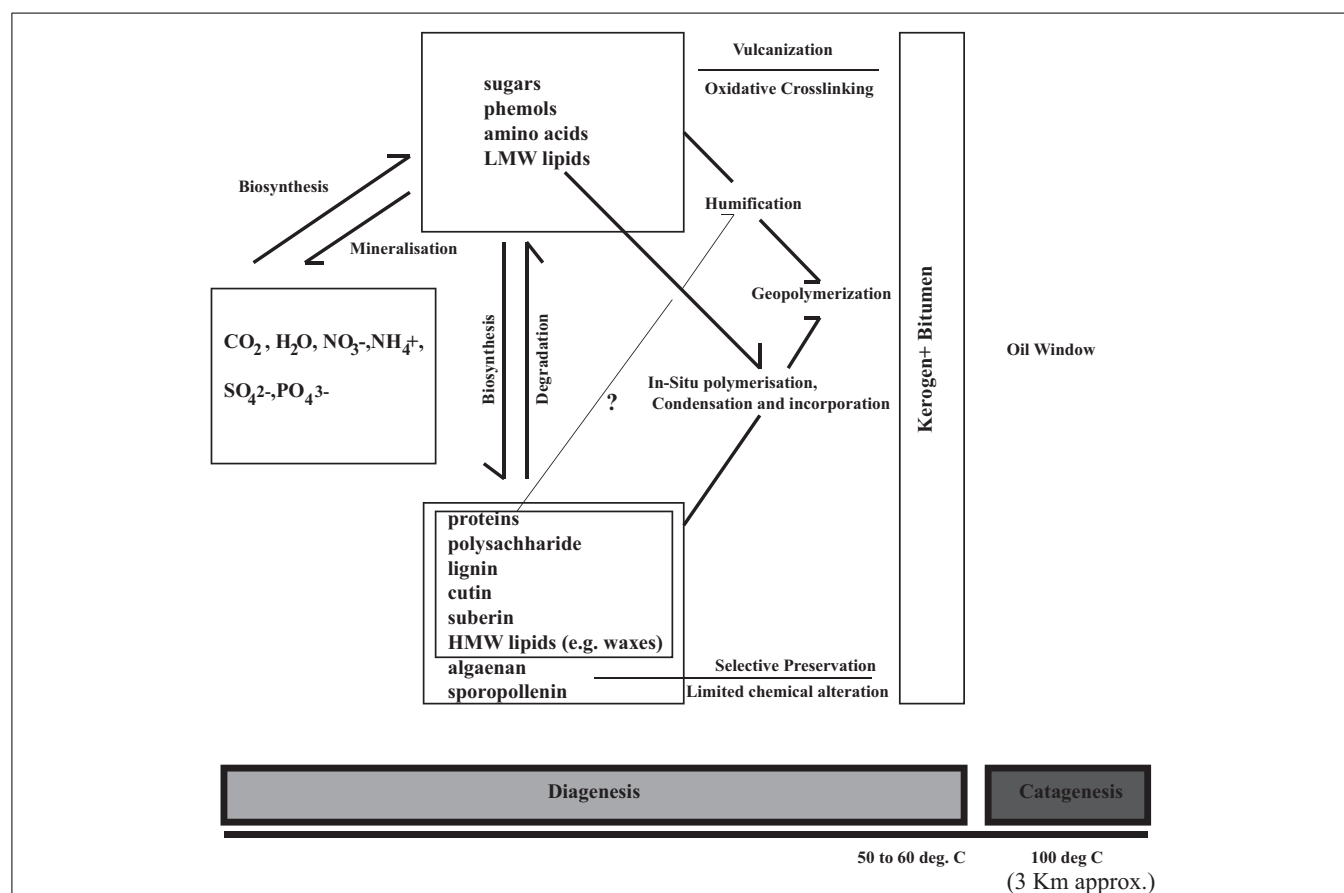

FIGURE 1 | A concept diagram proposing and integrating the pathways of organic matter preservation in tandem with selective preservation (that requires presence and limited change of precursor recalcitrant biopolymer).

cellular structure and cuticle of the modern, decayed, and fossil *Metasequoia* (Gupta et al., 2009).

Experimental heating of cutin is known to generate an aliphatic polymer with carbon chain length $<C_{20}$ (Gupta et al., 2007b), demonstrating that the *n*-alkyl component $>C_{20}$ is a product of incorporation of long-chain plant waxes (indicated by the odd over even predominance of the $>C_{27}$ *n*-alkanes) when cutan is absent in the modern leaf. The resistant nature of cutin compared with lignin and polysaccharides explains the ubiquitous presence of an *n*-alkyl component ($<C_{20}$) in fossil leaves even when polysaccharides are absent and lignin has decayed (Gupta et al., 2009). Experimental maturation of cutan, cutin, lipid waxes, lignin, and polysaccharides in plant leaves (and model compounds – 270 to 350°C, 700 bars) generated a resistant non-hydrolyzable aliphatic macromolecule similar to that detected in plant fossils (Gupta et al., 2007b); Stankiewicz et al. (2000) used similar methods for insects. By comparing the products derived from maturation of different pre-treated plant tissues, these experiments demonstrated that lipids are incorporated into the macromolecular material at 350°C (Gupta et al., 2007b; **Figure 1** shows a new integrated concept diagram). Thus, they indicate that labile organic compounds are a potential source of the aliphatic component of fossil organic matter and kerogen in the absence of a resistant aliphatic precursor in the living organism.

The mechanism leading to the formation of aliphatic components in petroleum from algal sources in marine kerogens is posited to derive from algaenan present in outer cell walls of algae (Goth et al., 1998). Experiments on the non-algaenan-producing alga *Chlamydomonas reinhardtii* at 260 and 350°C revealed a macromolecule with significant aliphatic component (Gupta et al., 2014) similar to that in the modern leaf experiments, also similar to high H content kerogens; derived directly from saturated and unsaturated C_{16} and C_{18} fatty acids here. The presence of amides, nitriles, and oximes in the heated algae is due to the reaction of lipids with the N-containing protein molecules as also seen in heated insects (Gupta et al., 2014). *Scenedesmus quadricauda* at 350°C (an algaenan-containing green alga – as a control) demonstrated survival of algaenan at these temperatures. Analysis of the solvent-insoluble residue of heated cyanobacterium (*Oscillatoria* sp.) and *Rhodopseudomonas palustris* (purple non-sulfur-containing bacteria) similarly produced a macromolecule with high aliphatic content in these studies. Algaenan thus does not give rise to a ubiquitous aliphatic composition in marine sedimentary organic matter (Goth et al., 1998) as a preserved biopolymer. These renew interests and caveats in organic diagenesis and selective preservation of biopolymers (such as algaenan and cutan) and their effect on long-term carbon sequestration (de Leeuw, 2007), where occurrence of recalcitrant biomolecules is limited in modern taxa.

Acknowledgments

References

Briggs, D. E. G. (1999). Molecular taphonomy of animal and plant cuticles: selective preservation and diagenesis. *Philos. Trans. R. Soc. Lond. B* 354, 7–16. doi:10.1098/rstb.1999.0356

de Leeuw, J. W. (2007). On the origin of sedimentary aliphatic macromolecules: a comment on recent publications by Gupta et al. *Org. Geochem.* 38, 1585–1587. doi:10.1016/j.orggeochem.2007.05.010

de Leeuw, J. W., and Largeau, C. (1993). "A review of macromolecular organic compounds that comprise living organisms and their role in kerogen, coal and petroleum formation," in *Org. Geochem.: Prin. and App*, eds M. H. Engel and S. A. Macko (New York: Plenum Press), 23–62.

de Leeuw, J. W., Versteegh, G. J. M., and van Bergen, P. F. (2006). Biomacromolecules of plants and algae and their fossil analogues. *Plant Ecol.* 189, 209–233. doi:10.1007/s11258-005-9027-x

Goth, K., de Leeuw, J. W., Puttman, W., and Tegelaar, E. W. (1998). Origin of messel oil shale kerogen. *Nature* 336, 759–761. doi:10.1038/336759a0

Gupta, N. S., Briggs, D. E. G., Collinson, M. E., Evershed, R. P., Michels, R., Jack, K. S., et al. (2007a). Evidence for the *in situ* polymerisation of labile aliphatic organic compounds during the preservation of fossil leaves: implications for organic matter preservation. *Org. Geochem.* 38, 499–522. doi:10.1016/j.orggeochem.2006.06.011

Gupta, N. S., Michels, R., Briggs, D. E. G., Collinson, M. E., Evershed, R. P., and Pancost, R. D. (2007b). Experimental evidence for formation of geomacromolecules from plant leaf lipids. *Org. Geochem.* 38, 28–36. doi:10.1016/j.orggeochem.2006.09.014

Gupta, N. S., Collinson, M. E., Briggs, D. E. G., Evershed, R. P., and Pancost, R. D. (2006a). Re-investigation of the occurrence of cutan in plants: implications for the leaf fossil record. *Paleobiology* 32, 432–449. doi:10.1666/05038.1

Gupta, N. S., Briggs, D. E. G., and Pancost, R. D. (2006b). Molecular taphonomy of graptolites. *J. Geol. Soc. Lond.* 163, 897–900. doi:10.1144/0016-7649 2006-070

Gupta, N. S., Steele, A., Fogel, M., Griffin, P., Adams, M., Summons, R. E., et al. (2014). Experimental formation of geomacromolecules from microbial lipids. *Org. Geochem.* 67, 35–40. doi:10.1016/j.orggeochem.2013.11.006

Gupta, N. S., Yang, H., Leng, Q., Briggs, D. E. G., Cody, G. D., and Summons, R. E. (2009). Diagenesis of plant biopolymers: decay and macromolecular preservation of *Metasequoia*. *Org. Geochem.* 40, 802–809. doi:10.1016/j.orggeochem.2009.04.004

Kok, M. D., Schouten, S., and Sinninghe Damsté, J. S. (2000). Formation of insoluble, nonhydrolyzable, sulfur-rich macromolecules via incorporation of inorganic sulfur species into algal carbohydrates. *Geochim. Cosmochim. Acta* 64, 2689–2699. doi:10.1016/S0016-7037(00)00382-3

Mösle, B., Collinson, M. E., Finch, P., Stankiewicz, B. A., Scott, A. C., and Wilson, R. (1998). Factors influencing the preservation of plant cuticles: a comparison of morphology and chemical comparison of modern and fossil examples. *Org. Geochem.* 29, 1369–1380. doi:10.1016/S0146-6380(98)00080-1

Riboulleau, A., Derenne, S., Largeau, C., and Baudin, F. (2001). Origin of contrasting features and preservation pathways in kerogens from the Kashpir oil shales (Upper Jurassic, Russian Platform). *Org. Geochem.* 32, 647–665. doi:10.1016/S0146-6380(01)00017-1

Stankiewicz, B. A., Briggs, D. E. G., Michels, R., Collinson, M. E., and Evershed, R. P. (2000). Alternative origin of aliphatic polymer in kerogen. *Geology* 28, 559–562. doi:10.1130/0091-7613(2000)28<559:AOOAPI>2.0.CO;2

Tegelaar, E. W., de Leeuw, J. W., Derenne, S., and Largeau, C. (1989). A reappraisal of kerogen formation. *Geochim. Cosmochim. Acta* 53, 3103–3106. doi:10.1016/0016-7037(89)90191-9

Tissot, B., and Welte, D. H. (1984). *Petrol. Form. and Occurr*, 2nd Edn. Berlin: Springer-Verlag.

Versteegh, G. M. J., Blokker, P., Wood, G. D., Collinson, M. E., Damsté, J. S. S., and de Leeuw, J. W. (2004). An example of oxidative polymerization of unsaturated fatty acids as a preservation pathway for dinoflagellate organic matter. *Org. Geochem.* 35, 1129–1139. doi:10.1016/j.orggeochem.2004.06.012

Watson, J. S., Fraser, W. T., and Sephton, M. A. (2012). Formation of a polyalkyl macro-molecule from the hydrolysable component within sporopollenin during

heating/pyrolysis experiments with *Lycopodium* spores. *J. Anal. App. Pyr.* 95, 138–144. doi:10.1016/j.jaap.2012.01.019

Conflict of Interest Statement: The author declares that the research was conducted in the absence of any commercial or financial relationships that could be construed as a potential conflict of interest.

Sporopollenin, the least known yet toughest natural biopolymer

Grahame Mackenzie[1,2]*, Andrew N. Boa[1], Alberto Diego-Taboada[1,2], Stephen L. Atkin[3] and Thozhukat Sathyapalan[4]

[1] Department of Chemistry, University of Hull, Hull, UK, [2] Sporomex Ltd., Driffield, UK, [3] Weill Cornell Medical College Qatar, Doha, Qatar, [4] Hull York Medical School, University of Hull, Hull, UK

Sporopollenin is highly cross-linked polymer composed of carbon, hydrogen, and oxygen that is extraordinarily stable and has been found chemically intact in sedimentary rocks some 500 million years old. It makes up the outer shell (exine) of plant spores and pollen and when extracted it is in the form of an empty exine or microcapsule. The exines resemble the spores and pollen from which they are extracted, in size and morphology. Also, from any one plant such characteristics are incredible uniform. The exines can be used as microcapsules or simply as micron-sized particles due to the variety of functional groups on their surfaces. The loading of a material into the chamber of the exine microcapsule is via multi-directional nano-diameter sized channels. The exines can be filled with a variety of polar and non-polar materials. Enzymes can be encapsulated within the shells and still remain active. *In vivo* studies in humans have shown that an encapsulated active substance can have a substantially increased bioavailability than if it is taken alone. The sporopollenin exine surface possesses phenolic, alkane, alkene, ketone, lactone, and carboxylic acid groups. Therefore, it can be derivatized in a number of ways, which has given rise to applications in areas, such as solid supported for peptide synthesis, catalysis, and ion-exchange chromatography. Also, the presence of the phenolic groups on sporopollenin endows it with antioxidant activity.

Keywords: sporopollenin, pollen, spores, exines, microcapsules

The Oxford English Dictionary defines a biopolymer as "any of various polymers occurring in living organisms." They are often categorized simply as carbohydrates, proteins, nucleic acids, polyisoprenoid lipids, and lignin. Sporopollenin seems to fall off the list or appears much lower in profile, despite its extraordinary properties that can exceed those of more widely known biopolymers. Sporopollenin makes up the fabric of the outer shell (exine) of plant spores and pollens and is arguably the toughest plant substance known. It has been referred to as the "diamond of the plant world" (Kesseler, 2004), as "probably one of the most extraordinary resistant materials known in the organic world" (Feagri and Iverson, 1964) and, in the plural sense, "the most resistant organic materials of direct biological origin found in nature and in geological samples" (Brooks and Shaw, 1978). In support of these statements, intact exines have been found in some of the most ancient sedimentary rocks found on the Earth's surface (Wellman et al., 2003). In 1814, John (1814) was first to comment on the inertness of tulip pollen wall material, which he called "pollenin." Such inertness was later reported in 1829 by Braconnot (1829) in the pollen wall of bullrush (*Scirpoides holoschoenus*), which he named "sporonin." Almost a century later Zetzsche et al. made a systematic study to characterize the material from the asexual spores of *Lycopodium clavatum* L. (club moss) (Zetzsche and Kälin, 1931; Zetzsche and Vicari, 1931). He combined the previous names to form

the word "sporopollenin," as the generic term for the resistant exine material forming both spore and pollen grain walls, since they appeared to be of the same or have a very similar chemical character. More simply, sporopollenin has been defined as "the resistant non-soluble material left after acetolysis" (Heslop-Harrison and Shaw, 1971; Shaw, 1971) (using a hot mixture acetic anhydride and concentrated sulfuric acid) (Erdtman, 1960) since it readily digests most other biopolymers. Perhaps because of this resilience, the structure and biosynthesis of sporopollenin has yet to be fully elucidated although significant progress has been made over the years (Brooks and Shaw, 1978; Hemsley et al., 1992; Shaw and Apperley, 1996; Ahlers et al., 2000; Fraser et al., 2012; Watson et al., 2012). There is evidence (Hemsley et al., 1998; Gabarayeva and Hemsley, 2006) for the involvement of self-assembly in the formation of exines and more recently evidence for genetic and molecular regulation in sporopollenin biosynthesis (Basketter et al., 1997; Ariizumi and Toriyama, 2011). Also, there is strong support for sporopollenin being built up *via* catalytic enzyme reactions present in the tapetum. In spite of the widely divergent exine morphology and patterning across plant taxa, the developmental processes of sporopollenin formation appear, surprisingly, not to vary significantly, which suggests the preservation of a common molecular mechanism (Fraser et al., 2012). The quest to unravel the structure of sporopollenin has attracted several workers and a variety of approaches over the years (Shaw, 1971; Schulze Osthoff and Wiermann, 1987; Guilford et al., 1988; Wehling et al., 1989; Shaw and Apperley, 1996). Cumulative evidence is in support of sporopollenin being a highly cross-linked polymer composed of carbon, hydrogen, and oxygen. The building blocks appear to be varied and complex, comprising straight- and branched-aliphatic chains, some of which are saturated, unsaturated, and polyhydroxylated (Ahlers et al., 2000). Other important building blocks involve oxygenated aromatic rings and phenylpropanoid moieties. Cross-linking of the blocks has been shown to involve ether cross-linking (Domínguez et al., 1998; Ahlers et al., 2000) but carbon–carbon cross-linking is likely. Exines can be extracted from spores or pollen by a variety of methods, all of which rely upon and demonstrate the extreme stability of sporopollenin to harsh chemical treatment and a wide range of digestive enzymes. The early extraction work was performed to provide a source material for structural characterization. Chemical methods have included successive treatments with hot acetone, potassium hydroxide, and phosphoric acid (Zetzsche and Huggler, 1928; Zetzsche and Kälin, 1931; Zetzsche and Vicari, 1931; Zetzsche et al., 1937) although sulfuric acid was suggested (Shaw and Apperley, 1996) to be a better alternative to phosphoric acid. Acetolysis, introduced by Erdtman (1960) is often used as a cleaning method for palynological sample preparation and has been used frequently since it is rapid and efficient. Interestingly, when used under relatively mild conditions acetolysis has relatively little impact on sporopollenin chemistry (Jardin et al., 2015). Domínguez et al. (1998) developed a method involving anhydrous hydrofluoric acid in pyridine in one-step and claimed that it isolated unaltered sporopollenin. An alternative one-step method used aqueous 4-methylmorpholine-*N*-oxide and sucrose in alkaline conditions (Loewus et al., 1985; Espelie et al., 1989; Couderchet et al., 1996). Most of the extraction methods produce sporopollenin that is nitrogen free by combustion elemental analysis, which is

indicative of sporopollenin being protein free. However, exines treated with sequential hot alkali and acid treatments were also shown to be protein free by mass spectrometry (MALDI-TOF-MS and ESI-QqToF-MS) and electrophoresis (SDS-PAGE), which are techniques in keeping with the Advisory Committee on Novel Foods and Processes (ACNFP) guidelines for the detection of trace protein in foods. It was proposed by Wiermann and Gubatz (1992) that all the harsh chemical methods denature sporopollenin in spore or pollen wall. For this reason, they embarked upon a detailed investigation using an extensive sequence of digestive enzymes to remove all biopolymers and leave only the natural sporopollenin intact (Schulze Osthoff and Wiermann, 1987). Clearly, it is important that sporopollenin be biologically degraded in nature "otherwise we would quite simply be submerged in these materials," as Faegri (1971) stated. Various bacteria are known to degrade sporopollenin under certain conditions (e.g., pH or aerobic milieu) (Faegri, 1971; Stanley and Linskens, 1974; Edlund et al., 2004). There is surprisingly little in the literature pertaining to characterized enzymes that are capable of degrading sporopollenin. Following pollination, the intine secretes an enzyme cocktail (acid phosphatase, ribonuclease, esterase, and amylase) to break up the exine, but the precise characterization of such enzymes not been made (Edlund et al., 2004). Similarly, an uncharacterized pollen esterase has been found in *Hordeum vulgare* L. (barley) pollen that hydrolyzes sporopollenin, in pore formation (Ahokas, 1976).

Exines are unique as microcapsules due to their resilience, consistency in size and characteristic morphology, the latter two features being peculiar to the plant taxa. The exines (**Figure 1**, left) are penetrated by a myriad of nano-diameter sized channels that provide access to the internal chamber (**Figure 1**, centre) for hydration and dehydration processes (Rowley et al., 2003). The biological role of the exines is to protect and transport the delicate genetic and nutrient payloads as part of the plant replication process. Therefore, the exines have evolved to be light shielding (Rozema et al., 2001; Atkin et al., 2011), antioxidant, elastic, and resilient, both chemically and physically. Such a wide range of properties endowed upon sporopollenin exines has attracted interest toward a wide range of applications, particularly where the raw pollen or spores can be obtained in bulk commercial amounts. Examples include club moss (*L. clavatum*) (**Figure 1**), sunflower (*Helianthus annuus*), pine (*Pinus*), and green algae (*Chlorella vulgaris*). The foremost of these is the club moss, which is perhaps the most robust and plentiful since it is used in herbal remedies (Orhan et al., 2007; Mandal et al., 2010) and pyrotechnics (Ellern, 1968). However, the use of pollen from cereal crops, such as rye, maize, and wheat, holds great potential due to the large amounts of such crops being grown worldwide. Exines have served in two roles: (i) as simple "microparticles" that are resilient, uniform, and have a multifunctional and highly decorated surface and (ii) resilient microcapsules with an accessible chamber that can be filled with a variety of polar and non-polar actives with relatively favorable weight-for-weight loadings (**Figure 1**, right). Initially, applications used only the former capability.

Applications as microparticles: the first reported application used exines extracted from *L. clavatum* using sequential treatment with hot alkali and acid (Mackenzie and Shaw, 1980). The aromatic moieties of the exines were chloromethylated and used as a
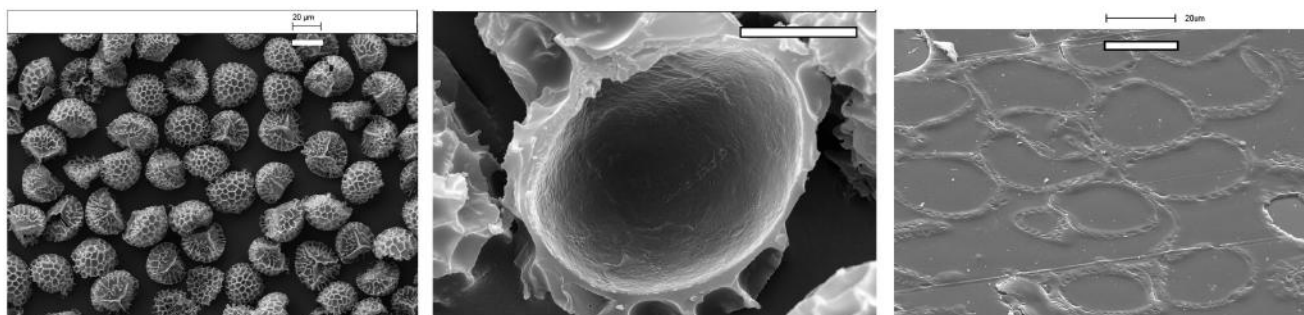
FIGURE 1 | Scanning electron microscopy (SEM) micrographs of *Lycopodium clavatum* L exines [left (bar = 20 µm)] exterior view of a cluster of exines [center (bar = 10 µm)], microtome section of a single exine showing the empty internal cavity, and [left (bar = 20 µm)] a microtome section of exines embedded in acrylic resin with internal cavities filled with the resin.

Merrifield-type resin to synthesize a tripeptide. Conveniently, the loading of the chloromethyl linker was similar to that found on commercial synthetic resins. The chemical resilience and consistency in particle size of exines, coupled with available aromatic and carboxylic acid functions, were put to use as an immobile phase in chromatography and ion-exchange processes (Shaw et al., 1988). The former could be sulfonated with chlorosulfonic acid to produce a strongly acid material and the carboxylic acid could be converted into basic amino functionalities, either by using different types of diamines or reductive amination using ammonia (Barrier et al., 2010). Various chemically modified and unmodified exines from *L. clavatum* have been used for metal remediation (Archibald et al., 2014). Modifications have also been reported to demonstrate the use of sporopollenin exines as a support for use in heterogeneous catalysis. Examples include sporopollenin-supported Schiff bases (Sahin et al., 2012) and palladium catalysts for use in Heck coupling reactions (Keles, 2013). More recently, the exines have been demonstrated to act as an efficient support for enzyme-catalyzed reactions (de Souza et al., 2015). The exine surface possesses ionizable groups (phenols and carboxylic acids) that become increasingly negatively charged with an increase in pH (Binks et al., 2011). This has facilitated their being able to adsorb at both air–water and oil–water interfaces, forming stabilized liquid marbles and emulsions, respectively. The surface conjugated phenol functionalities have been shown by cyclic voltammetry to cause either a two-electron two-proton, or a two-electron one-proton process, which suggests that a rapid electron transfer takes place over the over the surface. This is in accordance with the observed antioxidant behavior of sporopollenin for protecting encapsulated omega-3 oils. Furthermore, the exines have been shown to adsorb ultra-violet and visible light (Atkin et al., 2011; Lomax and Fraser, 2015), which might be expected in terms of their biological role of protecting the genetic material within the pollen or spore.

Applications as microcapsules: the capability of exines from *L. clavatum* to act as microcapsules (**Figure 1**) was demonstrated (Barrier et al., 2011) for a range of polar and non-polar materials, over a wide range of molecular weights, from water to proteins up to 2000 kDa (Atwe et al., 2014). Notably, neither the sporopollenin nor the encapsulation procedure was significantly deleterious to the enzymes' activity, thus offering the possibility of the exines

to act as micro-reaction vessels or transporters of enzymes. This concept was also shown to be effective for the encapsulation of a lipase and subsequent use as catalyst in a variety of reactions (Tutar et al., 2009; Yilmaz, 2012). *L. clavatum* exines were also shown to work as micro-reactors for inorganic reactions. Magnetite nanoparticles and low-soluble salts, such as calcium phosphates, were formed within the exines' chambers. The relatively large available space in the *L. clavatum* exine's chamber, coupled with the exine's amphiphilic surface properties have shown application by being able to sequester oil very efficiently from oil-in-water emulsions. Not surprisingly, the efficiency could be controlled by modifying the polarity of the exines by converting the exine's surface hydroxyl groups (alcohols, phenols, and carboxylic acids), into polar salts (Na^+ and K^+) or non-polar derivatives (ethers, esters, and acetates). The ester forms were shown to sequester oils in near quantitative fashion. The elasticity of the exines permitted encapsulated oils to be released from the microcapsules in a stepwise manner simply by repeated rubbing. It is of note that the exines can be obtained with the cellulose intine (under) layer remaining intact, by hydrolysis of the spores or pollen with strong base, such as aqueous potassium hydroxide (Diego-Taboada et al., 2012). These double layered microcapsules (intine plus exine) can also be alkylated and acylated to sequester oil efficiently from emulsions. Normally, encapsulation into the exine's available chamber is *via* the nano-diameter channels that penetrate them. However, it would appear that compression of the dry exines under some 5–10 tonnes/cm^2 can open the trilete scar feature of the exines, allowing entry of living yeast cells into the exines' chambers (Barrier et al., 2011; Hamad et al., 2011). After this process, the cells still remain viable within the chamber and the exines undamaged, which further illustrate the remarkable elasticity and physical robustness of the exines. The potential for sporopollenin exines to be used in food and pharmaceutical applications has been demonstrated by their having taste-masking properties to the tongue when encapsulated with, such as fish oil and ibuprofen (Diego-Taboada et al., 2013). Also, the exines were shown to encapsulate a commercial gadolinium(III) MRI contrast agent and allow slow release over 8 h in blood plasma (Lorch et al., 2009). *In vitro* studies have shown exines to have the potential to act as an effective drug delivery vector in which release can be triggered by pH (Beckett et al., 2009; Diego-Taboada et al., 2013).

However, more importantly, the potential for exines to be used to deliver specialized foods and drugs has been demonstrated by the significantly enhanced bioavailability of the omega oil eicosapentaenoic acid (EPA) in a double cross-over study in human volunteers. It was shown that the taking the EPA in the encapsulated form provided a *circa* 10-fold increase in bioavailability over taking the EPA alone. The mechanism involved may be associated with bioadhesion of the exine capsules in the gastrointestinal tract. A later *in vivo* study in mouse showed that the sporopollenin exines filled with ovalbumin as a model antigen could be used for oral immunization and which demonstrates the potential of the exines to be used for oral vaccination (Atwe et al., 2014). The authors offered evidence by confocal microscopy that the exines translocate across the mouse intestinal epithelium, which, the authors proposed, might be involved

in the stimulation of the immune system. This work further supports the potential of such microcapsules to have universality toward the delivery of polar and non-polar payloads. The unique three-dimensional shapes and surface topographies of pollens have attracted interest to synthesis inorganic mimics for use in drug delivery and adhesive microparticles with tuneable short- and long-range attractive forces (Goodwin et al., 2013).

For many years, sporopollenin has been studied as a curiosity due its robust nature and role in nature; however, it is only since 1980 that there has been a steady rise of interest in the potential uses of sporopollenin, particularly from *L. clavatum*. The authors believe that there will be more applications and uses in the years to come of this unique renewable polymer that is plentiful in nature from a wide variety of plant sources.

REFERENCES

Ahlers, F., Bubert, H., Steuernagel, S., and Wiermann, R. (2000). The nature of oxygen in sporopollenin from the pollen of typha angustifolia L. *Z. Naturforsch. C* 55, 129–136. doi:10.1515/znc-2000-3-401

Ahokas, H. (1976). Evidence of a pollen esterase capable of hydrolysing sporopollenin. *Experientia* 32, 175–177. doi:10.1007/BF01937750

Archibald, S. J., Atkin, S. L., Bras, W., Diego-Taboada, A., Mackenzie, G., Mosselmans, J. F. W., et al. (2014). How does iron interact with sporopollenin exine capsules? An X-ray absorption study including microfocus XANES and XRF imaging. *J. Mater. Chem. B* 2, 945–959. doi:10.1039/C3TB21523G

Ariizumi, T., and Toriyama, K. (2011). Genetic regulation of sporopollenin synthesis and pollen exine development. *Annu. Rev. Plant Biol.* 62, 437–460. doi:10.1146/annurev-arplant-042809-112312

Atkin, S. L., Barrier, S., Cui, Z., Fletcher, P. D. I., Mackenzie, G., Panel, V., et al. (2011). UV and visible light screening by individual sporopollenin exines derived from *Lycopodium clavatum* (club moss) and *Ambrosia trifida* (giant ragweed). *J. Photochem. Photobiol. B* 102, 209–217. doi:10.1016/j.jphotobiol.2010.12.005

Atwe, S. U., Ma, Y., and Gill, H. S. (2014). Pollen grains for oral vaccination. *J. Control. Release* 194, 45–52. doi:10.1016/j.jconrel.2014.08.010

Barrier, S., Diego-Taboada, A., Thomasson, M. J., Madden, L., Pointon, J. C., Wadhawan, J. D., et al. (2011). Viability of plant spore exine capsules for microencapsulation. *J. Mater. Chem.* 21, 975–981. doi:10.1039/C0JM02246B

Barrier, S., Loebbert, A., Boasman, A. J., Boa, A. N., Lorch, M., Atkin, S. L., et al. (2010). Access to a primary aminosporopollenin solid support from plant spores. *Green Chem.* 12, 234–240. doi:10.1039/B913215E

Basketter, D. A., Chamberlain, M., Griffiths, H. A., Rowson, M., Whittle, E., and York, M. (1997). The classification of skin irritants by human patch test. *Food Chem. Toxicol.* 35, 845–852. doi:10.1016/S0278-6915(97)00053-7

Beckett, S. T., Atkin, S. L., and Mackenzie, G. (2009). *Dosage Form.* US 07608270.

Binks, B. P., Boa, A. N., Kibble, M. A., Mackenzie, G., and Rocher, A. (2011). Sporopollenin capsules at fluid interfaces: particle-stabilised emulsions and liquid marbles. *Soft Matter* 7, 4017–4024. doi:10.1039/c0sm01516d

Braconnot, H. (1829). Recherches chimiques sur le pollen de *Typha latifolia* L., famille des typhacées. *Ann. Chim. Phys.* 2, 91–105.

Brooks, J., and Shaw, G. (1978). Sporopollenin a review of its chemistry paleochemistry and geochemistry. *Grana* 17, 91–98. doi:10.1080/00173137809428858

Couderchet, M., Schmalfuß, J., and Böger, P. (1996). Incorporation of oleic acid into sporopollenin and its inhibition by the chloroacetamide herbicide metazachlor. *Pestic. Biochem. Physiol.* 55, 189–199. doi:10.1006/pest.1996.0048

de Souza, S. P., Bassut, J., Marquez, H. V., Junior, I. I., Miranda, L. S. M., Huang, Y., et al. (2015). Sporopollenin as an efficient green support for covalent immobilization of a lipase. *Catal. Sci. Technol.* 5, 3288–3295. doi:10.1039/C4CY01682C

Diego-Taboada, A., Cousson, P., Raynaud, E., Huang, Y., Lorch, M., Binks, B. P., et al. (2012). Sequestration of edible oil from emulsions using new single and double layered microcapsules from plant spores. *J. Mater. Chem.* 22, 9767–9773. doi:10.1039/c2jm00103a

Diego-Taboada, A., Maillet, L., Banoub, J. H., Lorch, M., Rigby, A. S., Boa, A. N., et al. (2013). Protein free microcapsules obtained from plant spores as a model for drug delivery: ibuprofen encapsulation, release and taste masking. *J. Mater. Chem. B* 1, 707–713. doi:10.1039/C2TB00228K

Domínguez, E., Mercado, J. A., Quesada, M. A., and Heredia, A. (1998). Isolation of intact pollen exine using anhydrous hydrogen fluoride. *Grana* 37, 93–96. doi:10.1080/00173139809362649

Edlund, A. F., Swanson, R., and Preuss, D. (2004). Pollen and stigma structure and function: the role of diversity in pollination. *The Plant Cell* 16, S84–S97. doi:10.1105/tpc.015800

Ellern, H. (1968). *Military and Civilian Pyrotechnics*. New York, NY: Chemical Publishing Company Inc.

Erdtman, G. (1960). The acetolysis method. A revised description. *Svensk Botanisk Tidskrift* 54, 561–564.

Espelie, K. E., Loewus, F. A., Pugmire, R. J., Woolfenden, W. R., Baldi, B. G., and Given, P. H. (1989). Structural-analysis of lilium-longiflorum sporopollenin by C-13 NMR-spectroscopy. *Phytochemistry* 28, 751–753. doi:10.1016/0031-9422(89)80108-6

Faegri, K. (1971). "The preservation of sporopollenin membranes under natural conditions," in *Sporopollenin*, eds J. Brooks, P. R. Grant, M. Muir, P. Van Gijzel, and G. Shaw (London: Academic Press), 256–272.

Feagri, I., and Iverson, J. (1964). *Textbook of Pollen Analysis*. London: Blackwell.

Fraser, W. T., Scott, A. C., Forbes, A. E. S., Glasspool, I. J., Plotnick, R. E., Kenig, F., et al. (2012). Evolutionary stasis of sporopollenin biochemistry revealed by unaltered Pennsylvanian spores. *New Phytol.* 196, 397–401. doi:10.1111/j.1469-8137.2012.04301.x

Gabarayeva, N., and Hemsley, A. R. (2006). Merging concepts: the role of self-assembly in the development of pollen wall structure. *Rev. Palaeobot. Palynol.* 138, 121–139. doi:10.1016/j.revpalbo.2005.12.001

Goodwin, W. B., Gomez, I. J., Fang, Y., Meredith, J. C., and Sandhage, K. H. (2013). Conversion of pollen particles into three-dimensional ceramic replicas tailored for multimodal adhesion. *Chem. Mater.* 25, 4529–4536. doi:10.1021/cm402226w

Guilford, W. J., Schneider, D. M., Labovitz, J., and Opella, S. J. (1988). High-resolution solid-state C-13 NMR-spectroscopy of sporopollenins from different plant taxa. *Plant Physiol.* 86, 134–136. doi:10.1104/pp.86.1.134

Hamad, S. A., Dyab, A. F. K., Stoyanov, S. D., and Paunov, V. N. (2011). Encapsulation of living cells into sporopollenin microcapsules. *J. Mater. Chem.* 21, 18018–18023. doi:10.1039/c1jm13719k

Hemsley, A. R., Chaloner, W. G., Scott, A. C., and Groombridge, C. J. (1992). C-13 Solid-state nuclear-magnetic-resonance of sporopollenins from modern and fossil plants. *Ann. Bot.* 69, 545–549.

Hemsley, A. R., Vincent, B., Collinson, M., and Griffiths, P. C. (1998). Simulated self-assembly of spore exines. *Ann. Bot.* 82, 105–109. doi:10.1006/anbo.1998.0653

Heslop-Harrison, J., and Shaw, G. (1971). "Sporopollenin in the biological context," in *Sporopollenin*, eds J. Brooks, P. R. Grant, M. Muir, and P. Van Gijzel (London: Academic Press), 1–30.

Jardin, P. E., Fraser, W. T., Lomax, B. H., and Gosling, W. D. (2015). The impact of oxidation on spore and pollen chemistry. *J. Micropalaeontolog* 34, 139–149. doi:10.1144/jmpaleo2014-022

John, J. F. (1814). Über den befruchtungsstaub, nebst einer analyse des tulpenpollens. *J. Chem. Phys.* 12, 244–252.

Keles, M. (2013). Preparation of heterogeneous palladium catalysts supported on sporopollenin for heck coupling reactions. *Synthesis and Reactivity in Inorganic Metal-Organic and Nano-Metal Chemistry* 43, 575–579. doi:10.1080/15533174.2012.749895

Kesseler, I. H. M. (2004). *Pollen, The Hidden Sexuality of Flowers*. London: Papadakis Publisher.

Loewus, F. A., Baldi, B. G., Franceschi, V. R., Meinert, L. D., and McCollum, J. J. (1985). Pollen sporoplasts – dissolution of pollen walls. *Plant Physiol.* 78, 652–654. doi:10.1104/pp.78.3.652

Lomax, B. H., and Fraser, W. T. (2015). Palaeoproxies: botanical monitors and recorders of atmospheric change. *Palaeontology* 58, 759–768. doi:10.1111/pala.12180

Lorch, M., Thomasson, M. J., Diego-Taboada, A., Barrier, S., Atkin, S. L., Mackenzie, G., et al. (2009). MRI contrast agent delivery using spore capsules: controlled release in blood plasma. *Chem. Commun.* 42, 6442–6444. doi:10.1039/b909551a

Mackenzie, G., and Shaw, G. (1980). Sporopollenin. A novel, naturally occurring support for solid phase peptide synthesis. *Int. J. Pept. Protein Res.* 15, 298–300. doi:10.1111/j.1399-3011.1980.tb02580.x

Mandal, S. K., Biswas, R., Bhattacharyya, S. S., Paul, S., Dutta, S., Pathak, S., et al. (2010). Lycopodine from *Lycopodium clavatum* extract inhibits proliferation of HeLa cells through induction of apoptosis via caspase-3 activation. *Eur. J. Pharmacol.* 626, 115–122. doi:10.1016/j.ejphar.2009.09.033

Orhan, I., Kupeli, E., Sener, B., and Yesilada, E. (2007). Appraisal of anti-inflammatory potential of the clubmoss, *Lycopodium clavatum* L. *J. Ethnopharmacol.* 109, 146–150. doi:10.1016/j.jep.2006.07.018

Rowley, J. R., Skvarla, J. J., and El-Ghazaly, G. (2003). Transfer of material through the microspore exine – from the loculus into the cytoplasm. *Can. J. Bot.* 81, 1070–1082. doi:10.1139/b03-095

Rozema, J., Broekman, R. A., Blokker, P., Meijkamp, B. B., de Bakker, N., van de Staaij, J., et al. (2001). UV-B absorbance and UV-B absorbing compounds (para-coumaric acid) in pollen and sporopollenin: the perspective to track historic UV-B levels. *J. Photochem. Photobiol. B* 62, 108–117. doi:10.1016/S1011-1344(01)00155-5

Sahin, M., Gubbuk, I. H., and Kocak, N. (2012). Synthesis and characterization of sporopollenin-supported schiff bases and ruthenium(III) sorption studies. *J. Inorg. Organomet. Polym. Mater.* 22, 1279–1286. doi:10.1007/s10904-012-9739-z

Schulze Osthoff, K., and Wiermann, R. (1987). Phenols as integrated compounds of sporopollenin from *Pinus* pollen. *J. Plant Physiol.* 131, 5–15. doi:10.1016/S0176-1617(87)80262-6

Shaw, G. (1971). "The chemistry of sporopollenin," in *Sporopollenin*, eds J. Brooks, P. R. Grant, M. Muir, P. V. Gijzel, and G. Shaw (London: Academic Press), 305–334.

Shaw, G., and Apperley, D. C. (1996). C-13-NMR spectra of *Lycopodium clavatum* sporopollenin and oxidatively polymerised beta-carotene. *Grana* 35, 125–127. doi:10.1080/00173139609429483

Shaw, G., Sykes, M., Humble, R. W., Mackenzie, G., Marsden, D., and Pehlivan, E. (1988). The use of modified sporopollenin from *Lycopodium clavatum* as a novel ion- or ligand-exchange medium. *React. Polym. Ion Exchangers Sorbents* 9, 211–217. doi:10.1016/0167-6989(88)90034-7

Stanley, R. G., and Linskens, H. F. (eds) (1974). *Pollen: Biology, Biochemistry, Management*. Berlin: Springer-Verlag, 307.

Tutar, H., Yilmaz, E., Pehlivan, E., and Yilmaz, M. (2009). Immobilization of *Candida rugosa* lipase on sporopollenin from *Lycopodium clavatum*. *Int. J. Biol. Macromol.* 45, 315–320. doi:10.1016/j.ijbiomac.2009.06.014

Watson, J. S., Fraser, W. T., and Sephton, M. A. (2012). Formation of a polyalkyl macromolecule from the hydrolysable component within sporopollenin during heating/pyrolysis experiments with *Lycopodium* spores. *J. Anal. Appl. Pyrolysis* 95, 138–144. doi:10.1016/j.jaap.2012.01.019

Wehling, K., Niester, C., Boon, J. J., Willemse, M. T. M., and Wiermann, R. (1989). *p*-Coumaric acid – a monomer in the sporopollenin skeleton. *Planta* 179, 376–380. doi:10.1007/BF00391083

Wellman, C. H., Osterloff, P. L., and Mohiuddin, U. (2003). Fragments of the earliest land plants. *Nature* 425, 282–285. doi:10.1038/nature01884

Wiermann, R., and Gubatz, S. (1992). Pollen wall and sporopollenin. *Int. Rev. Cytol.* 140, 35–72. doi:10.1016/S0074-7696(08)61093-1

Yilmaz, E. (2012). Enantioselective enzymatic hydrolysis of racemic drugs by encapsulation in sol-gel magnetic sporopollenin. *Bioprocess Biosyst. Eng.* 35, 493–502. doi:10.1007/s00449-011-0622-z

Zetzsche, F., and Huggler, K. (1928). Untersuchungen über die membran des sporen und pollen I. 1. *Lycopodium clavatum* L. *Justus Liebigs. Ann. Chem.* 461, 89–108. doi:10.1002/jlac.19284610105

Zetzsche, F., and Kälin, O. (1931). Untersuchungen über die membran der sporen und pollen v. 4. Zur autoxydation der sporopollenine. *Helv. Chim. Acta* 14, 517–519. doi:10.1002/hlca.19310140151

Zetzsche, F., Kalt, P., Lietchi, J., and Ziegler, E. (1937). Zur konstitution des lycopodium-sporonins, des Tasmanins und des lange-sporonins. *J. Prakt. Chem.* 148, 267–286. doi:10.1002/prac.19371480903

Zetzsche, F., and Vicari, H. (1931). Untersuchungen über die membran der sporen und pollen. III. 2. *Picea orientalis*, *Pinus sylvestris* L., *Corylus avellana* L. *Helv. Chim. Acta* 14, 62–67. doi:10.1002/hlca.19310140105

Advantages of publishing in Frontiers

OPEN ACCESS

Articles are free to read, for greatest visibility

COLLABORATIVE PEER-REVIEW

Designed to be rigorous – yet also collaborative, fair and constructive

FAST PUBLICATION

Average 85 days from submission to publication (across all journals)

COPYRIGHT TO AUTHORS

No limit to article distribution and re-use

TRANSPARENT

Editors and reviewers acknowledged by name on published articles

SUPPORT

By our Swiss-based editorial team

IMPACT METRICS

Advanced metrics track your article's impact

GLOBAL SPREAD

5'100'000+ monthly article views and downloads

LOOP RESEARCH NETWORK

Our network increases readership for your article

Find us on